A SPACEBORNE SYNTHETIC APERTURE RADAR (SAR) PROCESSOR DESIGN.

P.J. KRITZINGER

SEPTEMBER 1991

Submitted to the University of Cape Town in partial fulfilment of the degree of Master of Science in Engineering.

DECLARATION

I, **Paul Johan Kritzinger**, submit this thesis in partial fulfilment of the requirements for the degree of Master of Science in Engineering. I claim that this is my original work and that it has not been submitted in this, or any similar form, for a degree at any University.

Signed

Signature of candidate

ABSTRACT

Synthetic Aperture Radar (SAR) has many possible applications for the Southern African region and therefore, because no expertise was available in SA for the decoding of SAR data, it was decided that a facility for SAR research should be created. This research facility was realised at the University of Cape Town.

This thesis is the first phase of a project launched by the research facility, which comprises of the software design of a general purpose digital processor for the decoding of spaceborne SAR data. The thesis is divided into two main sections. The first is concerned with the development of a unified theoretical basis to explain the mechanism of operation of SAR. The second section is concerned with the design of a spaceborne SAR processor.

In Chapter 2, it is proved that SAR can be treated in its entirety from a signal processing perspective. Most of the specialised theory and techniques used to discuss SAR processing are relatively standard processing techniques as used in the signal processing literature. Azimuth SAR processing is shown to be no more complicated than the digital correlation of a sampled signal, where this signal is simply the Doppler waveform associated with a moving target.

In Chapter 3, an algorithm design is proposed for a digital processor to decode spaceborne SAR data. This design is general enough to accommodate data from a variety of spaceborne SAR systems, each with its own orbital geometry and system parameters. Range correlation, range walk correction, azimuth correlation and the effects of range migration are considered. The decode algorithms are designed to display the necessary insensitivity to numerical error in predicted satellite orbital geometry and system parameter values. Simulated data is used to test the validity and sensitivity of these algorithms.

To illustrate the operation of the decode algorithms in terms of numerical values, real system and orbital values are used throughout Chapter 3. These values were obtained from the "Shuttle Imaging Radar B Experiment" (SIR-B).

The proposed software design was implemented at UCT and tested on raw radar data of Cradock in South Africa. This data was obtained from the SIR-B experiment. A fully processed SAR image of the region, obtained using the algorithm design outlined in this thesis, is included in Chapter 3.

ACKNOWLEDGEMENTS

I would like to thank Professor M.R. Inggs for making this research possible and for the help and guidance he gave me during the period of this thesis. I would also like to extend my thanks to Mr M.W. van Zyl for the many helpful discussions that we had during this period.

The financial support received from the Foundation for Research and Development (FRD) is acknowledged.

TABLE OF CONTENTS

GLOSSARY

Standard terms as used in this thesis are defined in alphabetical order. In most cases standard radar terminology is used. In some cases, terms are defined that are either new or that differ in some way from the usual definition. In all cases, however, the terms used in this thesis correspond to the definitions given in the list below.

The first appearance of a standard term in the text of this thesis is bolded and enclosed in quotation mark. Subsequent appearances are treated as normal text.

NOTE: All standard terminology appearing in the list below, is bolded for cross referencing purposes.

Absolute time. The absolute time reference t of the radar system. This is also termed **azimuth time**.

Along-track direction. Another name for the **azimuth direction** in a SAR geometry.

Along-track velocity. The vector component of relative target velocity as resolved in the **azimuth or along-track direction**.

Aspect angle. The angle between the position of **zero doppler** and the target position, relative to the radar antenna.

Azimuth array. Any one dimensional array making up a row in the **SAR matrix**.

Azimuth bin. An azimuth sample in the **SAR matrix**.

Azimuth data. The sampled data contained within a particular **azimuth array**.

Azimuth direction. Defined to be in a direction perpendicular to the **range direction** and lying on a plane which contains the relative velocity vector V of the target and the position of the antenna.

Azimuth time. Equal to the **absolute time** reference t of the radar system.

Azimuth processing window. The spatial (or frequency) extent of target motion that is necessary to produce the length of **azimuth waveform** used during azimuth correlation.

Azimuth reference function. A reference function that is generated for azimuth correlation purposes.

Azimuth subarray. A term used to describe the sub sections of the **azimuth array** that must be shifted during range walk correction.

Azimuth waveform. This waveform is made up of the complex set of discrete phase samples as recorded in a series of received radar **range waveforms**.

Bandwidth. The range of positive frequencies present in the spectrum of a real signal.

Beam angle. The angle between the **boresight** of the antenna and the target position.

Beam pattern. The pattern describing the energy density of a radar antenna as a function of angle.

Beamwidth. The 3dB angular width of the main lobe of an **antenna pattern**.

Boresight. The direction of maximum energy density in a radar antenna.

Chirp pulse. A linearly frequency modulated (FM) continuous wave (CW) signal.

Chirp rate. The rate of frequency modulation of the **chirp pulse**.

Coherent carrier. The sinusoidal signal component (referenced to the coherent local oscillator of the radar system) of the transmitted radar pulse.

Cross-track direction. Another name for the **range direction** in a SAR geometry. The range direction being defined as having the same direction as a line connecting the spatial position of the radar antenna with the spatial location of the **doppler centroid position** of a particular point target response.

Cross-track velocity. The vector component of relative target velocity as resolved in the **range or cross track direction.**

Depth of focus. The change in slant range distance that can be tolerated before the azimuth reference function must be updated for azimuth correlation purposes.

Doppler bandwidth. The total frequency spread (positive and negative) contained within the **azimuth waveform** generated by a point target over the extent of the **azimuth processing window**.

Doppler centroid. The name given to the constant Doppler frequency term present in the equation for the azimuth waveform of a point target.

Doppler centroid position. Defined to be the position of a point target as calculated by means of the target positioning algorithm (described in this thesis). The azimuth time origin (t=0) is chosen to be coincident with this target position.

Doppler frequency. The frequency term associated with a moving target.

Doppler rate. The name given to the linearly increasing frequency term, present in the azimuth waveform.

Doppler waveform. Another name for the **azimuth waveform**.

Envelope function. The envelope of the transmitted and/or received radar pulse.

Ephemeris. The position, velocity, and acceleration information associated with a satellite at a particular time.

Footprint. Another name for the **target area.**

Inertial reference frame. A reference frame that is defined to be stationary with respect to a rotating earth. It has as its origin the earth geocentre with the Z-axis along the rotational axis of the earth (positive north). The X-axis is defined to be in the direction of the vernal equinox. The Y-axis is orthogonal to the right hand system as defined by the X and Z axes directions.

In-phase signal. The radar receive waveform after In-phase demodulation.

Phase offset. A phase offset term present in the transmitted radar pulse as a result of the presence of a modulating **coherent carrier**.

Phase delay. The phase term present in the received radar waveform. This term is caused by the propagation delay between transmit and receive.

Pixel. A single sample of magnitude terrain reflectivity in the final correlated SAR image array.

Point target. An infinitesimally small point as seen by a radar antenna.

Pulse repetition frequency. The rate at which the radar system transmits radar waveforms. This is simply the inverse of the **pulse repetition interval.**

Pulse repetition interval. The time interval between separate radar transmit pulses.

Pulse sampling interval. The finite time window over which the radar **receive waveform** is sampled.

Quadrature detection. The detection of both the **In-phase** and **Quadrature** components of a received radar signal.

Quadrature signal. The radar receive waveform after Quadrature demodulation.

Radial (or range) distance. The radial or range distance is defined to be the one way distance as measured from the target to the antenna. Two way radial distance is defined to be the distance from the antenna to the target and back to the antenna.

Range array. Any one dimensional array making up a column in the **SAR matrix**.

Range bin. A range sample in the **SAR matrix**.

Range curvature. Defined as the component of target motion not covered by the **range walk** component.

Range data. The sampled data contained within a particular **range array**.

Range direction. Defined as having the same direction as a line connecting the spatial position of the radar antenna with the doppler centroid position of the point target.

Range migration curve. The name given to the curve describing the radial movement of the peak of the range correlated envelope through the **SAR matrix** as a function of **azimuth time**.

Range reference function. A function that is generated for range correlation purposes.

Range time. This is a time reference specific to each separately transmitted radar pulse. The range time of the radar system differs from **absolute time** in that the range time origin is reset to zero every time a new radar pulse is transmitted by the radar.

Range walk. Defined as the difference in one way **radial distance** (range) to a point target at the start of the **azimuth processing window** relative to the end of the window.

Range waveform. A waveform consisting of the **In-phase** and **Quadrature** signals, combined as follows: $I() + j.Q()$.

Raw data. The sampled radar data as contained in the SAR matrix before processing.

Receive waveform/pulse. A single radar pulse as received on the input of the radar receiver. (In other words as received by the radar antenna)

Resolution. The 3dB width of the main lobe of a correlated radar signal.

SAR matrix. A two dimensional matrix of discrete radar data. The columns of this matrix make up the **range arrays**. The rows of this matrix make up the **azimuth arrays**.

Signal to noise ratio. The ratio of maximum target energy to noise energy in a radar detector.

Target. The name given to the object or objects imaged by the radar.

Target (illumination) area. The surface of the earth illuminated within the 3dB limits of the antenna **beam pattern.**

Target illumination period. The length of time over which a target is illuminated by a single radar pulse.

Target observation period. The length of time for which a point target is located within the 3dB limits of the antenna **beam pattern**.

Time-bandwidth product. The time duration of a signal multiplied by the frequency **bandwidth** occupied by that signal.

Transmit waveform/pulse. A single radar pulse as transmitted by the radar transmitter.

Zero doppler position. The direction along which a target has zero relative radial velocity towards a SAR antenna. Since there is no radial velocity, no **doppler frequency** is generated.

VARIABLE DEFINITIONS

Variables as used in this thesis are defined. The variables are arranged in English and then Greek alphabetical order.

NOTE: All standard terminology appearing in the list below, as defined in the Glossary, is bolded for cross referencing purposes.

A	A scaling factor included in the equation of the received radar waveform to model the effects of signal propagation loss, antenna beam pattern, etc.
B	A scaling factor associated with the **beam pattern** (flux density pattern) of a radar antenna.
c	The speed of light.
dt	The sampling period of the radar receiver.
d	The distance between the **zero Doppler position** and **Doppler centroid** of a point target.
D	The time delay between transmitting and receiving a single radar pulse.
f_o	Radar transmit frequency.
$f_a()$	A function describing the **azimuth waveform.** The azimuth waveform comprises the complex set of discrete phase samples present in the **range waveform.**
$F_a()$	The Fourier transform of the **azimuth waveform.**

f_c The **Doppler centroid**. The name given to the constant doppler frequency term, present in the **azimuth waveform**.

f_d The **Doppler frequency** associated with a moving target.

f_{if} The video offset frequency. (The offset frequency at which the received radar signal is sampled)

f_r The **Doppler rate**. The name given to the linearly increasing frequency term, present in the **azimuth waveform**.

$f_r()$ A function describing the **range waveform**. The range waveform consists of the **In-phase and Quadrature signals** combined as follows: I() + j.Q().

$g()$ The function describing a single transmitted radar pulse or waveform.

$h()$ The received radar pulse or waveform.

h_t The average terrain height over the **target area**.

$I()$ The **In-phase signal**. This function describing the radar receive waveform after In-phase demodulation.

L_a The synthetic aperture length. This is equal to the spatial length associated with an **azimuth reference function**.

M The number of azimuth samples contained in a single **azimuth subarray**.

n A discrete integer variable associated with a particular radar pulse.

$p()$ The function describing the **envelope** of a single transmitted radar pulse.

P The target position vector $P = [P_1, P_2, P_3]$ at time t=0.

PRF	The pulse repetition frequency.
Q()	The **Quadrature signal**. This function describing the radar receive waveform after Quadrature demodulation.
r()	The relative radial distance between the radar receiver and the imaged target.
r_e	The geoidal sea level radius at a particular point on the earth's surface.
r_o	This is defined as the relative radial distance from the antenna to the **zero doppler position** of a point target.
r_s	The slant range distance. This can be defined as the radial distance from the radar antenna to the **Doppler centroid position** of a point target.
RW	Range walk.
S	The satellite position vector $S = [S_1, S_2, S_3]$ at time t=0.
t	The **absolute time** reference of the radar system.
t'	The **range time** of the radar system. The range time of the radar system differs from **absolute time** in that the range time origin is reset to zero every time a new radar pulse is transmitted by the radar.
t_o	The offset (expressed in time) of the correlated **range waveform** caused by the doppler modulation of the radar receive pulse over the **target illumination period.**
T	The time interval between separate radar transmit pulses. In the radar literature this variable is usually defined as the **pulse repetition interval** or PRI.

T_a The length of time represented by an **azimuth reference function.**

T_s The tangential vector component of satellite motion. $T_s = [T_{s1}, T_{s2}, T_{s3}]$.

$v()$ The relative instantaneous velocity between antenna and target. This is simply defined as the derivative of the relative radial distance.

V The relative velocity of a target as measured with respect to the antenna.

V_a The relative **along-track velocity** of a target.

V_c The relative **cross-track velocity** of a target.

V_p The target velocity vector $V_p = [V_{p1}, V_{p2}, V_{p3}]$ at time t=0.

V_s The satellite velocity vector $V_s = [V_{s1}, V_{s2}, V_{s3}]$ at time t=0.

$y_a()$ The correlated **azimuth waveform.**

$y_o()$ The point target response after range and azimuth correlation.

$y_r()$ The correlated *range waveform.*

α The **aspect angle.** This is defined as the angle between the position of **zero doppler** and the target position, relative to the radar antenna.

β_a The **bandwidth** (defined as positive frequency spread) of the absolute value of the correlated **azimuth waveform.**

β'_a The total frequency spread contained in the **azimuth waveform**. Since the azimuth waveform is purely complex it is incorrect to attach any meaning of **bandwidth** to this variable.

β_r The **bandwidth** (defined as positive frequency spread of a real signal) of the correlated envelope of a received radar pulse.

β'_r The **bandwidth** of the received radar waveform or radar pulse.

γ The radar incident angle. This is defined as the angle between a normal to a point on the earth surface and a line connecting that point with the radar antenna.

ΔF The depth of focus.

δ_{at} The **resolution** of a target in the **azimuth dimension**, expressed as a function of time.

δ_a The **resolution** of a target in the **azimuth dimension**, expressed as a function of ground distance.

δ_{rt} The **resolution** of a target in the **range dimension**, expressed as a function of time.

δ_r The **resolution** of a target in the **range dimension**, expressed as a function of ground distance.

θ The **phase delay** term present in the received radar waveform. This term is due to the propagation delay between transmit and receive.

λ_o Radar transmit wavelength.

σ_a The spatial azimuth distance separating two **azimuth bins**.

σ_r The radial distance separating two **range bins.**

τ Width of a single radar transmit pulse expressed as a function of time.

ϕ A **phase offset** term present in the transmitted radar pulse as a result of the presence of a **coherent carrier** .

ψ The **beam angle.** This is defined as the angle between the **boresight** of the antenna and the target position.

ω_e A vector describing the angular velocity of the earth.

CHAPTER 1

INTRODUCTION

A Brief History of Synthetic Aperture Radar:

The beginning of Synthetic Aperture Radar (SAR) can be traced back to the early 1950's and a man by the name of Carl Wiley of the Goodyear Aircraft Corporation. He proposed that a frequency analysis of reflected radar signals from a moving target would produce better azimuth resolution than could be obtained from the azimuth beamwidth of the radar antenna[1]. In 1953 Dr Sherwin of the University of Illinois and Dr Cutrona of the University of Michigan suggested that "... an extremely long radar antenna could be synthesised by using the forward motion of an aircraft to carry the radar antenna to positions which could be treated as though they were the individual antenna elements of a linear antenna array."[2] Their proposals were finally put to the test in the form of "Project Michigan". The project was centred at the Institute of Science and Technology at the University of Michigan. The project was a success and in 1960 the U.S. Army unveiled the first operational airborne SAR.

The next important development was the successful flight of the Seasat spaceborne Synthetic Aperture Radar in 1978. This experiment proved the feasibility of mapping the earth from space. Resolution of 25 meters was obtained in the ground range and azimuth directions[3]. Since then there have been two further spaceborne radar missions. The first was the "Shuttle Imaging Radar A" (SIR-A) flown on board the shuttle Columbia in 1981 and the second was SIR-B flown on board the shuttle Challenger in 1984.

Further missions are planned namely: SIR-C in 1995, the Canadian satellite "RADARSAT", and the European sponsored "ERS-1". The latter two will be free flying satellites that will enable global coverage of the earth's surface. These SAR satellites will be used primarily as remote sensing tools. Radar images of the earth will be recorded day, night and through cloud cover.

Applications of SAR as a remote sensing tool are numerous. ERS-1 and RADARSAT will be used for ship detection and location, iceberg detection, sea state monitoring, geological mapping, agricultural mapping and also surveying applications[4 5].

The Objectives of the SAR Program at the University of Cape Town:

When the SAR project was started at the University of Cape Town (UCT), under the supervision of Professor M.R. Inggs, there was no expertise available in South Africa for the decoding of Synthetic Aperture Radar data. Since this method of remote sensing has many possible applications for the Southern African region it was decided that an attempt should be made to create a facility at UCT for SAR research. The long term aim of this project is to decode and interpret SAR data taken over this region by the various proposed SAR satellites.

The Objectives of this Thesis:

This thesis comprises the first phase of the above mentioned project and is concerned with the software design of a general purpose digital processor for the decoding of spaceborne SAR data. The thesis is divided up into two main sections, namely Chapter 2 and Chapter 3. Chapter 2 is concerned with the development of a unified theoretical basis to explain the mechanism of operation of SAR. Chapter 3 is concerned with the design of a spaceborne SAR processor. The algorithms developed as part of this design have been implemented by Welsh on raw radar data as recorded by the SIR-B mission over Cradock, South Africa. Image results are included in this thesis.

Chapter 2:

Chapter 2 is concerned with developing a unified theoretical approach to Synthetic Aperture Radar. This is done in the context of 25 years of active research in this field.

Most of the literature on Synthetic Aperture Radar treats SAR as a problem specific to radar imaging. This has resulted in the processing aspect being obscured by terms and definitions, used only by the radar community. It will be proved in this chapter that SAR can be treated in its entirety from a signal processing perspective. Most of the seemingly specialised theory and techniques used to discuss SAR processing are relatively standard processing techniques as used by the signal processing community.

This chapter serves to lay down a theoretical framework for the design of a SAR processor which is the subject of Chapter 3.

Chapter 3:

This chapter is concerned with the software design of a SAR processor for the decoding of Spaceborne Synthetic Aperture Radar data. Similar such processors have been documented in the SAR literature and include ones operating at Jet Propulsion Laboratories - California, Farnborough - England, and the German Aerospace Research Establishment.

The main requirement of any SAR processor is to accept raw Synthetic Aperture Radar data as input, then to digitally decode this data and finally to produce a SAR image of the earth's surface. The processor should also be designed to accommodate data from a variety of spaceborne SAR systems, each with its own orbital geometry and system parameters.

The purpose of this chapter is to develop algorithms for the decoding of SAR data that meet the following requirements:

a) The algorithms must be flexible enough to cope with a variety of SAR geometries and system specifications.

b) The algorithms must be robust.

c) The algorithms must be efficient in terms of processing time.

d) The amount of human interaction involved in processing an image must be limited as far as possible.

Synthetic Aperture Radar data will be received from a variety of spaceborne SAR missions. Each of these systems will have different orbital and system parameters. Therefore, a software design is required that is flexible enough to cope with these changes. This has been achieved by formulating all algorithms and equations in terms of a closed set of predefined input variables. Once the relevant SAR system and orbital information is known the processor can be customised by simply changing the numerical values of these input variables.

The algorithms must be robust. It cannot be expected that the numerical values of the input variables passes to the data processor are exact. Practical constraints result in a certain amount of uncertainty in measured orbital and system values. For this reason the algorithms must be tested for their sensitivity to such variations. Error bounds are obtained on all the input parameters and sensitivity analyses are performed on all stages of the software design. These analyses are performed by testing the algorithms on simulated radar data with artificially introduced orbital and/or system error. In all cases algorithms are chosen that display the necessary insensitivity to numerical error.

Synthetic Aperture Radar processing is computationally intensive and involves thousands of Fast Fourier Transforms on data sets of the same magnitude. For this reason any algorithms must be efficient in terms of processing time.

The SIR-B system and orbital information is used as an example throughout this chapter to illustrate the operation of the decode algorithms in terms of numerical values. This has been done to clarify the operation of these algorithms and to obtain a "feel" for the quantities involved in spaceborne SAR processing. The algorithms developed as part of this design have been implemented by Welsh in a high level software language and tested on raw radar data as recorded by the SIR-B mission. Image results obtained by running prototypes of this software are included in this thesis.

CHAPTER 2

THE DEVELOPMENT OF SYNTHETIC APERTURE RADAR FROM A SIGNAL PROCESSING PERSPECTIVE.

2.1 INTRODUCTION

Most of the literature on synthetic aperture radar (SAR) treats SAR processing as a problem specific to radar imaging. This has resulted in the processing aspect being obscured by terms and definitions, used only by the radar community. (A problem that is also highlighted in an article by Munson[6]) It will be proved in this chapter that SAR can be treated in its entirety from a signal processing perspective. Most of the seemingly specialised theory and techniques used to discuss SAR processing are relatively standard processing techniques as used by the signal processing community.

The author feels that there are a number of advantages to be gained from treating SAR as a signal processing problem, namely:

a) Once SAR has been reduced to a straight signal processing problem, standard Fourier techniques of waveform analysis can be applied directly to the production of SAR images without the need for a redevelopment of basic theory in the radar literature. More modern signal processing techniques can be applied directly to SAR data decoding without the need for a signal processing specialist to get involved in a study of radar.

b) If SAR can be treated in terms of very basic signal processing theory, the whole complexity surrounding this imaging system is reduced and a deeper insight into the operation of SAR is obtained.

The signal processing theory and mathematical derivations contained in this chapter, are closely referred to in Chapter 3.

2.2 A BASIC TRANSMIT/RECEIVE SYSTEM FOR A COHERENT RADAR.

In its most basic form, a Synthetic Aperture Radar system closely resembles that of a coherent pulsed radar (or Pulse Doppler Radar[7]). A simplified block diagram of such a system is shown in Figure 2-1.

A pulse modulator unit modulates a coherent sinusoid of frequency f_o with some "**envelope**" function of width τ. The equation for the envelope can be written as

$$\begin{aligned} p(t,\tau) &= p(t) && -\frac{\tau}{2} < t \le \frac{\tau}{2} \\ &= 0 && \textit{elsewhere} \end{aligned} \qquad (2\text{-}1)$$

For a simple Pulse Doppler Radar the envelope is usually of the following form

$$\begin{aligned} p(t,\tau) &= 1 && -\frac{\tau}{2} < t \le \frac{\tau}{2} \\ &= 0 && \textit{elsewhere} \end{aligned}$$

In Synthetic Aperture Radar systems the envelope is more commonly a linearly frequency modulated signal

$$p(t,\tau) = e^{j.\pi a(t')^2} \qquad -\frac{\tau}{2} < t \leq \frac{\tau}{2} \qquad (2\text{-}2)$$
$$= 0 \qquad \textit{elsewhere}$$

This is commonly known in the radar literature as a "**chirp pulse**". The factor a is called the "**chirp rate**" and refers to the rate of frequency modulation used.

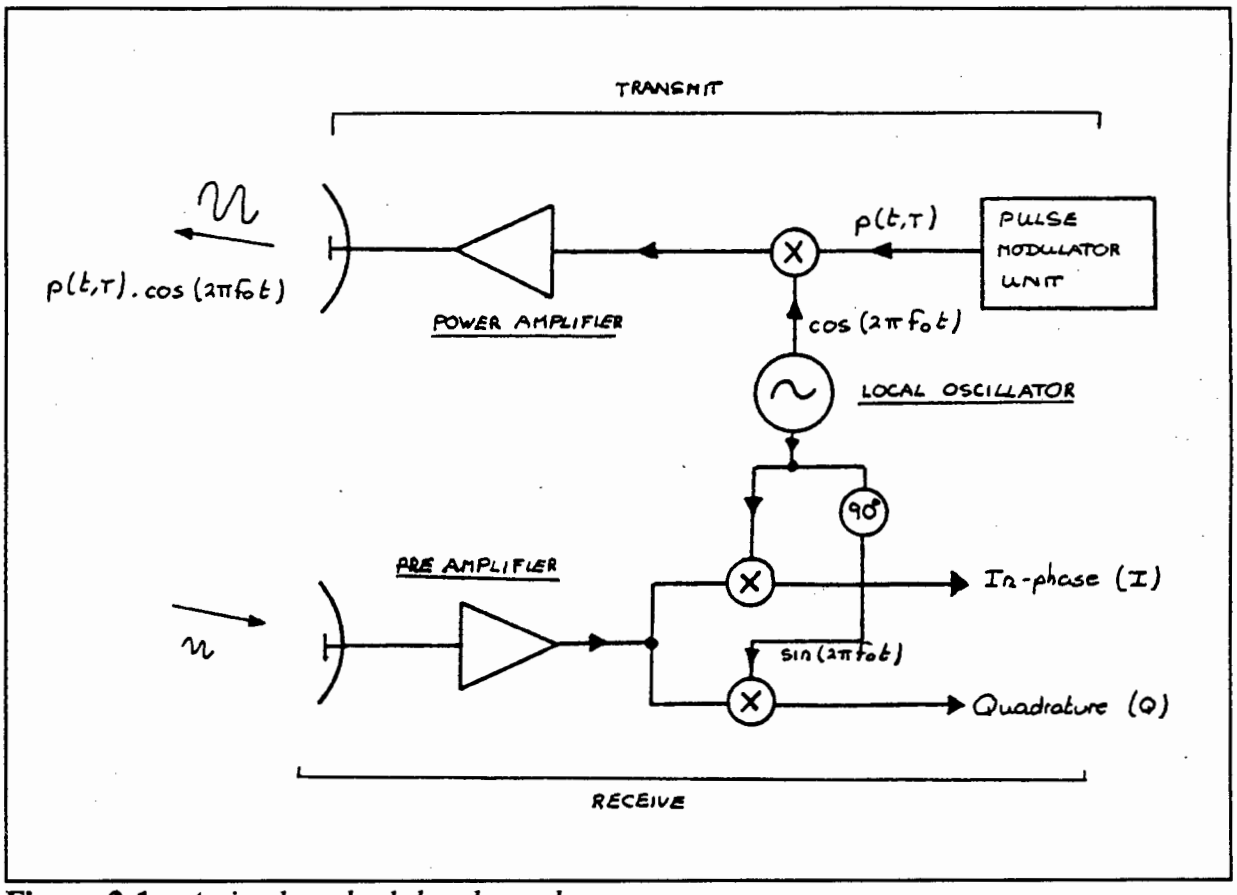

Figure 2-1: *A simple pulsed doppler radar system.*

After pulse modulation, the composite waveform

$$p(t,\tau) \cdot \cos(2\pi f_o t)$$

is amplified and transmitted.

Upon reflection from a target, an attenuated and doppler shifted replica of this pulse is received back at the radar. A demodulation is performed on the return signal to produce an **"In phase"** (I) and **"Quadrature"** (Q) waveform[8].

In most radar systems only one antenna is used and the functions of transmit and receive are multiplexed in time[9] as shown in Figure 2-2.

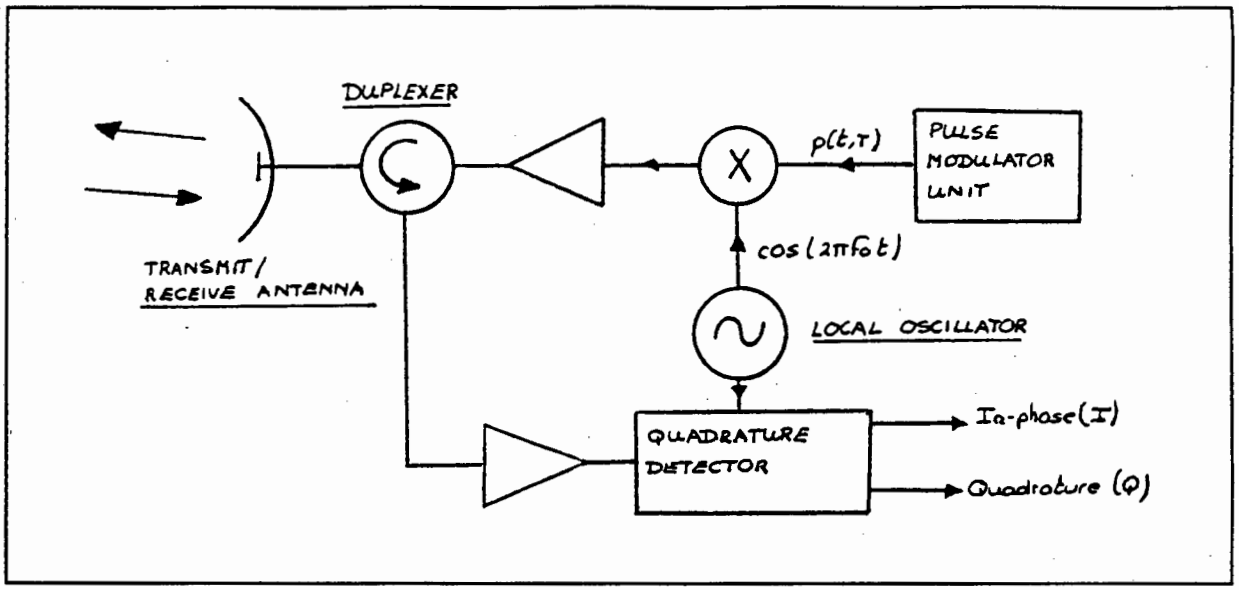

Figure 2-2: *A simple pulsed doppler radar system with single transmit/receive antenna.*

The buffering between the transmit and receive circuitry is achieved by making use of a duplexer[10].

Although modern Synthetic Aperture Radar systems are more involved than the ones shown above (see for example Hovannesian[11]), the actual physical manipulation of the transmit and receive waveform can always be simplified down to the operations shown in Figure 2-2. Therefore, this figure can be used to mathematically characterise the analogue operation of a typical SAR system.

2.3 A MODEL OF THE TARGET MOTION.

A "**target**" can be defined as being any specific point located within the antenna beam pattern of a radar system. A coherent radar system, like the one shown in Figure 2-2, can measure radial "**target**" distance by illuminating the target with a transmitted pulse and then recording the target reflection.

The "**radial distance**" to the target is measured at discrete intervals of time by illuminating it with a train of separately transmitted radar pulses or waveforms[†]. If the assumption is made that during separate pulse illuminations the target is considered stationary, the radial position of that target (as seen by the radar) can be discretised as

$$r(t) = r(nT)$$

where n is defined as a discrete integer variable associated with a particular radar pulse and T is the time interval separating each of these pulses. (T is often called the "**pulse repetition interval**" of a radar system.)

Over the period of time during which a target can be detected a set of such distance measurements are made. This set is represented as

$$r(t) = \sum_{n=-(\frac{N}{2}-1)}^{\frac{N}{2}} r(nT)$$

where N is defined as the total number of elements in that set.

[†]The radial distance is defined to be the one way distance as measured from the target to the antenna.

2.4 A MODEL OF THE TRANSMIT WAVEFORM.

A coherent radar system transmits a waveform that consists of a coherent carrier modulated by some envelope function. Upon transmission of this signal, the coherent carrier component is an exact copy of the coherent oscillator waveform at that time.

For purposes of mathematical convenience it is useful to maintain a local time reference whose origin is reset to zero upon transmission of each new radar pulse. This time reference will be termed "**range time**". To differentiate between range time and the absolute time of the system, a superscript will be attached to the range time variable.

In terms of this newly defined range time a transmitted pulse is written as

$$g(t') = p(t',\tau).\cos(2\pi f_o t' + \phi)$$

Writing the transmitted pulse in terms of range time rather than absolute time, has necessitated the introduction of a arbitrary "**phase offset**", ϕ, into the coherent carrier term. Although the radar system's coherent oscillator must be synchronised to the absolute time of the system (condition of coherency) it does not necessarily occupy the same phase offset with respect to the successive range time origins. However, the envelope of successive radar pulses is identical in each case.

A set of transmitted pulses can now be written as

$$g_n(t') = \sum_{n=-(\frac{N}{2}-1)}^{\frac{N}{2}} \left[p(t',\tau) \cdot \cos(2\pi f_o t' + \phi_n) \right]$$

where the phase offset term is subscripted to reflect the possible change in its value on a pulse to pulse basis.

2.5 A MODEL OF THE RECEIVE WAVEFORM.

The transmitted radar signal propagates through space, hits the target at a discrete position and is reflected back towards the receive antenna. With each successively received radar pulse is associated a new delay time

$$D_n = \frac{2 \cdot r(nT)}{c} \tag{2-3}$$

where c is defined to be the speed of light.

A single received pulse is written as

$$\begin{aligned} h_n(t') &= A_n \cdot \left[p(t'-D_n, \tau) \cdot \cos(2\pi f_o (t'-D_n) + \phi_n) \right] \\ &= A_n \cdot \left[p(t'-D_n, \tau) \cdot \cos(2\pi f_o t' - 2\pi f_o D_n + \phi_n) \right] \end{aligned}$$

This waveform is simply a delayed and scaled copy of the coherent oscillator waveform, modulated by a delayed envelope function. The constant A_n in the above equation represents a scaling factor, which is included to model the effects of radar signal propagation loss[12], antenna beam shaping[13] [14], target reflection characteristics[15], receiver amplification and receiver losses on the amplitude level of the received waveform. The value of this scaling factor is usually a function of time and position (hence the indexing on the variable), although initially it will be assumed to have a constant value of one.

Defining the delay term present in the coherent carrier as a "**phase delay**" equal to

$$\theta_n = 2\pi f_o D_n \tag{2-4}$$

the received radar pulse can be rewritten as

$$h(t') = p(t'-D_n, \tau) \cdot \cos(2\pi f_o t' - \theta_n + \phi_n) \tag{2-5}$$

A set of such receive pulses is then written as

$$h(t') = \sum_{N=-(\frac{N}{2}-1)}^{\frac{N}{2}} \left[p(t'-D_n, \tau) \cdot \cos(2\pi f_o t' - \theta_n + \phi_n) \right]$$

Once more, discrete indexing is used to denote variables that change on a pulse to pulse basis.

2.6 QUADRATURE DETECTION OF THE RECEIVED RADAR WAVEFORM.

2.6.1 ANALOGUE DEMODULATION.

As shown in Figure 2-2 the received waveform is demodulated to baseband via In-phase and Quadrature demodulation. This process is more commonly termed "**quadrature detection**" in the radar literature and is treated extensively by Wehner. In his words: "Quadrature detection is used in various types of coherent radar systems to recover echo signal phase relative to the transmitted carrier."[16]

The process of quadrature detection can be described as follows: The received radar waveform is split into two channels. The one signal is multiplied (using analogue techniques) by an exact replica of the local oscillator waveform and the other signal is multiplied by a replica of the local oscillator waveform delayed by 90°. The resulting waveforms are Low Pass Filtered to produce an In phase and Quadrature signal respectively.

It is proved in Appendix A1 that quadrature detection of a received radar pulse, of the form given in Equation 2-5, produces an In-phase signal

$$I(t') = \frac{1}{2} . p(t'-D_n,\tau) . \cos(\theta_n)$$

and a Quadrature signal

$$Q(t') = \frac{1}{2} . p(t'-D_n,\tau) . \sin(\theta_n)$$

The original envelope function is unaltered; but the coherent carrier term has been reduced to a constant scaling factor which is dependent on the phase delay term present in the original radar receive waveform.

Meanwhile, the phase offset term that was present in the original receive waveform has been removed by the process of demodulation. This term is cancelled by using an exact copy of the local oscillator waveform in the demodulation process (see Appendix A1).

In summary, two **real** signals are obtained whose values are directly related to the two-way pathlength between the target and the antenna.

2.6.2 DIGITAL DEMODULATION.

In some of the more modern coherent radar systems, the range waveform is not demodulated to baseband. Rather, this signal is sampled and digital techniques are used to produce a result that is equivalent to analogue demodulation†.

Another characteristic of these modern systems is that the timing of the pulse modulator unit is synchronised to integral periods of the coherent oscillator. For this reason the coherent

†Analogue demodulation produces a certain amount of phase instability between the resultant In Phase and Quadrature signals (The desired phase shift being 90°). However, digital demodulation avoids this problem.

carrier always occupies a zero phase offset with respect to the range origin. The transmit waveform can, therefore, be written in this case as

$$g(t') = p(t',\tau) \cdot \cos(2\pi f_o t') \tag{2-6}$$

without the presence of any phase delay term.

The receive waveform is then given as

$$h(t') = p(t'-D_n,\tau) \cdot \cos(2\pi f_o t' - \theta_n) \tag{2-7}$$

A digital technique for achieving a result equivalent to quadrature detection is now outlined:

In Appendix A2 it is proved that the Fourier transform of the received signal is equal to

$$\mathcal{F}[h(t')] = \frac{\cos(\theta_n)}{2} \cdot \{P(2\pi f - 2\pi f_o) + P(2\pi f + 2\pi f_o)\}$$

$$+ \frac{\sin(\theta_n)}{2.j} \cdot \{P(2\pi f - 2\pi f_o) - P(2\pi f + 2\pi f_o)\}$$

where $P(2\pi f)$ is defined to be the Fourier transform of the envelope function $p(t',\tau)$.

Removing the negative frequency component of this spectrum and performing a digital frequency shift to baseband (a simple translation of sampled array values) gives

$$\frac{\cos(\theta_n)}{2} \cdot P(2\pi f) + \frac{\sin(\theta_n)}{2.j} \cdot P(2\pi f)$$

The inverse Fourier transform of this signal produces a demodulated and complex "time" signal

$$p(t'-D_n).\cos(-\theta_n) + p(t'-D_n).\sin(-\theta_n)$$

or

$$p(t'-D_n,\tau) \cdot e^{-j.\theta_n}$$

This result is equivalent to that achieved by analogue demodulation except for the sign change on the phase delay term and the combination of the In-phase and Quadrature terms into a complex pair. This equivalence is also proved independently by Fitch[17]. The exact digital methods for achieving the mathematical manipulations, shown above, are given in Section 3.3.2

A set of quadrature detected radar waveforms are written as

$$f_r(t') = \sum_{n=-(\frac{N}{2}-1)}^{\frac{N}{2}} \left[p(t'-D_n, \tau) \cdot e^{-j.\theta_n} \right]$$

The same result as the one above was obtained by Wu[18] for the special case of a rectangular envelope. However, he assumes analogue demodulation in his derivation.

In summary, for a target assumed to be stationary during illumination, the received waveform upon demodulation consists of two separate independent terms, namely:

a) A delayed replica of the envelope of the transmit signal.

b) A phasor whose phase value is dependent on the two way pathlength between the target and the radar.

2.7 SYNTHETIC APERTURE RADAR PROCESSING.

Figure 2-3 shows the basic geometry involved in Synthetic Aperture Radar imaging. (see also Kovaly[19]) An antenna, mounted on a moving platform such as an aircraft or satellite, is responsible for transmitting a set of radar pulses of the form given in Equation 2-6. The time, *T*, between transmission of these pulses is termed the pulse repetition interval or PRI.

The transmitted radar pulses illuminate a "**target area**" on the surface of the earth. **If only one "point target" is considered**, the time delay between transmission and reception of the radar pulse is proportional to the relative radial distance, r_n, between the target and the antenna, as a function of discrete time, t.

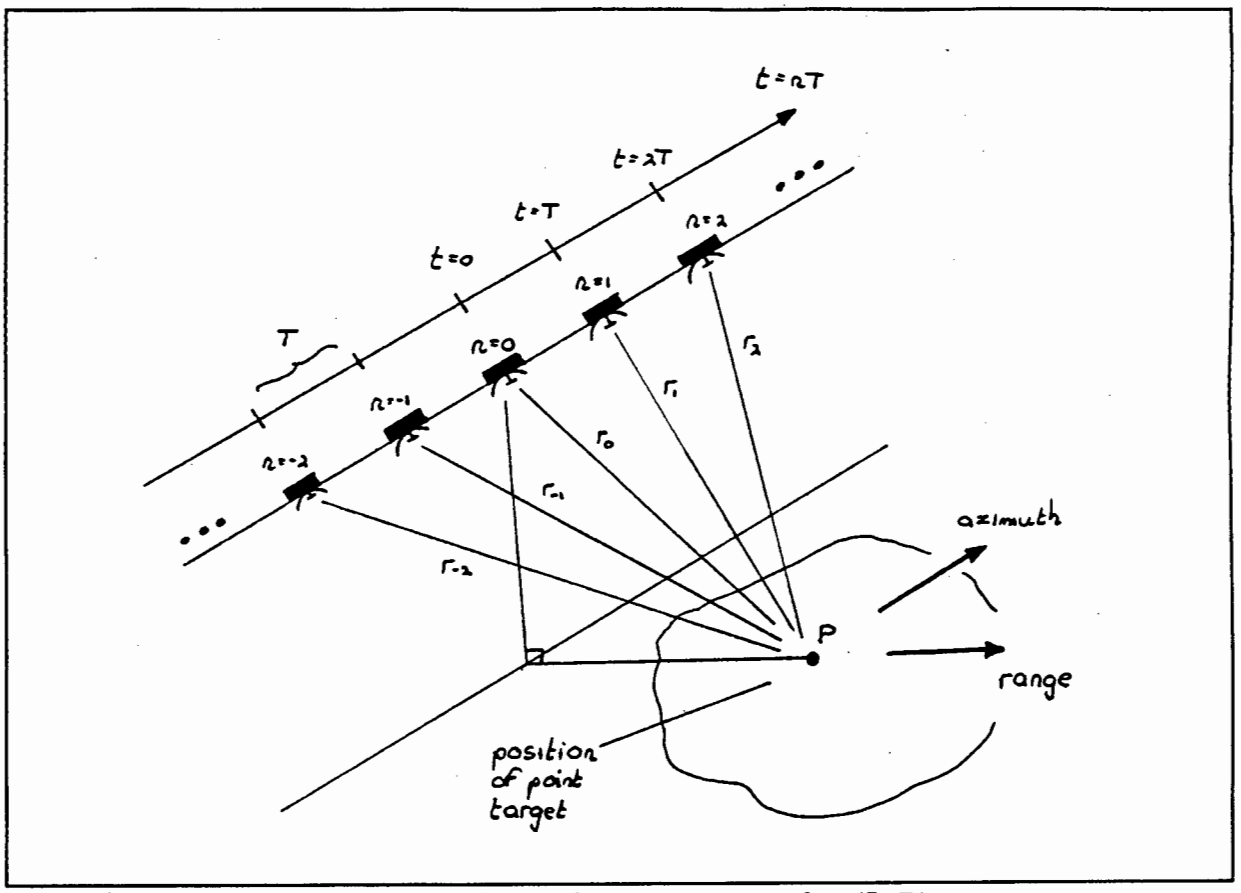

Figure 2-3: *The basic geometry of a synthetic aperture radar (SAR)*

Each separately received radar waveform is quadrature detected to produce a point target return

$$f_r(t') = p(t'-D_n,\tau) \cdot e^{-j.\theta_n} \qquad \textbf{(2-8)}$$

which will be know in further discussion as the "**range waveform**".

A Synthetic Aperture radar image of a point target can be created by manipulating a set of such range waveforms

$$f_r(t') = \sum_{n=-(\frac{N}{2}-1)}^{\frac{N}{2}} \left[p(t'-D_n, \tau) \cdot e^{-j.\theta_n} \right]$$

$$= p(t'-D_n, \tau) \cdot \sum_{n=-(\frac{N}{2}-1)}^{\frac{N}{2}} \left[e^{-j.\theta_n} \right]$$

The "**range direction**" shown in Figure 2-3 is defined, loosely, as having the same direction as a line connecting the radar antenna with a particular point target P located on the surface of the earth. The "**azimuth direction**" is defined, loosely, as the direction of motion of the radar platform. (Both these terms are defined more accurately in Section 2.17.2)

Resolution of a point target in range is obtained purely by manipulation of the envelope function $p(t'-D_n, \tau)$ and the process is termed "**range processing**". Resolution of a point target in the azimuth direction is termed "**azimuth processing**". Azimuth resolution is achieved by manipulating the set of complex phase samples

$$f_a(t) = f_a(nT) = \sum_{n=-(\frac{N}{2}-1)}^{\frac{N}{2}} \left[e^{-j.\theta_n} \right] \qquad \textbf{(2-9)}$$

This set will be called the discrete "**azimuth waveform**".

2.8 RANGE PROCESSING IN SYNTHETIC APERTURE RADAR.

Range processing involves a) detecting the received range waveform in the presence of noise and b) resolving range returns reflected from closely spaced targets in the range dimension.

A processing technique that acts as a suitable compromise between the above two functions is matched filtering. A matched filter optimises the maximum signal to noise ratio of a received signal[20] [21], while at the same time providing good resolution extraction capabilities[22]. The process of matched filtering has been shown to be equivalent to a correlation of the received waveform with an exact replica of that waveform (usually termed the "**range reference function**")[23].

Matched filtering (or correlation) is used extensively in SAR processing. Resolution in the range direction is achieved by performing a correlation on the range waveform (Equation 2-8) after demodulation of the received radar signal. As Rihaczek[24] points out, this correlation is limited to the envelope $p(t,\tau)$. The complex phase term resulting from the presence of the coherent carrier in the received radar waveform is not included in this process.

The achievable resolution in time between two closely spaced targets is loosely defined in the Synthetic Aperture Radar literature as being equal to the inverse of the bandwidth occupied by transmitted (and therefore received) radar signal[25] [26].

This definition is not strictly correct.

In the Signal Processing literature, bandwidth is defined for a **real** signal as "... the interval of **positive** frequencies over which the magnitude (of the frequency spectrum of a signal) remains within a given numerical factor...a popular numerical factor is -3dB..."[27]. On the other hand, time resolution is defined as the time interval over which the amplitude of a correlated signal remains within 70 percent (-3dB) of the maximum value. By inspection of various standard waveforms (and the 3dB bandwidth they occupy) it is possible to give the time resolution of a correlated waveform as

$$\delta_{rr} = \frac{1}{2\beta_r}$$

where β_r is defined as being the 3dB bandwidth of that correlated signal[28].

This is in contradiction to the commonly quoted formula for the range resolution of a Synthetic Aperture Radar system. The reason for this discrepancy lies in the fact that SAR authors tend to use the 3dB bandwidth of the received radar signal, as their bandwidth figure.

As Figure 2-4 shows, this bandwidth β'_r is equal to twice the bandwidth of the envelope $p(t,\tau)$ alone.

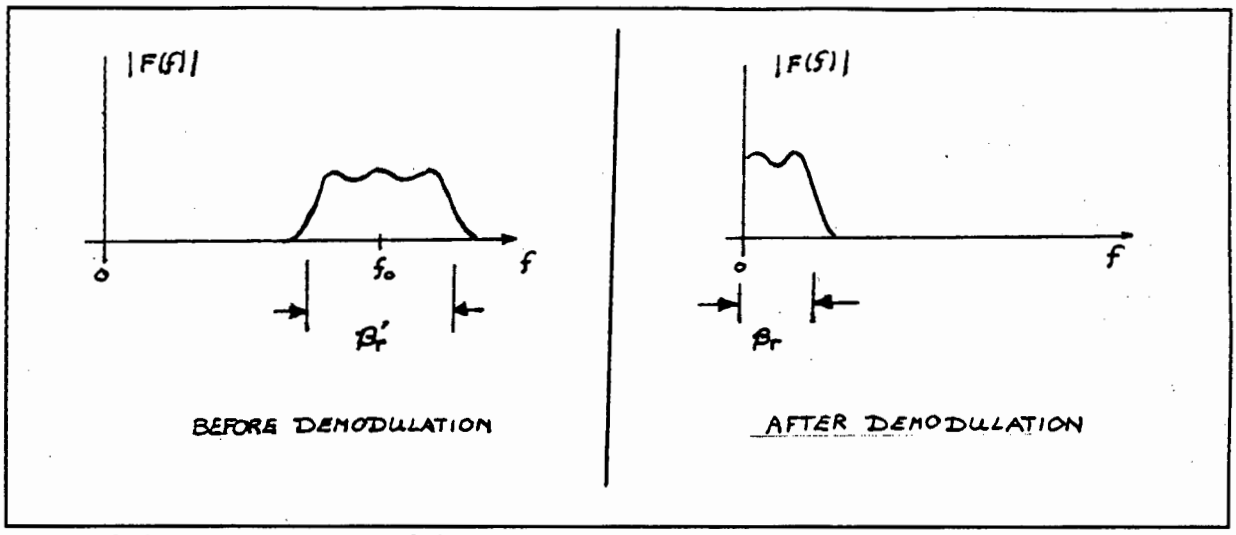

Figure 2-4: *A comparison of the real 3dB bandwidth of a radar signal before and after demodulation to baseband.*

Since matched filtering takes place only on the envelope of the return radar signal, the above definition of bandwidth is obviously incorrect.

In conclusion then, the range resolution in time is given as

$$\delta_{rt} = \frac{1}{2\beta_r}$$

with the bandwidth β_r being defined as the positive 3dB frequency spread of the (assumed real) envelope after correlation.

In Synthetic Aperture Radar applications the envelope is complex. Therefore, the bandwidth is undefined. However, it is proved in Appendix A3 that a correlation of this complex function produces a real signal with a bandwidth equal to half the "frequency spread" (positive and negative frequencies) of the original complex chirp envelope. This frequency spread is

equal in magnitude to the bandwidth β'_r of the received radar signal. For this reason the time resolution of a correlated chirp pulse can be written as

$$\delta_{rr} = \frac{1}{2\beta_r} = \frac{1}{\beta'_r} \qquad \textbf{(2-10)}$$

2.9 AZIMUTH PROCESSING IN SYNTHETIC APERTURE RADAR.

2.9.1 THE SAMPLING OF A CONTINUOUS DOPPLER WAVEFORM.

SAR azimuth processing can be developed as a special case of discrete signal processing by regarding the azimuth waveform of Equation 2-9

$$f_a(t') = e^{-j.\theta_n}$$

$$= e^{-j.\frac{2\pi f_o}{c}.[2r(nT)]}$$

to be samples of a continuous complex waveform

$$f_a(t') = e^{-j.\frac{2\pi f_o}{c}.[2r(t)]} \qquad \textbf{(2-11)}$$

Using the standard definition for the instantaneous frequency of a complex phasor[29], the frequency of this continuous waveform is calculated as

$$f = \frac{-f_o}{c}.[2v(t)] \qquad \textbf{(2-12)}$$

This equation is equivalent to the one given by Skolnik[30] for the **"Doppler frequency"** of a moving target. Therefore, the continuous azimuth waveform represents the doppler waveform of a moving target as referred to widely in the radar literature[31 32 33].

However, it has been suggested by Munson that "...the azimuth resolving method relies on the geometry of the imaging scenario rather than the Doppler effect."[34] In the Author's opinion this statement is incorrect. There is no difference between the operation of a doppler radar and a SAR†. The differences between the two systems arise in the methods used to process the discrete samples (Equation 2-9) of the azimuth or doppler waveform. (This point is discussed further in Section 2.13)

2.9.2 THE SAMPLING OF A CONTINUOUS WAVEFORM AS A SIGNAL PROCESSING PROBLEM.

The sampling process described in the above section is commonly known as ideal impulse sampling. The discrete frequency spectra generated by the process of impulse sampling are discussed in detail by Stremler[35] and De Fatta[36]. To prevent any loss in information content, caused by an effect known as **aliasing**, it is necessary to sample the continuous azimuth or doppler waveform at a rate of twice the maximum modulus†† frequency contained within that signal.

A result derived by Rihaczek[37] shows that an instantaneous frequency in the time domain maps into an equivalent position in the Fourier frequency spectrum. Therefore, it can be said that the minimum sampling rate (or minimum pulse repetition frequency) required of this azimuth waveform is

$$\begin{aligned} PRF_{min} &= 2.|f_d|_{max} \\ &= 2.\left[\frac{f_o}{c}.\,|2v(t)|_{max}\right] \end{aligned} \qquad \textbf{(2-13)}$$

---

†In fact, up to now no mathematical distinction has been made between the operation of a simple pulsed doppler radar and that of a SAR.

††If the time signal is real, the negative frequency spectrum is simply a copy of the positive spectrum. In such cases the minimum sampling rate can be written as twice the maximum positive frequency contained within that signal. For the more general case of a complex time signal this minimum sampling frequency is in fact twice the largest **modulus** frequency contained within that spectrum.

where $|f_d|_{max}$ is the maximum modulus doppler frequency contained within that waveform. This formula has been obtained elsewhere in the radar literature[38].

Many SAR authors quote a minimum sampling rate that is half the above mentioned value[39] [40]. This contradiction arises due to a difference in the definition of the maximum doppler frequency. In their case the maximum doppler frequency is quoted as a number equal to the maximum **range** of doppler frequencies covered[41]. This definition is obviously wrong if the effects of aliasing are to be prevented. This contradiction is discussed further in Section 2.17.3

2.9.3 AZIMUTH RESOLUTION

The azimuth or doppler waveform

$$f_a(t') = e^{-j.\frac{2\pi f_o}{c}.[2\,r(t)]}$$

has an instantaneous frequency

$$f_d = -\frac{f_o}{c}.[2v(t)]$$

The bandwidth of this azimuth signal is directly related to the range of frequencies f_d contained within that signal. Noting the dependence of frequency on instantaneous target velocity it can be said that the bandwidth is directly proportional to the range of velocities covered by the target during the time for which that target is observed.

If a finite bandwidth is generated, matched filtering techniques (digital matched filtering techniques) can also be used on the azimuth waveform to obtain point target resolution in the azimuth direction†

†The implicit assumption from now on, is that the azimuth sampling rate (PRF) is chosen high enough to prevent aliasing of the azimuth waveform.

For a target moving with random velocity it is possible that a large doppler frequency spread could be generated over the **"target observation period"**. Given a large enough receiver signal to noise ratio, and assuming that an accurate enough reference function has been estimated for use in the azimuth correlation process, resolution of that target can be achieved† [42] [43].

2.10 THE EFFECTS OF A MOVING TARGET ON THE INDEPENDENCE OF RANGE AND AZIMUTH PROCESSING.

If a target is stationary during pulse illumination (as has been assumed up to now), the matched filtering of the range envelope can take place independently of the complex phasor term. For any realistic target there is a certain amount of motion during each separate pulse illumination. It will now be shown that this movement is a detrimental on the range correlation process.

For the special case of an envelope function that is rectangular (as is the case in a simple pulsed doppler radar system), it can be proved[44] that the range waveform is more correctly written as

$$\begin{aligned} f_r(t') &= p(t'-D_n,\tau)\,.\,e^{2\pi f_d t' - 2\pi f_o D_n} \\ &= \left\{ p(t'-D_n,\tau).e^{-j.\frac{2\pi f_o}{c}.[2v(t).t']} \right\}.e^{-j.\theta_n} \end{aligned} \qquad \textbf{(2-14)}$$

An inspection of the above equation reveals that apart from the envelope function being multiplied by a discrete phase delay term, it is also modulated continuously over the pulse duration by a continuous function of time. This function can be recognised from Equation

†This particular problem is currently being addressed in a Doctoral study by M.W. van Zyl at the University of Cape Town.

2-11 as being that of the doppler waveform.† (This effect is also represented diagrammatically by Skolnik[45]). The continuous modulation of the envelope by the doppler waveform mirrors the radial movement of the target relative to the antenna over the short duration of time for which that target is illuminated.

For the case of a transmit envelope that is rectangular in shape, a set of demodulated pulses (of the form shown in the equation above) can be recognised as a set of "natural" rather than "impulse" samples of the continuous doppler waveform. These signal processing specific terms are discussed in detail by authors such as Stremler[46] and Tretter[47].

Skolnik[48] shows that if a correlation (where the reference function is assumed to be a replica of the **original** envelope function) is performed on this modified range waveform (Equation 2-14), a breakdown begins to occur in the matched filtering process. This breakdown can be represented by means of two dimensional plots (ambiguity diagrams), where the output of the matched filter is plotted for various values of target velocity[49].

In all but the earliest SAR systems, the range envelope is not a rectangular envelope but a frequency modulated (FM) or chirp signal. In a simple pulsed radar, the bandwidth (and therefore resolution) is inversely proportional to the time duration of that pulse. The problem is that the shorter the pulse, the smaller the total signal energy that can be transmitted. However, the bandwidth of a chirp waveform is not limited by the duration of the pulse, so pulses of large bandwidth and relatively large signal power may be transmitted[50].

Matched filtering of chirp pulses and the effects of target motion are discussed in detail by Hovanessian[51]. His analyses show that the continuous doppler modulation of the chirp envelope does not cause a substantial reduction in target resolution, but rather a shift in the observed target position††.

---

†This result is further proof of the fact that the mechanism of operation of a synthetic aperture radar is the same as that of a doppler radar.

††Or stated differently, the peak of the matched filter output for a particular point target occurs at a slightly different range time to the one that would be observed if the target had been stationary during pulse illumination.

This offset in range time is given by Hovanessian as:

$$t_o = -\frac{\tau f_d}{\beta'} \qquad (2\text{-}15)$$

τ *The time duration of single radar pulse.*

f_d *Doppler frequency at the instant of target observation.*

β' *The bandwidth of the transmitted range waveform.*

For most SAR systems this shift in the observed range position of a target is negligible in comparison to the resolution of the final image and can, therefore, be ignored†.

To summarize using the words of Rihaczek: " (In the SAR case) Target doppler... typically is so small compared with the doppler resolution capability of a single pulse that the target can be considered stationary over the pulse duration... This means that the range measurement and azimuth measurement can be treated independently of each other."[52] This conclusion is also reached by authors such as Fitch[53] and Kovaly[54]

2.11 AZIMUTH PROCESSING IN SIDELOOKING SYNTHETIC APERTURE RADAR.

Figure 2-5 shows the basic geometry of a sidelooking Synthetic Aperture Radar in two dimensional space. Point P denotes the position of a point target. The vector velocity, V, of this point target is measured relative to the antenna and is assumed to be constant with time. Point A represents that position on the target trajectory where the relative radial velocity between target and antenna is zero. By Equation 2-12 this also represents the position of zero doppler. The angle between this position and any other target position will be known as the **"aspect angle"**. The distance between this position and the antenna will be known as r_o. The antenna **"beam pattern"** is also shown.

---

†The magnitude of the range shift for the Shuttle Imaging Radar B (SIR-B) case is calculated in Appendix B8.

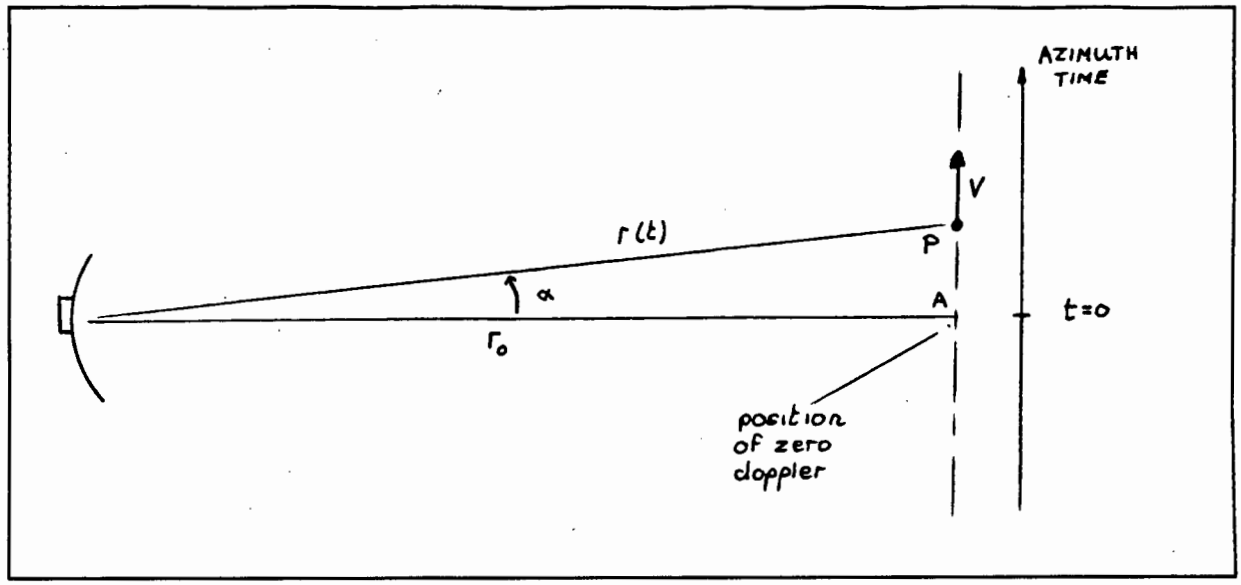

Figure 2-5: *A typical simplified geometry for the sidelooking SAR case.*

For the purposes of an initial development it will be assumed that:

a) the boresight of the antenna lies along the zero doppler position and

b) the position of zero time ($t=0$) coincides with the zero doppler position.

A more general treatment will, however, be given in Section 2.17

2.11.1 THE EQUATION FOR THE AZIMUTH WAVEFORM.

The instantaneous radial velocity component of the target motion (shown in Figure 2-5) is given by simple trigonometry as

$$v(t) = V.\sin(\alpha)$$

where α is defined as the aspect angle at that instant.

Any change in doppler frequency is dependent on a change in this aspect angle. The bandwidth of the azimuth waveform (and therefore azimuth resolution) is directly related to the range of aspect angle through which the target is observed by the antenna. This very

fundamental view of the azimuth resolving capability of sidelooking SAR is also stressed by Kovaly[55] and Brown. In fact Brown[56] gives an expression for spatial azimuth resolution that depends only on this change in aspect angle:

$$\delta_a = \frac{\lambda_o}{2\sin\left(\frac{\Delta\alpha}{2}\right)}$$

λ_o Transmit radar wavelength.

$\Delta\alpha$ Change in aspect angle (in radians) over which the target is observed.

In Appendix A4 it is shown that for the sidelooking SAR case it is possible to approximate the relative radial distance between the target and antenna as

$$r(t) = r_o + \frac{V^2 t^2}{2r_o}$$

where r_o is the distance between the antenna and the zero doppler position (point A in Figure 2-5). The approximation used is a two term binomial series expansion. For sidelooking SAR, the maximum aspect angle at which the target is observed is usually of the order of 2 or 3 degrees. Therefore, an approximation of this nature is assumed by most researchers in the SAR field to be adequate[57] [58].

Using this approximation to radial distance (and ignoring any constant terms) it is possible to rewrite the continuous azimuth waveform (as given in Equation 2-11) as

$$f_a(t) = e^{-j.\frac{-2\pi f_o}{c}\left[\frac{V^2 t^2}{r_o}\right]} \qquad \textbf{(2-16)}$$

and the instantaneous doppler frequency as

$$f_d = -\frac{f_o}{c}.\left[\frac{V^2 t}{r_o}\right] \qquad \textbf{(2-17)}$$

The azimuth waveform is now in the standard form of a complex chirp pulse as described by Rihaczek[59] and Wu[60]. By noting that for small angles the trigonometric ratio

$$\sin(\alpha) = \frac{Vt}{r_o}$$

can be approximated by

$$\alpha = \frac{Vt}{r_o} \tag{2-18}$$

the azimuth waveform can be written as a function whose instantaneous chirp frequency is given by the aspect angle, α, at that time.

2.11.2 AZIMUTH RESOLUTION.

Resolution in azimuth is achieved by a discrete correlation of the sampled azimuth waveform.

In Appendix A6 it is shown that a correlation of this complex chirp signal produces a purely real result

$$y_a(t) = \beta'_a K . \frac{\sin(\pi \beta'_a t)}{\pi \beta'_a t} \tag{2-19}$$

where β'_a is defined as a numerical value equal to the range of frequencies (positive and negative) occupied by the azimuth signal and K is an arbitrary constant.

In Appendix A6 it is also shown that the bandwidth, β_a, of this real function is equal to half the total doppler frequency spread, β'_a, contained within the azimuth waveform. Therefore, the resolution in azimuth (as a function of time) is given by Equation 2-10 as

$$\delta_{at} = \frac{1}{2\beta_a} = \frac{1}{\beta'_a} \tag{2-20}$$

2.12 THE ANALOGY BETWEEN SAR AND DISCRETE ANTENNA THEORY.

Many authors in the Synthetic Aperture Radar literature compare the azimuth resolving mechanism used in sidelooking SAR systems to that used in discrete antenna array systems[61 62 63]. It is more correct to view the azimuth resolving mechanism of both systems in terms of more fundamental signal processing theory as follows: **Azimuth resolution is achieved by utilising the azimuth signal bandwidth generated by a changing aspect angle between the target and the radar.**

In the case of sidelooking Synthetic Aperture Radar the linear antenna array is synthesised by the forward motion of the radar platform[64]. The distance between the "discrete dipoles" is given by the pulse repetition interval (PRI) used, multiplied by the velocity of this platform relative to the target. At each discrete interval a phase measurement is made (Equation 2.9) which constitutes a sample of the doppler or azimuth waveform at that point.

In a real antenna array the "phase measurement" can be regarded as an "ideal impulse sample" of the doppler waveform[65] †. For each separate dipole it is as if the doppler waveform is frozen in time at that point.

The presence of only one transmit/ receive pair in a Synthetic Aperture Radar forces one to move the radar to different points in space. This movement means that the doppler waveform is not sampled ideally, since during the measurement interval, the doppler waveform continues to change. As discussed in Section 2.9.2 a large change in this doppler waveform during the sampling period can corrupt the measured sample value.

The processing method used to achieve resolution in a discrete antenna array system is described by Elachi[66] and Hecht[67]. This is equivalent to "vector addition", described by Hughes[68] as a method for achieving azimuth resolution in SAR. Vector addition and correlation have been proved to be equivalent by McCord[69].

---

†A very clear mathematical description of the process of pathlength or phase measurement by each of the discrete dipoles in an array antenna is given by Hecht. (Reference 62)

In conclusion, both the mechanisms of operation and the processing techniques used in sidelooking SAR and discrete antenna systems are equivalent. In both cases an increase in the length of the "discrete antenna array" will increases the overall change in aspect angle. This can be utilised to produces better resolution.

Practical antenna arrays are a fraction of the length of synthetic arrays. This allows the more general azimuth correlation technique to be approximated by a simple coherent integration of the phase samples from each dipole. (In the SAR case this simplified technique is usually given the name of "unfocussed azimuth processing"[70 71])

2.13 THE ANALOGY BETWEEN SAR AND PULSE DOPPLER RADAR.

It has been claimed by the author (Section 2.9.1) that there is no difference between the operation of a Doppler radar system and a sidelooking SAR system. The distinction between the two arises only in the methods used to process the discrete samples of the doppler waveform.

A Doppler radar is concerned with the identification and resolution of targets moving with different velocity. Processing is done under the assumption that a single target moves with a constant radial velocity over the target illumination period. For this case the azimuth or Doppler waveform (Equation 2-11) reduces to

$$f_a(t) = e^{-j.\frac{2\pi f_o}{c}.[2(vt+r_o)]}$$

$$= C.e^{\frac{-4\pi}{\lambda_o}.vt}$$

where v is defined as being the assumed constant relative radial velocity of the target.

This waveform contains a constant frequency component which is dependent on the velocity of the target. Processing is employed to estimate this frequency component as a measure of the target velocity[72] [73].

In Synthetic Aperture Radar, however, the target does not move with constant radial velocity and the recorded azimuth waveform has a Doppler bandwidth associated with it. This bandwidth is utilised by matched filtering techniques to produce spatial rather than frequency resolution.

In conclusion it can be said that the operation of sidelooking SAR, Doppler radar (MTI radar) and linear antenna arrays all depend directly on the sampling of the Doppler waveform. The distinction arises in the way the sampled Doppler waveform is interpreted for the particular application in question. This refutes an argument, made in a recent paper by Munson, that azimuth resolution in Synthetic Aperture Radars is not dependent on the Doppler effect[74].

2.14 THE EFFECTS OF THE REAL BEAM PATTERN ON AZIMUTH RESOLUTION IN SIDELOOKING SAR.

The beamwidth of an antenna is defined as the angle within which the radiated power of that antenna is within 70 percent (-3dB) of the maximum value[75] [76]. Skolnik[77] describes how the theoretical minimum beamwidth is obtained for an antenna having uniform current distribution across its aperture. This minimum beamwidth is inversely proportional to the length of the antenna. The best obtainable azimuth resolution happens† to be equal to this theoretical minimum beamwidth[78] [79]. Since the antenna beam diverges, the spatial azimuth resolution decreases in direct proportion to the distance of the target from the antenna[80].

In the case of Synthetic Aperture Radar, azimuth resolution is achieved by utilising the Doppler frequency spread that is generated when a target is illuminated through a range of

†Both the resolution and the physical beamwidth of a transmit antenna depends directly on the length of that antenna.

aspect angle. In a sidelooking SAR the range of aspect angle over which processing is done, is limited (see Section 2.15) to the 3dB beamwidth of the real SAR antenna[81] [82]. This limits the frequency spread contained within the processed azimuth waveform. Any higher Doppler frequencies (point target returns from a larger aspect angle) present in the azimuth waveform are filtered out using analogue techniques[83] or as part of the digital processing[84]. For this reason it is possible to rewrite the equation for the complex azimuth waveform as

$$\begin{aligned} f_a(t) &= e^{-j.\frac{2\pi f_o}{c}.\left[\frac{v^2 t^2}{r_o}\right]} && -\alpha_{3dB} < t \le \alpha_{3dB} \\ &= 0 && \textit{elsewhere} \end{aligned} \qquad (2\text{-}21)$$

with α_{3dB} defined as the aspect angle corresponding to the 3dB width of the antenna beam.

The equation for azimuth resolution is now rewritten as

$$\delta_{az} = \frac{1}{2|f_{d_{3dB}}|}$$

with $|f_{d3dB}|$ representing the positive Doppler frequency associated with the 3dB limit of the antenna beamwidth. Since the aspect angle is limited by the 3dB antenna beamwidth it can immediately be said that the resolution of a sidelooking SAR is directly proportional to the real antenna beamwidth. This is the exact opposite to the case in a conventional radar.

In general, the shape of the real antenna beam pattern is not fixed and by manipulating the current amplitude distribution on the surface of the antenna it is possible to synthesise a variety of beam patterns[85]. It has been shown[86] that the Far Field (or Fraunhoffer) beam pattern of an antenna is given by the Fourier transform of the current distribution over the surface of that antenna. The manipulation of antenna current distribution in conjunction with "beam pattern prediction techniques" using the Fourier transform falls under the very general signal processing topic of "windowing" as discussed by Brigham[87].

By using these antenna aperture "windowing" techniques directive antenna gain is traded off for an increase in the 3dB beamwidth of that antenna[88]. In other words, the azimuth resolution can be increased at the expense of "**signal to noise ratio**" in the final SAR image[89] [90]. For large phased array antennas with very large directive gain, these "windowing"

techniques are particularly pertinent and have been employed in a number of spaceborne SAR systems[91] [92].

Given this new perspective it is possible to throw fresh light on some of the more ambiguous statements made in the SAR literature concerning azimuth resolution:

The frequency dependence of azimuth resolution.

Equation 2-12 predicts that an increase in transmit frequency causes a proportional increase in azimuth resolution. This presupposes that the target is illuminated through the same aspect angle. Antenna theory predicts that an increase in transmit frequency causes a proportional reduction in the real beamwidth[93]. Therefore, the increase in resolution is exactly counterbalanced by the decrease in resolution caused by the reduction in the aspect angle change between target and antenna. This has lead a number of authors, including Cutrona[94], to state that azimuth resolution in SAR is independent of the transmit frequency used.

This is not the complete story. A reduced beamwidth caused by a higher transmit frequency produces an increased antenna gain which increases the final signal to noise ratio of the SAR image. There is no reason why the mainlobe antenna beam pattern could not be broadened using windowing techniques at the expense of this increased signal to noise ratio[95] †. This would, in effect, produce a SAR image with better azimuth resolution and with the same signal to noise ratio as an image recorded at the original frequency.

---

†Antenna windowing (tapering) by using amplitude modulation techniques has the detrimental effect that the total output power of the antenna drops. The windowing technique proposed for the SIR-C experiment uses phase modulation across the length of the antenna. This modulation technique does not affect the total output power of the antenna. (See reference 89)

The range dependence of azimuth resolution.

For sidelooking synthetic aperture radar the azimuth resolution is independent of range[96]. This is true since the total aspect angle contained within the 3dB azimuth beamwidth of the real antenna is the same at any distance from that antenna. However, the signal to noise ratio of an imaged target falls off rapidly with distance.

The dependence of azimuth resolution on antenna size.

It is argued by Munson (amongst others) that azimuth resolution improves with decreasing antenna size[97]. This statement implies that it is necessary to employ a smaller antenna to improve azimuth resolution (assuming a constant transmit frequency). It is true that the 3dB beamwidth of an antenna increases in inverse proportion to the size of the antenna, but it is also true that the transmitted signal power falls off rapidly with decreasing antenna size. There is no reason why a large antenna with high output power and suitable aperture windowing in the antenna azimuth plane could not be used to obtain the required resolution.

2.15 THE EFFECTS OF THE REAL BEAM PATTERN ON AZIMUTH PROCESSING IN SIDELOOKING SAR.

Up to this point the amplitude scaling factor B that must be included in any mathematical model of the received radar waveform has been ignored. In sidelooking SAR the predominant effect influencing this scaling factor is the real antenna beam pattern as a function of azimuth aspect angle. The effect that this scaling might have on the azimuth matched filtering process will now be considered.

Taking this scaling effect into consideration, the azimuth or doppler waveform of Equation 2-11 is rewritten as

$$f_a(t) = B(\alpha(t)).e^{-j.\frac{2\pi f_o}{c}.[2r(t)]}$$

where $B(\alpha)$ is the amplitude (flux density) of the real antenna beam pattern as a function of azimuth aspect angle, α.

The only role that the real beam pattern plays in the azimuth matched filtering process is to weight each complex phase sample by an amplitude value dependent on the aspect angle at which that sample is recorded. This point is also made by Ausherman[98]. Stated differently, the sampled azimuth waveform is modulated in amplitude by a sampled envelope function, where the shape of this envelope function is given directly by the real antenna beam pattern as a function of angle.

For the special case of a sidelooking Synthetic Aperture Radar the azimuth waveform can be written in terms of this scaling factor as

$$f_a(t) = B(\alpha(t)).e^{-j.\frac{2\pi f_o}{c}.\left[\frac{V^2t^2}{r_o}\right]} \qquad -\alpha_{3dB} < t \le \alpha_{3dB} \qquad \text{2-22}$$

$$= 0 \qquad \textit{elsewhere}$$

where the aspect angle α is given by Equation 2-18 as

$$\alpha(t) \approx \frac{Vt}{r_o}$$

This equation for the azimuth waveform describes a linear FM chirp modulated by an amplitude envelope function. For the case of a chirp signal with a large "**time-bandwidth**" product† (as defined by Rihaczek[99]), it has been proved that the frequency spectrum has

†In sidelooking Synthetic Aperture Radar the time-bandwidth product of the azimuth signal is assumed to be sufficiently large.

a similar quadratic phase characteristic and is modulated by the same envelope as the time function[100].

Using a result derived by Rihaczek[101] and Harger[102] it is proved in Appendix A5 that the frequency spectrum for this azimuth waveform can be written mathematically as

$$F_a(f) = \sqrt{\frac{r_o}{2\lambda_o V^2}} \cdot B\left(\frac{\lambda_o}{-2V}.f\right) . e^{j.\frac{\pi}{2\lambda_o}.\left[\frac{r_o}{V^2}.f^2\right]} . e^{-j.\frac{\pi}{4}} \qquad -f_{3dB} < t \leq f_{3dB}$$

$$= 0 \qquad \textit{elsewhere}$$

(2-23)

where f_{3dB} represents the positive doppler frequency associated with the 3dB limit of the antenna beamwidth.

In the words of Harger[103] "... as a target passes through the azimuth pattern, the latter is replicated in the frequency domain as the envelope of the spectrum. Time or azimuth position is related uniquely to spectral location..."

a) The effects of antenna beam pattern on azimuth resolution.

It is now possible to give a more mathematical explanation as to why azimuth processing is limited to the 3dB width of the antenna beam in sidelooking SAR. Azimuth resolution was defined in Section 2.15 to be proportional to the real 3dB bandwidth of the processed azimuth signal. Even if a greater antenna beamwidth was utilised in the azimuth correlation, the 3dB bandwidth would effectively be determined by the 3dB beamwidth as shown in Figure 2-6. Since the magnitude of the antenna beam (for a rectangular aperture with uniform current distribution) falls off rapidly outside this limit, any increase in resolution obtained by utilising the higher frequencies in the signal can be considered negligible.

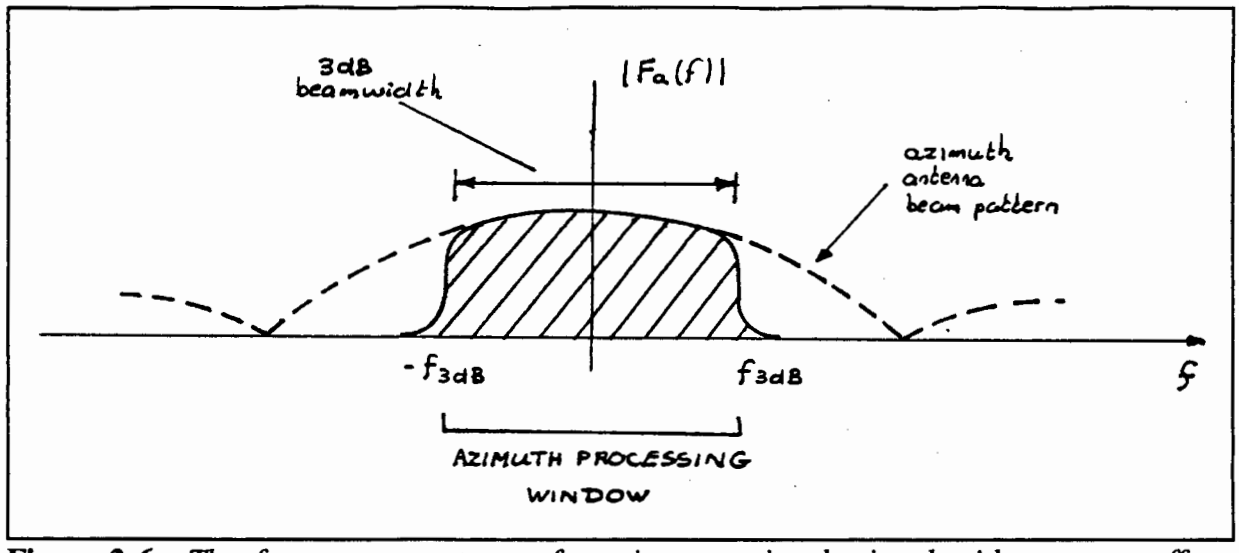

Figure 2-6: *The frequency spectrum of continuous azimuth signal with antenna effects included.*

b) Including the effects of the antenna beam pattern in the azimuth reference function.

For a matched filter to achieve the maximum theoretical signal to noise ratio on the output signal, the reference function must be an exact replica of the point target return signal. Therefore, (see Fitch[104] and Wu[105]) the reference function should include the effects of a modulating beam pattern. In the author's opinion any increase in signal to noise ratio obtained by including the effects of beam pattern is small. For this reason the azimuth waveform will be assumed to be given by Equation 2-22, without any beam pattern scaling factor. The corresponding frequency domain spectrum will then have an envelope that is rectangular in shape.

c) The beam pattern as a spectral window.

Matched filtering of a chirp signal was shown in Appendix A6 to give rise to a time domain response with good mainlobe resolution but with relatively high and usually undesirable sidelobes[106] [107]. This is caused by the relatively sharp signal transition

at the boundaries of the frequency spectrum associated with this chirp pulse (see Figure 2-6). In the signal processing literature this effect is known as "ringing" of the time response† and is described by authors such as Fitch[108] and De Fatta[109]. The effects of ringing can be reduced by windowing the frequency spectrum and this process is described in detail by authors in the digital signal processing literature such as Oppenheim & Schafer[110].

Since the beam pattern imposes an amplitude taper on the frequency spectrum, it has been compared to a window function. Heimiller argues that "...(the) shape of the physical antenna beam shape gives a result similar to amplitude weighting with a slight decrease in resolution but with improved sidelobe level."[111] For reasons given below the beam pattern cannot be considered to be a suitable window:

a) The amount of amplitude taper imposed on the frequency spectrum (within the 3dB limits) is not enough to cause a significant decrease in the level of sidelobes in the correlated point target response.

b) In azimuth processing it is sometimes convenient to split the Doppler bandwidth into separate sections and to correlate each section independently†† (see Section 3.9.5). This causes an asymmetrical beam pattern over each of these sections. The theory of windowing requires that the amplitude tapering of the frequency spectrum be symmetrical with respect to the centre of each particular spectrum.

In Section 3.12 it is discussed how **artificial** windowing techniques can be implemented to get the desired results.

---

†This effects is also called the Gibbs phenomenon.

††This is done to produce multiple looks of the same target area.

2.16 DOPPLER AMBIGUITIES IN AZIMUTH PROCESSING.

It was assumed in Section 2.9.2 that a sampling period, T, could be defined that would be small enough to prevent any aliasing of the azimuth frequency spectrum. In practical terms this is impossible to do. As Harger explains, the extent of the azimuth beam pattern and, subsequently, Doppler frequency content is determined by geometry[112]. The Far Field antenna pattern is, infinite in azimuth spatial extent so theoretically the highest frequency contained within the azimuth signal is infinite. For practical reasons the PRI has to be limited and therefore some signal aliasing will occur. Raney[113] and Noack[114] give examples of where aliasing effects have corrupted the final SAR image.

The effects of doppler ambiguity is understood by a direct application of signal processing theory. Figure 2-7 represents the magnitude frequency response of the sampled azimuth signal. Only the processing bandwidth is shown because the process of correlation will automatically force the higher frequencies contained in the azimuth signal to zero (as explained in Section 2.14). The sampling process causes repeated frequency spectra to be generated at multiples of the sampling frequency. This effect is explained in detail by Oppenheim & Schafer[115].

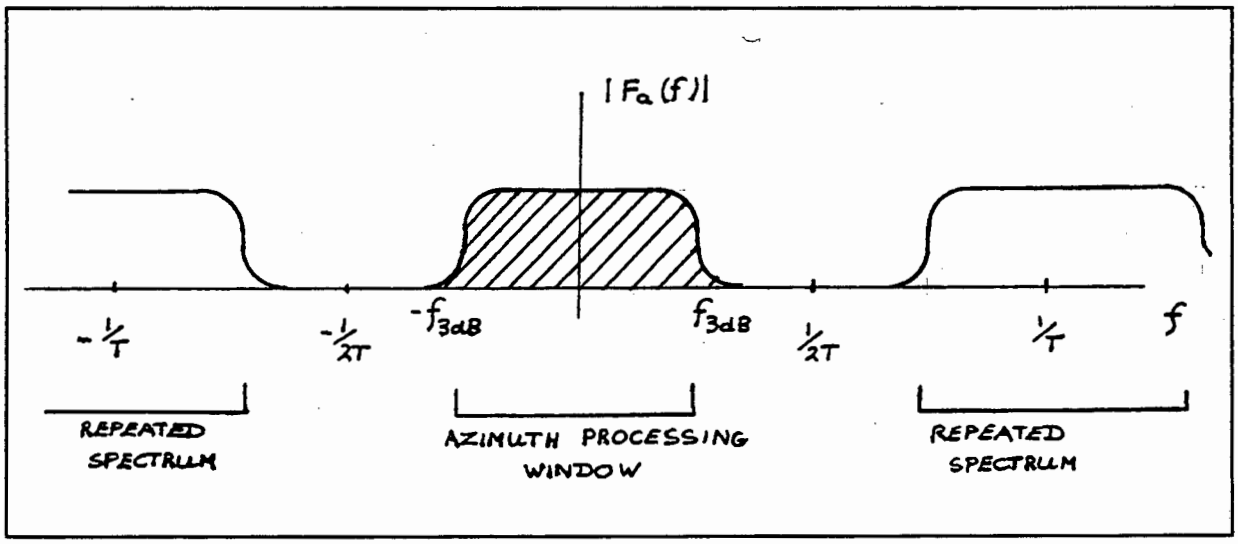

Figure 2-7: *Frequency spectrum of the sampled azimuth signal (antenna beam weighting effects are not included).*

The frequency spectrum can be interpreted as follows: Any radar return signal from a target, which has associated with it a frequency spectrum situated at a multiple of the sampling frequency, will be aliased in such a way as to be indistinguishable from a target return located within the 3dB antenna beamwidth. (Hence the existence of a complex "one to many mapping" between time and frequency).

The envelope of this extended frequency spectrum is modulated by the beam pattern of the antenna. Rihaczek points out that the beamwidth of an antenna is typically so small that the small angle approximations made in predicting the antenna pattern as a function of angle (and presumably the approximation of a target return to a chirp pulse) will hold well to within several beamwidths about the main beam[116]. The antenna beam pattern is assumed to modulate directly both the primary spectrum and several of the repeated signal spectra in the frequency domain. This is shown diagrammatically in Figure 2-8.

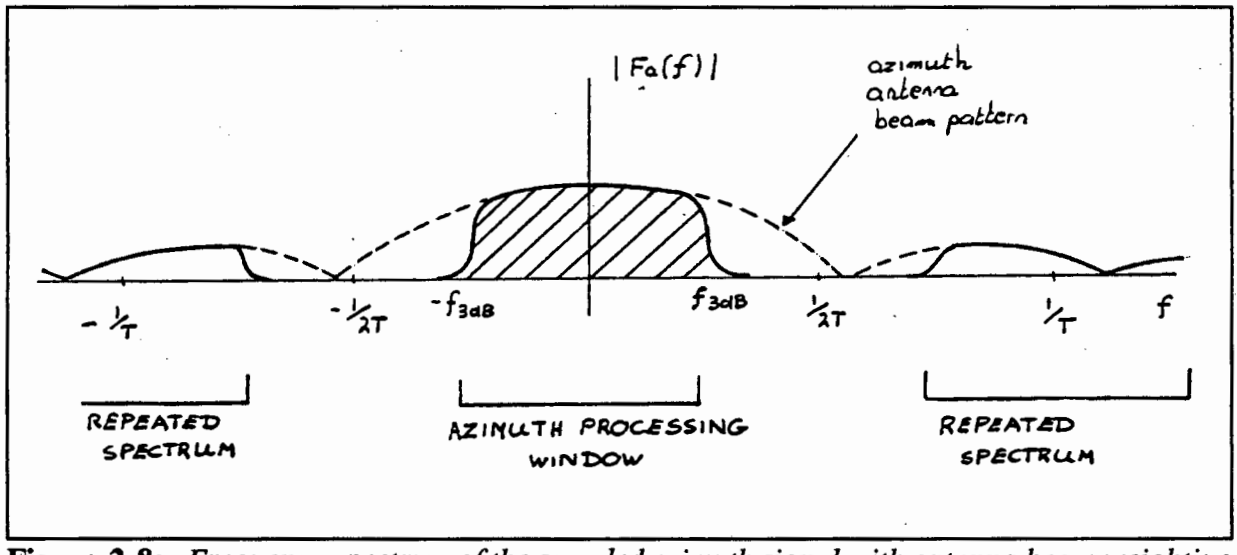

Figure 2-8: *Frequency spectrum of the sampled azimuth signal with antenna beam weighting effects included.*

The antenna pattern modulates the frequency spectrum in such a way as to reduce the level of ambiguous signal mapped into the SAR image. Design techniques for limiting the doppler ambiguities are discussed by various authors such as Raney[117], Heimiller[118], Harger[119] and Bayma[120], and are not repeated here.

2.17 THE EFFECTS OF SPATIAL GEOMETRY ON THE POSITION OF THE AZIMUTH PROCESSING WINDOW.

2.17.1 DEFINING A DOPPLER CENTROID AND DOPPLER RATE.

It has been assumed up to now that the position of zero doppler corresponds to the boresight of the antenna. In reality the geometry of the imaging situation is such that this is not (in general) true. This problem is discussed in detail in Section 3.8.3. A small error in predicted target/ antenna geometry will cause the antenna boresight to shift away from the zero doppler position. The effects of such a shift on the resulting frequency spectrum is shown in Figure 2-9.

If the azimuth processing window is left in the position occupied in Figure 2-9 a number of complications arise. Firstly, the signal to noise ratio of the azimuth waveform is impaired by the fact that the direction of maximum antenna power output is not aligned with the processing window. Secondly, the ambiguity specifications are no longer valid, causing an increased amount of image corruption.

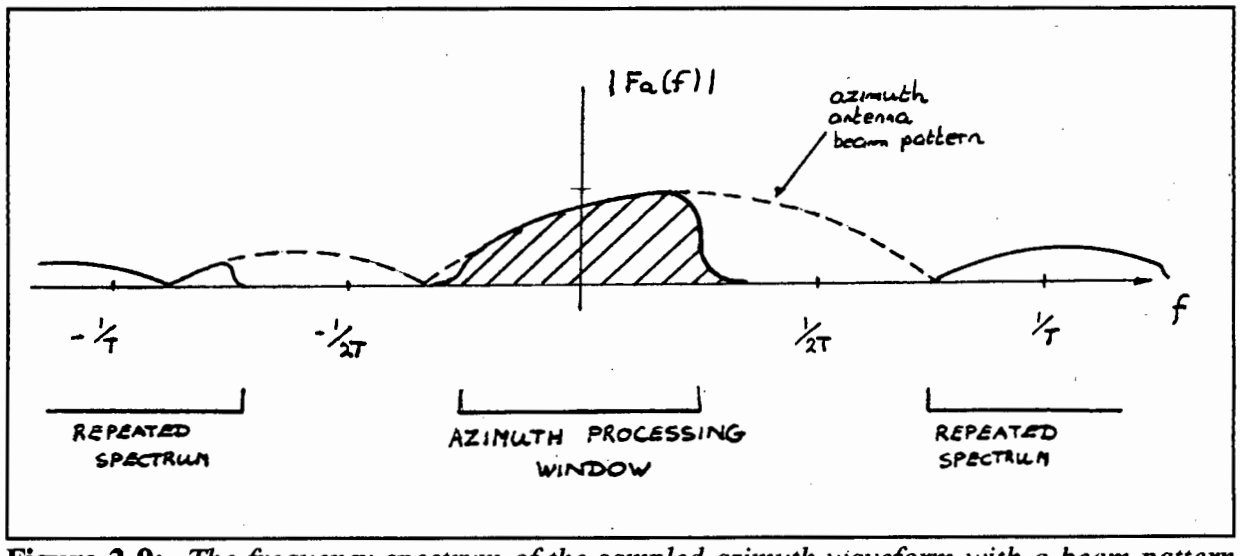

Figure 2-9: *The frequency spectrum of the sampled azimuth waveform with a beam pattern that is shifted away from the zero doppler (or zero frequency) position.*

Therefore, significant misalignment must be avoided. This can be done if the geometry of the imaging situation can be predicted with enough accuracy. This problem is addressed in Section 3.6. Once a more accurate boresight direction is estimated, the processing window can be shifted by a suitable modification of the azimuth reference function. The frequency spectrum for this modified signal is shown in Figure 2-10.

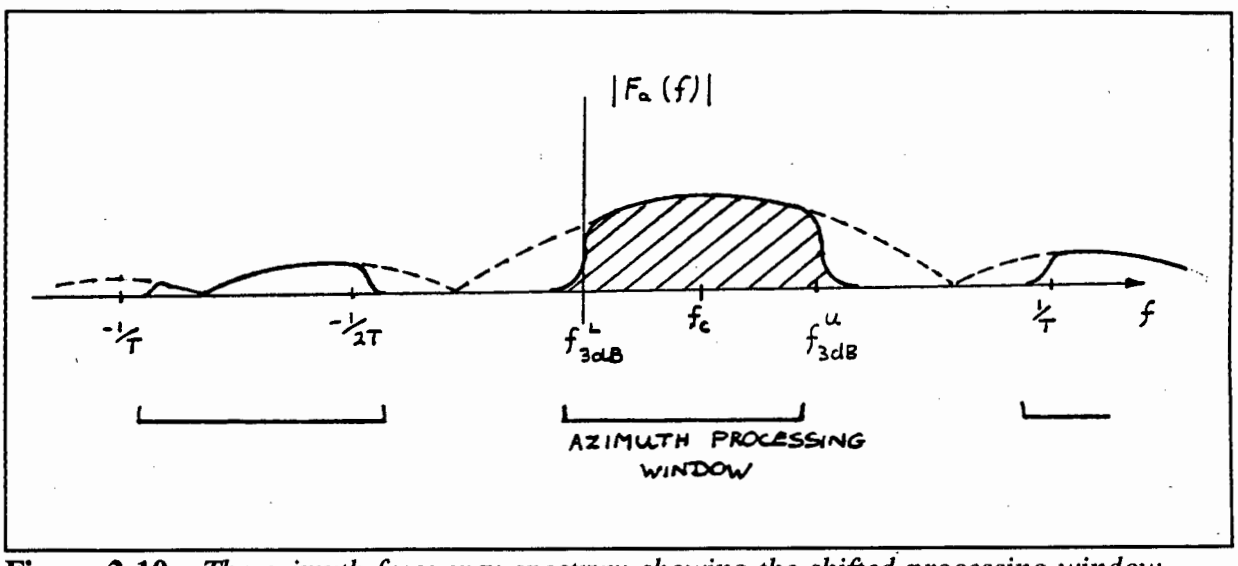

Figure 2-10: *The azimuth frequency spectrum showing the shifted processing window.*

Geometrically this procedure is equivalent to processing the radar reflections from a target located in an area that is offset from the zero doppler position. This is shown in Figure 2-11. The centre of the target illumination area is shifted a perpendicular distance *d* away from the line of zero doppler.

Once more a two term binomial expansion is used to obtain an approximation to the relative radial distance, *r(t)*. In Appendix A7 this is shown to be equal to

$$r(t) = r_o + \frac{d^2}{2r_o} + \frac{1}{2r_o}.(V^2t^2+2Vt.d)$$

where $t=0$ is defined as the time when the target occupies a position at the centre of this illumination area.

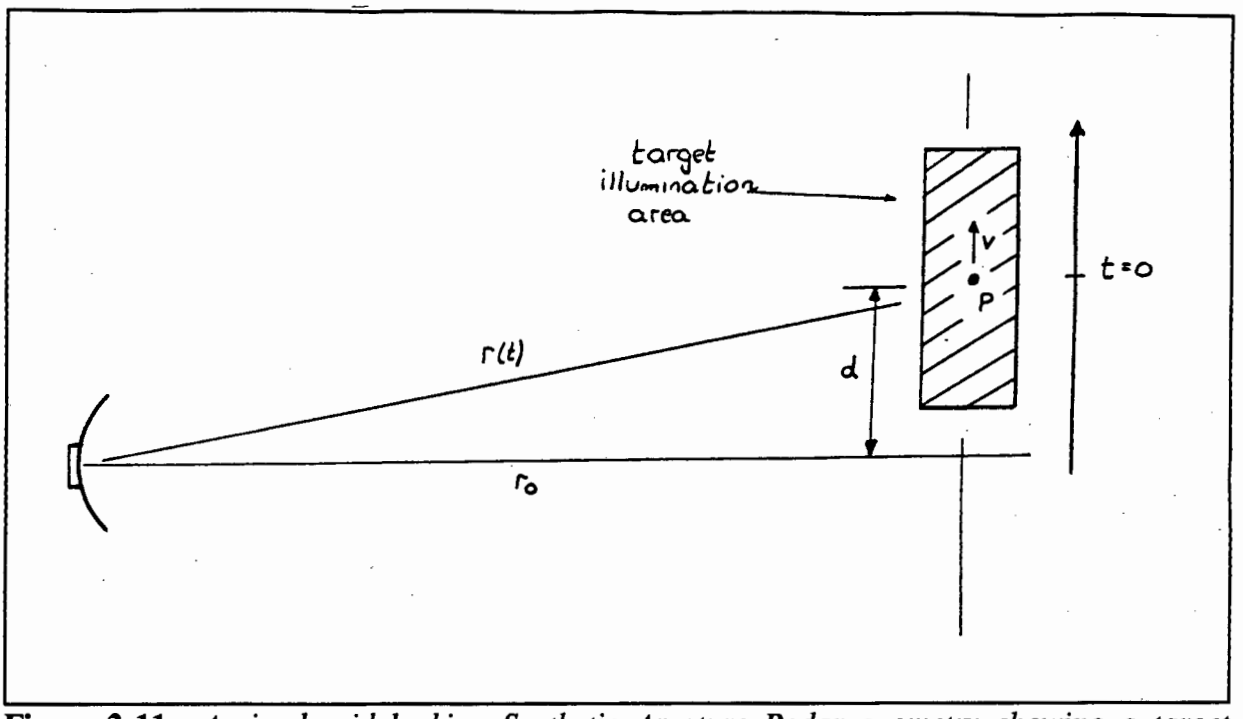

Figure 2-11: *A simple sidelooking Synthetic Aperture Radar geometry showing a target illumination area that is offset from the zero Doppler position.*

Ignoring any constant terms the continuous azimuth waveform of Equation 2-22 is now rewritten in terms of this approximation as

$$f_a(t) = e^{-j.\frac{2\pi f_o}{c}.\left[\frac{V^2t^2}{r_o}+\frac{2dVt}{r_o}\right]} \qquad \alpha^L_{3dB} < t \le \alpha^U_{3dB}$$

$$= 0 \qquad \textit{elsewhere}$$

(2-24)

where α^L_{3dB} and α^U_{3dB} represent the aspect angles at the upper and lower bound of the 3dB antenna beamwidth, respectively.

In this case the instantaneous doppler frequency is given as

$$f_d = \frac{-2f_o}{c}.\left[\frac{V^2t}{r_o}+\frac{d.V}{r_o}\right] \qquad \textbf{(2-25)}$$

The equation for doppler frequency consist of two separate terms. The first term is a constant exponential carrier which arises due to the offset position of the processing window. The second term is a linear frequency term which is identical to the one obtained in the case of a processing window that is centred about zero doppler. (see Equation 2-17) The constant exponential term is usually defined in the SAR literature[121] as the **"Doppler centroid frequency"**, f_c. The linear term is given the name of **"Doppler rate"** or f_r.

Making the substitutions

$$f_c = \frac{-2f_o}{c} \cdot \frac{Vd}{r_o} \tag{2-26}$$

and

$$f_r = \frac{-2f_o}{c} \cdot \frac{V^2}{r_o} \tag{2-27}$$

the azimuth reference function can be rewritten as

$$f_a(t) = e^{j.2\pi\left(\frac{1}{2}f_r t^2 + f_d t\right)} \tag{2-28}$$

and the doppler frequency as

$$f_d = f_r.t + f_d \tag{2-29}$$

The azimuth reference function is again in the form of a complex chirp, but is now modulated by a complex exponential carrier. In Appendix A8 it is shown that a correlation of this function with an identical reference produces a point target response

$$y_a(t) = \beta_a' K . \frac{\sin(\pi \beta_a' t)}{\pi \beta_a' t} . e^{-j.\frac{2\pi f_o}{c} \cdot \left[\frac{2Vd}{r_o}\right]} \tag{2-30}$$

where β_a' is defined as a numerical constant equal to the range of frequencies (positive and negative) occupied by the azimuth function. K is an arbitrary scaling constant.

The result of this correlation is a complex signal. In all SAR azimuth processing an absolute value is taken of the final correlated result. This is done so as to remove any constant

complex phase offset terms that might be generated as a result of terrain reflectivity effects[122] and constant radial distance terms. (These constant radial distance terms having been left out of the azimuth reference function up to now)

Taking an absolute value of the correlated azimuth signal also has the effect of removing any complex carrier terms that might be present. In Appendix A8 it is shown that taking an absolute value of the correlated azimuth signal (Equation 2-30) produces a final result

$$y_a(t) = \left| \beta_a' K . \frac{\sin(\pi \beta_a' t)}{\pi \beta_a' t} \right| \qquad (2\text{-}31)$$

This result is the same as that produced for the case where the azimuth spectrum was assumed to be centred around zero frequency. This signal is real and therefore a resolution can be defined. (as is done in Section 2.11.2)

2.17.2 DEFINING THE "ALONG TRACK" AND "CROSS TRACK" VELOCITY COMPONENTS OF TARGET MOTION.

It is now possible to clarify, in a precise manner, some of the standard terminology that will be used in further discussion of sidelooking SAR systems.

All target motion is measured relative to the antenna. The "**Doppler centroid position**" is defined to be the position of a point target located at the centre of the target illumination area at time t=0 (see Figure 2-12). The "**range direction**" has the same direction as a line connecting the spatial position of the radar antenna with the doppler centroid position. The component of the target velocity vector, V, as resolved in this direction is known as the "**cross track**" velocity or V_c. The "**azimuth direction**" is defined to be in a direction perpendicular to the "range direction" and lying on a plane which contains the relative velocity V of the target and the position of the antenna. The component of target velocity, V, as resolved in this direction is known as the "**along track**" velocity component, V_a.

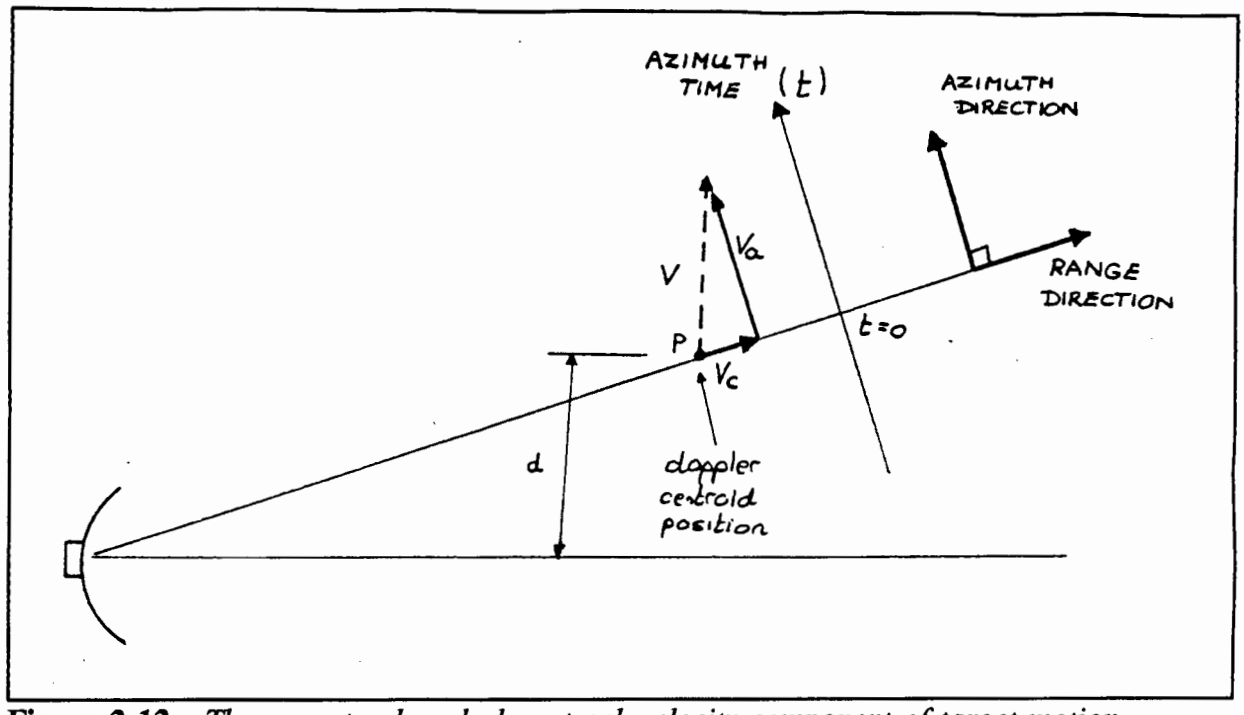

Figure 2-12: *The cross track and along track velocity component of target motion.*

The vector diagram in Figure 2-12 is two dimensional. The terminology can be applied equally well to a three dimensional geometry.

2.17.3 PROCESSING ALIASED DOPPLER SIGNALS.

In some cases (see Section 3.8.2) it is possible that the geometry of the imaging situation is such that the mainlobe of the antenna beam pattern illuminates a frequency range in an ambiguous region of the azimuth frequency spectrum. This is illustrated in Figure 2-13. However, if the geometry of the imaging situation is known with sufficient accuracy, the location of the target illumination area can be established. It is then possible to generate an accurate reference function. If this function is then sampled at the same frequency as the PRF used, the reference function will be aliased in exactly the same way as the original target return signal. Digital correlation of these two signals can then take place. No problems will occur if the level of signal returns from targets located within ambiguous areas on either side of the target illumination area are reduced sufficiently by the attenuating effects of the antenna beam pattern.

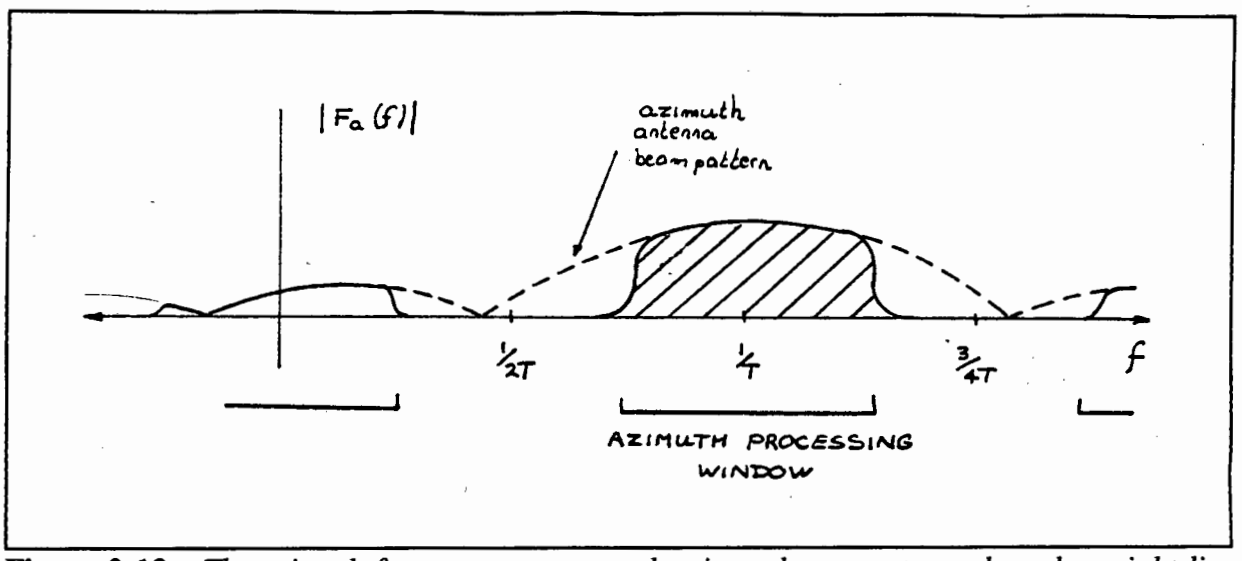

Figure 2-13: *The azimuth frequency spectrum showing a beam pattern whose boresight lies in an ambiguous region of that spectrum.*

In the light of the above discussion it is necessary to reconsider the question of azimuth sampling. In Section 2.9.2 it was stated that the minimum azimuth sampling rate or PRF_{min} must be equal to twice the maximum doppler frequency contained within the azimuth processing window. Any sampling rate below this figure causes ambiguities. Obviously if this ambiguity can be resolved from an investigation of the imaging geometry there is no need to maintain this sampling rate. In this case, the minimum sampling rate can be reduced to a value equal in magnitude to the **range** of doppler frequencies contained within the azimuth processing window. However, any further reduction in the sampling rate cannot be tolerated as it will cause a corruption of the azimuth signal. This is caused by foldover (aliasing) effects within the actual processing bandwidth.

The above point also clears up the discrepancy that exists in the SAR literature (see Section 2.9.2) as to what the minimum sampling rate of the azimuth signal ought to be.

CHAPTER 3

THE PROCESSING OF SYNTHETIC APERTURE RADAR DATA FROM THE SIR-B EXPERIMENT

3.1 INTRODUCTION

3.1.1 THE DESIGN OF A DIGITAL PROCESSOR FOR THE DECODING OF SPACEBORNE SAR DATA.

This thesis is the first phase of a long term project to develop a general purpose digital processor for the decoding of spaceborne Synthetic Aperture Radar data, at the University of Cape Town (UCT). Similar such processors have been documented in the SAR literature and include ones operating at JPL-California[123] [124], Farnborough-England[125] and the German Aerospace Research Establishment[126]. Reference is made to all three of these systems.

The main requirements of a SAR processor are characterised by Noack as:

a) The input of raw SAR data.
b) The digital decoding of this data using the best available system and satellite (shuttle) orbit information.
c) The production of a SAR image.

This processor must be general enough to accommodate data from a variety of spaceborne SAR systems, each with its own orbital geometry and system parameters. The required flexibility, therefore, cancels out the possibility of a pure hardware solution to the SAR processing problem. Noack describes how a software solution must be developed that allows the "... formulation of all terms and notations to be used in mathematical models and equations, in a general and coherent scheme."[127]

The purpose of this chapter is to generate a software design for the decoding of SAR data that meet the following requirements:

a) The algorithms must be flexible enough to cope with a variety of SAR geometries and system specifications.

b) The algorithms must be efficient in terms of processing time.

c) The amount of human interaction involved in producing an image must be limited as far as possible.

The algorithms developed as part of this software design have been implemented by Welsh[128] in a high level software language and tested on raw radar data as recorded by the SIR-B mission. Image results obtained by running prototypes of this software are included in this thesis.

3.1.2 THE SOURCE OF THE RAW RADAR DATA USED TO TEST THE SOFTWARE DESIGN.

The SIR-B SAR system was launched aboard Flight 41-G of the space-shuttle Challenger into a nominally circular orbit with an inclination of 57 degrees. The mission took place during October 1984. SIR-B coverage of Southern Africa was limited to one data take and a subset of the raw data recorded during this take was obtained from JPL for processing purposes[129].

Raw radar data acquired in the Cradock region of Southern Africa was processed. The official description of this data set as obtained from the "menu tape" supplied with the raw data is as follows:

Table 3-1: **SIR-B**
Digitally Correlated Menu Tape.
Request No. 3008

Site name: **AGULHAS/MOLOPO**	Centre Time: **281/15:20:11.755**
Data Take-Scene No: **X1-035.60-079**	Correlation Date: **06/23/90**
Centre Lat/Long: **-32° 16.5 min / 25° 38.9 min**	Centre Incident Angle: **35.8**
Centre Resolution (R. x A.): **24.0m x 29.2m**	Pixel Size: **12.5**
Track (Deg. to True North): **139.9°**	Bits Per Sample: **6**

A copy of the complete "menu tape" is provided in Appendix D1. An areal photograph and topographic map covering a section of the area in question were obtained for comparison with the decoded radar data. Copies are included in Appendix D2.

3.1.3 SYSTEM AND ORBITAL PARAMETERS USED IN THE DECODING OF SIR-B DATA.

The correlation algorithms developed for the decoding of spaceborne SAR data require the radar system and satellite orbital parameters specified in Table 3-2 and Table 3-3. In this case the numerical values associated with these parameters pertain to the SIR-B experiment at the time of the data take over Cradock.

The algorithms are general enough such that the processing of raw SAR data obtained at another time, or by a different spaceborne satellite system, involves only a change in the numerical values of the parameter list given below.

Table 3-2: Radar System Parameters

Chirp Pulse Duration (τ): 30.4μs *	Video Offset (f_{if}): 7.2MHz *
Chirp Pulse Bandwidth (β'_r): 12MHz *	Sampling Rate ($1/dt$): 30.355MHz ***
Pulse Rep. Frequency ($1/T$): 1463.8Hz **	Transmit Frequency (f_o): 1282 MHz **

Table 3-3: Orbital Parameters

a) Satellite position:

X position (S_1): 282.449km **
Y position (S_2): -5637.355km **
Z position (S_3): -3419.207km **

b) Satellite velocity:

X velocity (V_{s1}): 4763.469m **
Y velocity ($Vs2$): 3359.391m **
Z velocity (V_{s3}): -5143.152m **

c) Satellite attitude:

Roll: 85.0° **
Pitch: 0° **
Yaw: 0° **

d) Slant range to near edge of swath:

Slant Range (r_s): 227.29km **

*Paper by Curlander[130]

**SIR-B Menu Tape

***SIR-B Experimental Report[131]

The data required for the SIR-B experiment was obtained from a number of sources as indicated by the superscripted asterices. In all cases the numerical value is given to the best significance known at the time of writing.

The standard abbreviations adopted in this thesis for these relevant variables are included in brackets in the above tables. Any further reference to parameters in these tables will be given in terms of these abbreviations.

3.1.4 THE ACCURACY AND AVAILABILITY OF THE PARAMETER SPECIFICATIONS.

The usefulness of any SAR correlation algorithm is limited by:

a) The availability of the parameters required for implementation of that algorithm.

b) The accuracy to which the parameters in question are known.

The radar system parameters listed in Table 3-2 and Table 3-3 are all standard measurable in any spaceborne SAR system. In recent years much emphasis has been placed on the accurate measurement (or estimation) of these specific parameters. This is documented by authors such as Huneycutt[132], Ahmed[133] and Noack[134] in discussions on the proposed SIR-C, Radarsat and ERS-1 spaceborne SAR missions. The quality of the final SAR image will obviously depend directly on the accuracy of these parameters. For this reason, sensitivity analyses are performed on the range and azimuth correlation algorithms developed in this thesis.

3.2 A SIMPLIFIED SPACEBORNE SAR GEOMETRY

A typical spaceborne SAR viewing geometry[135] is sketched in Figure 3-1. An antenna mounted on a spaceborne satellite illuminates a "**target area**" (or "**footprint**") on the surface of the earth. The boundary of this target area is given by the spherical 3dB width of the antenna beam. Point P is assumed to be a point target located in the target area. The motion of this point is shown relative to an observer on the antenna. (In other words the antenna is assumed to be stationary and all motion is measured with respect to that antenna). The "**incident angle**" γ is defined as the angle between the line connecting the target position P with the radar antenna and the earth normal at that point. For SIR-B the average incident angle over the target field of interest is given in the menu tape as approximately 36°.

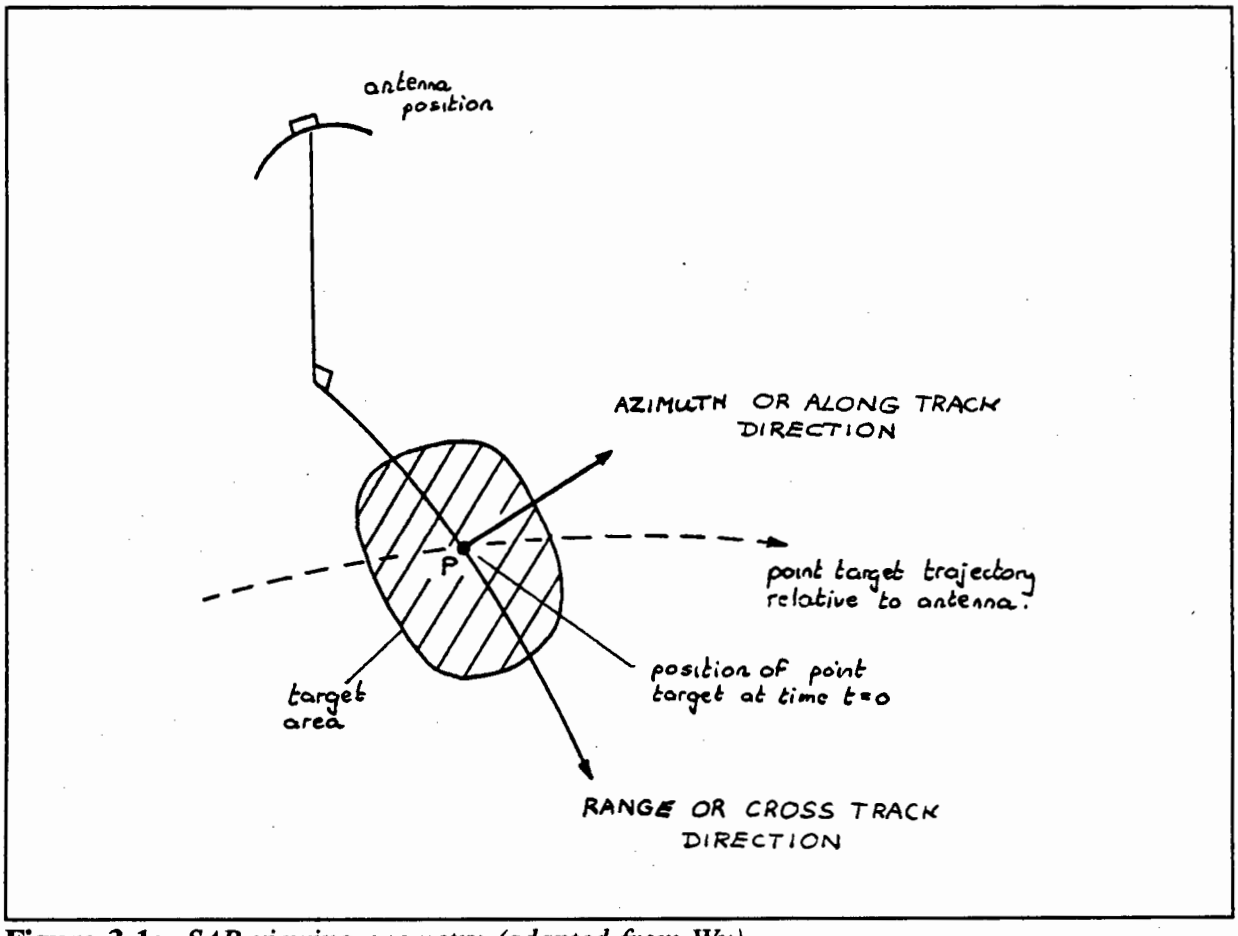

Figure 3-1: *SAR viewing geometry (adapted from Wu)*

The processing algorithms will initially be developed to resolve a single point target in the range and azimuth directions as described in Section 2.7. The resolving of other targets in the target field is discussed in Section 3.11 under the heading of "Depth of Focus".

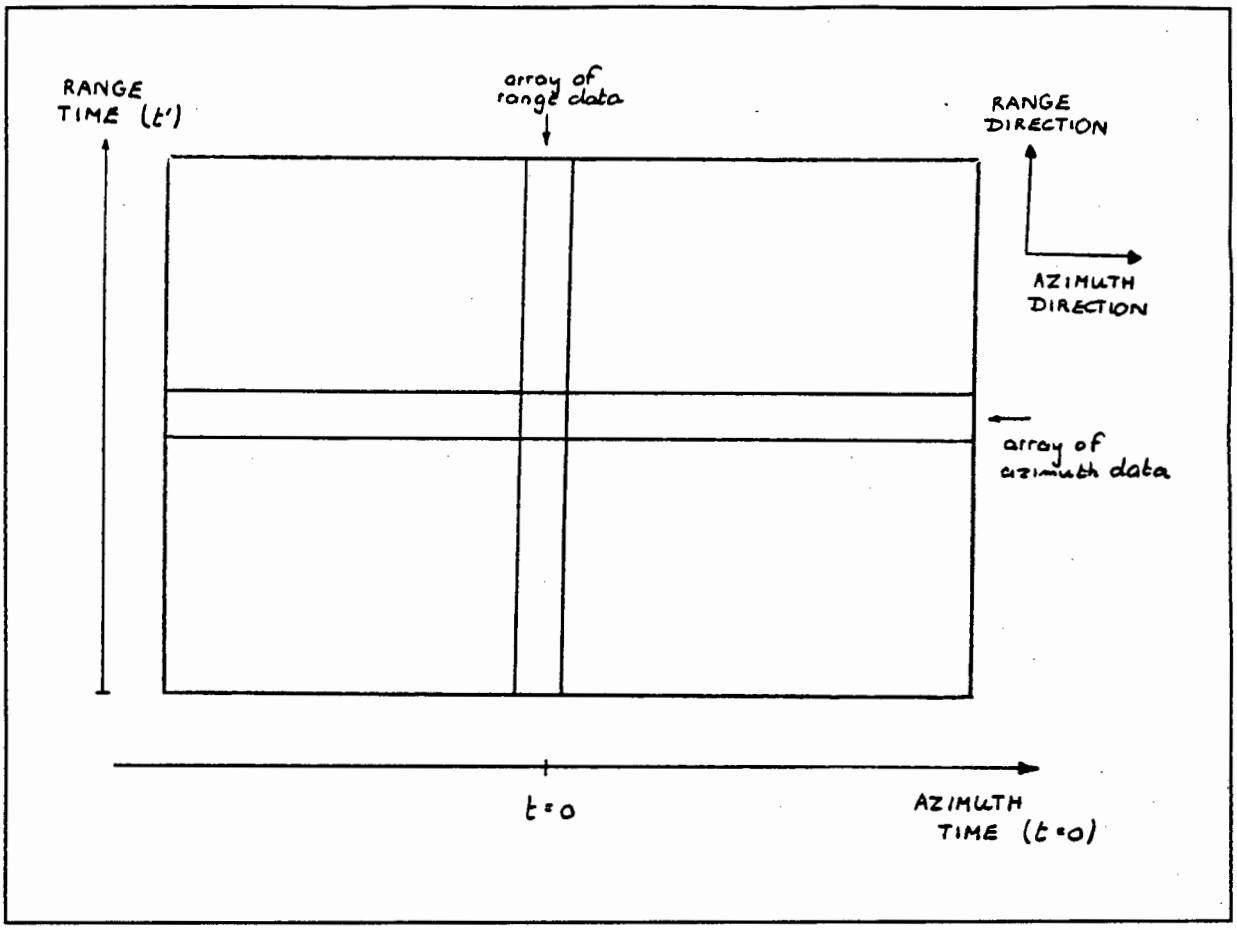

Figure 3-2: *A 2D array of SAR data.*

The format of the sampled data recorded by the spaceborne SAR sensor can be described as follows:

> At each PRI a radar pulse is transmitted and after a fixed delay time the composite return waveform is sampled and recorded over a finite time window ("**pulse sampling window**") as described by Elachi[136]. To simplify the terminology, a set of such samples will be termed a set of "**range data**". A number of such sets of range data, recorded at intervals of the PRI over the point target illumination period, forms a two dimensional discrete matrix of data as shown in Figure 3-2. This will be known as the "**SAR matrix**" in future reference.

The range data is represented as columns in this matrix. The one dimensional arrays making up the rows of the matrix are referred to as sets of "**azimuth data**". The approximate directions of increasing range (cross track) and increasing azimuth (along track) are also shown.

3.3 RANGE PROCESSING

In all modern Synthetic Aperture Radar systems, resolution in range is achieved by modulating the transmitted coherent carrier (on a pulse to pulse basis) with an envelope displaying two characteristics: A unity magnitude response and a phase response resembling that of a linear FM or chirp pulse. (see Section 2.2) Therefore, the radar transmit signal is written in the standard form of Equation 2-7 as

$$g(t') = \Re e \left[p(t',\tau) \cdot e^{j.2\pi f_o t'} \right] \qquad \textbf{(3-1)}$$

with an envelope function

$$p(t',\tau) = e^{-j.\pi a(t')^2} \qquad -\frac{\tau}{2} < t' \leq \frac{\tau}{2}$$

$$= 0 \qquad \textit{elsewhere}$$

and a carrier term

$$e^{j.2\pi f_o t'}$$

The term, a, present in the equation for the envelope function is known as the "**chirp rate**" and is given by Munson[137] as the transmitted signal bandwidth, β_r', divided by the duration, τ, of that signal.

3.3.1 IN-PHASE AND QUADRATURE DEMODULATION USING THE FAST FOURIER TRANSFORM ALGORITHM.

In all spaceborne SAR systems the radar receive signal is not demodulated to baseband but rather to some intermediate frequency (offset video) where it is sampled. A digital technique was developed in Section 2.6.2 to produce a result equivalent to analogue I and Q demodulation and can be summarised as follows:

1) Perform a Discrete Fourier Transform (DFT) on the sampled range waveform.
2) Set the negative frequency spectrum to zero.
3) Remove the offset video by a digital shift of the positive spectrum to baseband.
4) Perform an inverse DFT.

One of the most efficient techniques for implementing the DFT is to make use of the Fast Fourier Transform (FFT) algorithm. This transform, as discussed by Bergland[138] and Roberts & Mullis[139], is only an approximation to the DFT of a sampled signal but will produce good results if implemented correctly.

An FFT can only be implemented on an array consisting of a "power of two" number of samples. Barber[140] describes how a set of range data can either be truncated to fit this size of array or padded up with zeroes.

Assuming an FFT is performed on this contiguous "power of two" array of size (N), a frequency spectrum will be obtained that resembles the one shown in Figure 3-3. The FFT produces an approximation to the actual DFT spectrum, where positive frequencies are displayed in array positions: [0] ⇒ [N/2-1] and negative frequencies in positions: [N/2] ⇒ [N-1]. The envelope of this spectrum approximates that predicted by Rihaczek for a chirp signal with large time-bandwidth product[141].

The formulae linking positions (in this transformed array) to frequency are given by Roberts and Mullis[142] and can be summarized as follows:

a) Array position [N] corresponds to the frequency at which the original time signal was sampled. In other words *1/dt*.

b) The distance *df* between samples in the frequency spectrum is given by *1/(N.dt)*.

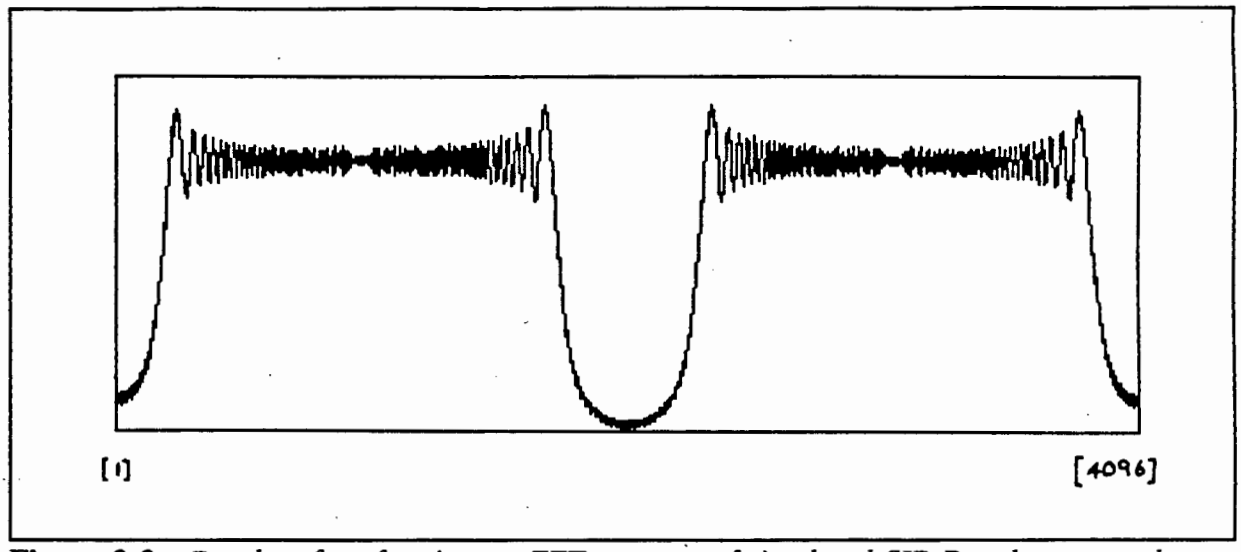

Figure 3-3: *Results of performing an FFT on a set of simulated SIR-B radar range data.*

Digital demodulation is performed by setting the negative frequency spectrum to zero and shifting the positive spectrum to baseband in such a way that it lies symmetrically with respect to the frequency origin. This will remove the intermediate, or video, offset frequency[143]. The number of array positions through which this spectrum must be shifted to the left is given by: f_{if}/df. The result of this operation is sketched in Figure 3-4.

On performing an inverse FFT, a time array of length (N) is obtained. For a single point target return this time signal reduces to the standard range waveform given in Equation 2-11 as

$$f_r(t') = p(t'-D_n,\tau) \cdot e^{-j.\theta_n}$$

where the complex phasor term was shown in Section 2.6.2 to represent a sample of the azimuth or doppler waveform at that point and $p(t\text{-}D_n,\tau)$ represents the unaltered chirp envelope function.

For the SIR-B case this envelope function can be written as

$$p(t',30.4\mu s) = e^{j\cdot\left[\frac{12MHz}{30.4\mu s}\right](t')^2} \qquad \frac{-30.4\mu s}{2} < t' \leq \frac{30.4\mu s}{2}$$

$$= 0 \qquad \textit{elsewhere}$$

with a chirp rate given by the transmitted signal bandwidth, β_r', divided by the pulse width, τ.

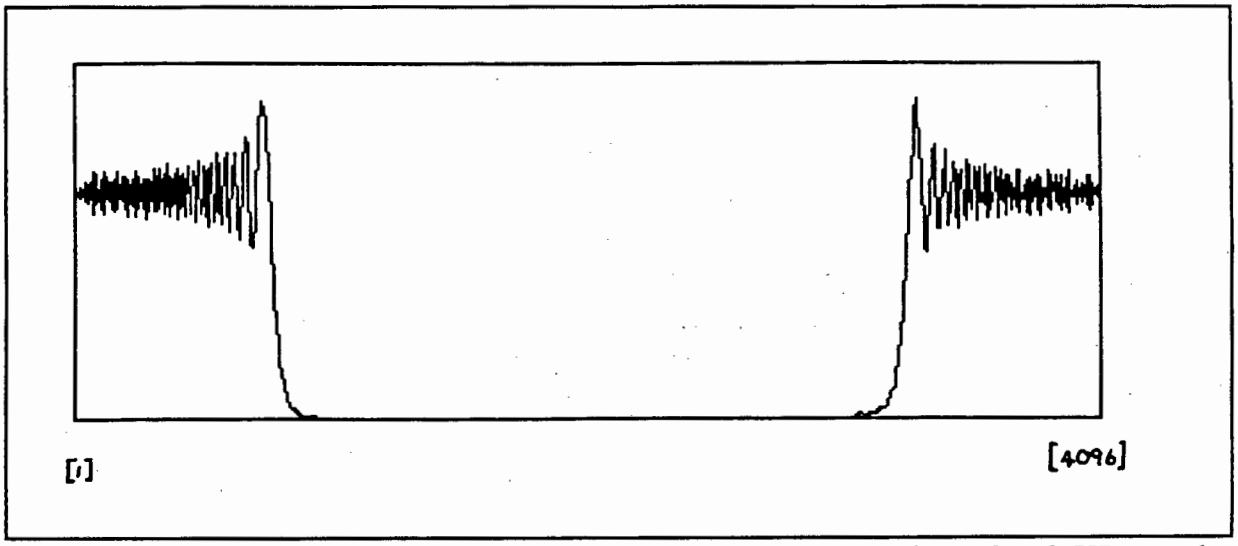

Figure 3-4: *FFT frequency spectrum after digital demodulation of simulated SIR-B radar range data.*

3.3.2 RANGE CORRELATION USING THE FFT ALGORITHM.

As was explained in Section 2-8 range resolution is obtained by correlating each set of range waveforms with a replica of the transmitted envelope function, which is known as the range reference function.

A digital correlation technique is described by Barber[144] and Wu[145] and can be summarized as follows:

1) A separate DFT is performed on each set of range data of length (N).
2) The DFT is calculated on a sampled version of the range reference function. The sampling rate *dt* is the same as that used in the radar receiver to record the set of range data.
3) This reference function is conjugated and a DFT performed on it.
4) The conjugate DFT of this reference function is then multiplied in turn with each set (or row) of Fourier transformed range data.
5) The inverse DFT is calculated on the result to form a set of correlated range data.

The correlation technique can be performed very efficiently using the FFT algorithm[146]. As explained in Section 3.3.1 the set of range data must be "modified" to form a range array of length (N). The sampled reference function is also padded up with zeroes to form an array of the same length (N). The FFT can then be used in steps 1 to 5 as an approximation to the DFT.

Bergland describes how problems can occur with this approximation. A correlation using the FFT technique described above corresponds to a correlation of sampled and **also periodic** time function[147]. The repetition cycle of these two periodic time functions (the range waveform and the reference function) is exactly equal to the length of time represented by the padded arrays. For this reason this process is usually given the name of "cyclic convolution" in the signal processing literature and is discussed in detail by Bracewell[148] and Oppenheim & Willsky[149].

If (R) is the number of array bins occupied by the reference function, then the results of correlation will be valid in the array index range: [0] → [(N-1)-R]. For larger array indices the process of cyclic convolution will have caused a corruption due to the partial correlation of the reference function with the "repeated" range waveform.

In practice, the range data that is correlated is finite in extent. This is either due to the finite time window over which the received radar return is sampled, or due to the truncation of the range array to a "power of two" length. A point target return (of width τ) which straddles the ensuing discontinuity will only be partially correlated by the reference function[150].

If (D) is the number of array bins occupied by the range data this partial correlation will occur in the time region corresponding to array indices: [D-R] ⇒ [D]. However, this breakdown in the correlation process is "graceful" with a linear degradation in signal to noise ratio and resolution over the duration indicated.

For the SIR-B case the number of array bins (D) occupied by the range data is equal to 3415. To obtain a "power of two" this array was zero padded up to a length of 4096 or 2^{12}. The number of array bins (R) occupied by the range reference function is calculated to be 923.† The corruption of correlated data, caused by the cyclic convolution effect, limits the valid output data to array indices: [0] ⇒ [3172]. Corruption in a point target response, caused by the discontinuous data window, occurs over array indices: [2491] ⇒ [3414].

For the above reasons, the length of range array used in subsequent processing of the azimuth signal was limited to the first 2491 range array values.

3.3.3 INTERPOLATION USING THE FFT ALGORITHM.

The range processing algorithm involving demodulation and correlation can be combined efficiently into a single range processing algorithm as described by Welsh[151]. Diagram 3-5 shows the results of range processing on some simulated data for the SIR-B case. A single point target return is assumed. This signal is over sampled (or in the words of Barber "interpolated") and the reason is as follows: The process of demodulation, as described in Section 3.3.1, reduces the maximum frequency content of the range data to half the original value, as shown in Figure 3-4. By the Nyquist theorem this allows a halving of the required sampling rate in time[152]. An efficient digital technique for achieving this is described by

†The number of array bins occupied by the range reference function is given by the length of this function, τ, divided by the receiver sampling period dt.

Barber[153] and involves reducing the length of the Fourier transformed range array, after demodulation and correlation, to (N/2). The effect of this reduction in sampling rate on a simulated point target response is shown in Figure 3-6.

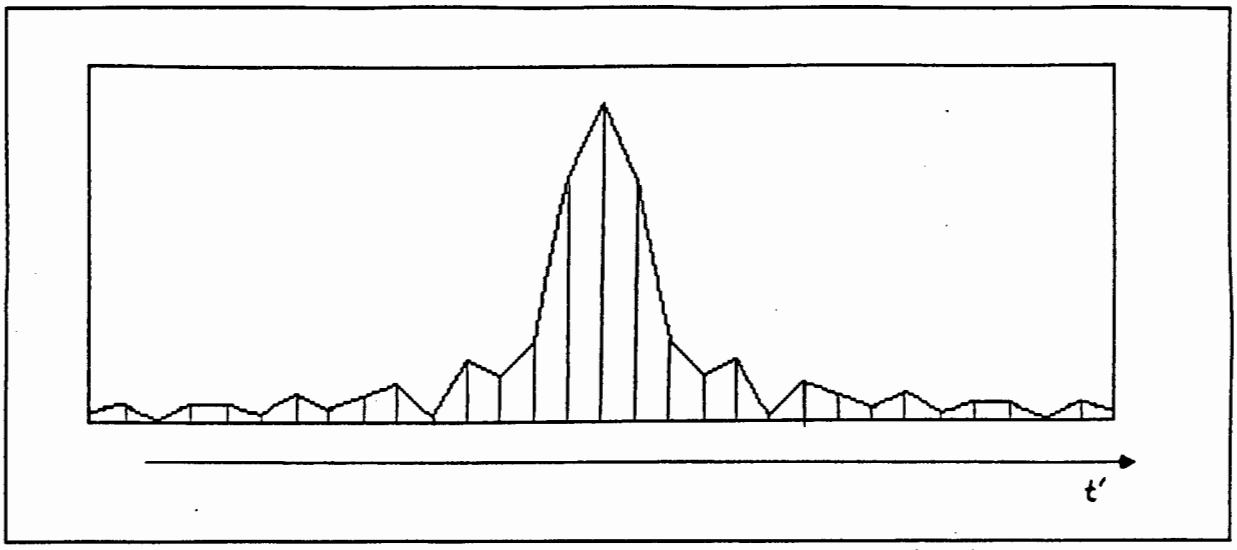

Figure 3-5: *Contents of range array after range processing of a simulated point target return. (SIR-B case)*

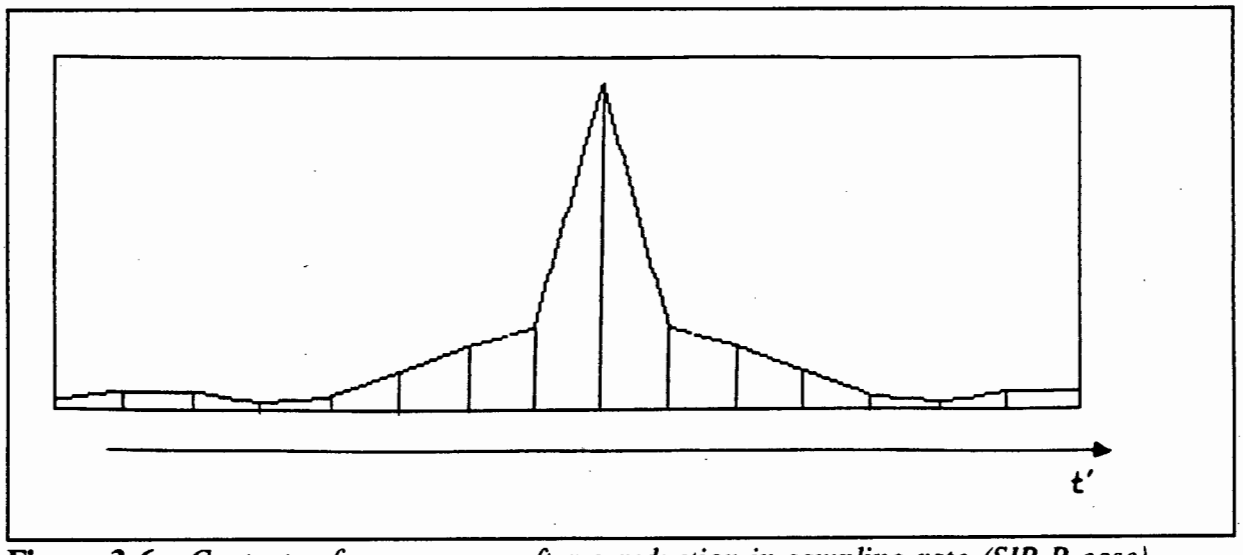

Figure 3-6: *Contents of range array after a reduction in sampling rate (SIR-B case)*

The obvious advantage of reducing the sampling rate is to limit the size of memory required in any subsequent processing. However, retaining the finer sampling in time has speed advantages in azimuth processing. Since sufficient memory can be made available on most

modern day computer systems, it was decided to leave the range array in its "interpolated" form.

3.3.4 A SENSITIVITY ANALYSIS OF THE RANGE CORRELATION PROCESS.

The accuracy of the correlation in range is directly dependent on the accuracy with which the chirp rate, a, is known in the calculation of the range reference function. For the SIR-B case, this parameter is known to a significance of 3 digits. The effects of a unit variation in the least significant digit of the chirp rate on the output of range processing is shown in Figure 3-7 for the case of a simulated point target. The point target response can be seen to be relatively insensitive to this variation.

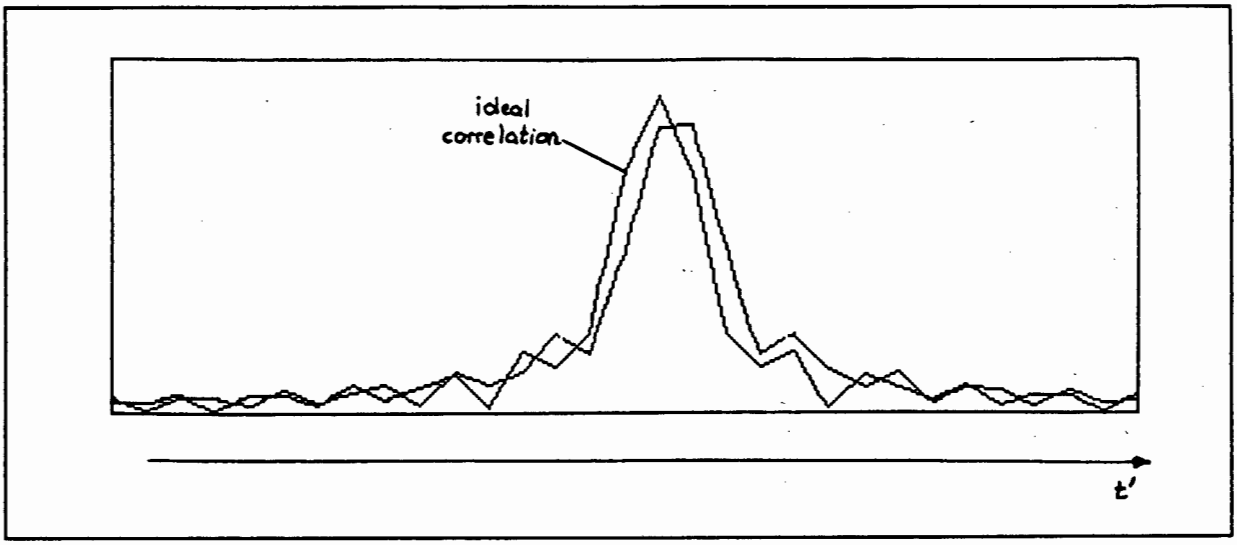

Figure 3-7: *The sensitivity of the range correlation process to changes in the reference function chirp rate.*

In more modern spaceborne SAR systems the accuracy with which system parameters such as chirp rate, PRF and transmit frequency are known, is very good. In particular, the proposed SIR-C system will derive all these system functions directly from a stable local oscillator (or STALO) clock whose frequency is known to a significance of 8 digits[154]. For this reason it will be possible to perform the range correlation very accurately in future SAR missions.

3.3.5 RANGE RESOLUTION.

In Appendix A3 an equation is given for a correlated complex chirp function. Using this result the correlated range waveform can be written as

$$y_r(t') = \left\{ 2\beta_r K_o \cdot \frac{\sin(\pi.2\beta_r.(t' - D_n))}{\pi.2\beta_r.(t' - D_n)} \right\} . e^{-j.\theta_n} \qquad (3\text{-}2)$$

with the first term representing the correlated (and delayed) chirp envelope function and the second term representing a sample of the doppler or azimuth waveform. β_r is equal to the bandwidth of the correlated chirp envelope and was shown in the sidelooking SAR case (see Section 2.8) to be equal to half the bandwidth, β_r', of the transmitted radar signal.

The range resolution in time, δ_n, can be calculated using Equation 2-10. This resolution is given in terms of a one way radial resolution by Elachi[155] as

$$\delta_{radial} = \delta_{rt} \cdot \frac{c}{2} \qquad (3\text{-}3)$$

and in terms of a ground range resolution as

$$\delta_r = \delta_{rt} \cdot \frac{c}{2\sin(\gamma)}$$

where γ is defined as the incident angle.

The transmit bandwidth, β_r', is given in Table 3-2 as 12 MHz and the incident angle in the SIR-B menu tape as 36 degrees. Substituting these values into the above gives a ground range resolution of 21 meters.

3.4 UNFOCUSSED AZIMUTH PROCESSING

For small synthetic aperture lengths the azimuth processing can be simplified to a coherent addition of the azimuth phase samples. As is described in Section 2.12, this technique is known as unfocussed azimuth processing.

The effective synthetic aperture length, L_a, over which coherent addition is performed, is usually limited such that the relative two way phase change (as measured form the centre of the synthetic antenna to one extremum) between the target and antenna does not exceed 90 degrees[156]. Cutrona gives this maximum aperture length as

$$L_a = \sqrt{r_o \lambda_o}$$

where r_o is defined as the relative radial distance from the antenna to the zero doppler position of a point target and λ_o is defined as the wavelength of the transmitted radar signal[157].

This synthetic length corresponds to a spatial azimuth resolution[158] of

$$\delta_a = \frac{1}{2}\sqrt{r_o \lambda_o}$$

In Appendix B1 it is calculated, for the SIR-B case, that the maximum unfocussed aperture length is equal to 250 meters (or 50 consecutive azimuth data values), and the corresponding azimuth resolution is equal to 125 meters.

Unfocussed azimuth processing was implemented on the range correlated SAR matrix to produce the image shown in Figure 3-8[159].

This image corresponds to an area which includes Buffelskop located in the Gannahoek mountain range, South of Cradock. The corresponding geography is easily discernable on aerial photographs and topographical maps of the area. (see Appendix D2)

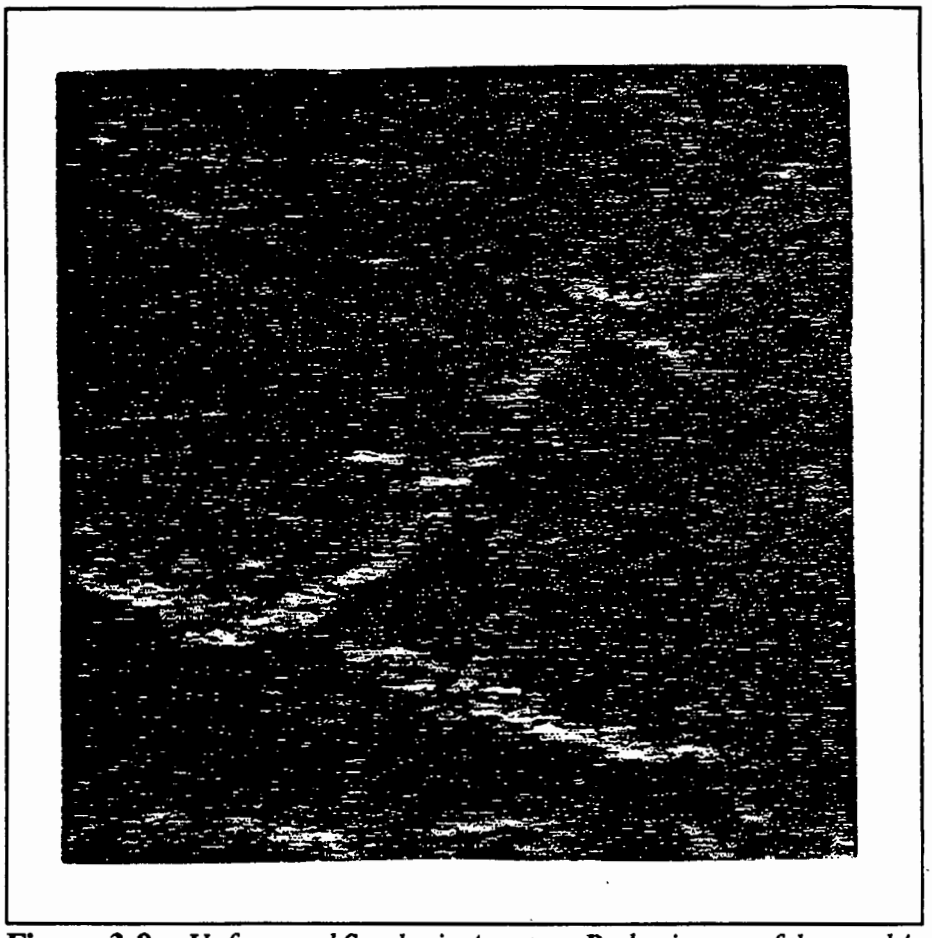

Figure 3-8: *Unfocussed Synthetic Aperture Radar image of the earth's surface. (The SIR-B experiment)*

3.5 FOCUSSED AZIMUTH PROCESSING

3.5.1 INTRODUCTION

It was shown in Section 2.16 that the azimuth waveform for a single point target return can be approximated by a complex chirp function of the form

$$f_a(t) = e^{j.2\pi.\left(\frac{1}{2}f_r t^2 + f_d t\right)} \qquad \alpha_{3dB}^{L} < t \leq \alpha_{3dB}^{U}$$

$$= 0 \qquad \textit{elsewhere}$$

An azimuth reference function can be calculated providing that the following two parameters can be estimated accurately:

a) A doppler centroid value, f_c, that is coincident with the azimuth boresight direction of the antenna.

b) The doppler rate, f_r.

"Autofocussing" and "clutterlock" techniques, as described by authors such as Li[160] and Elachi[161], are often used to estimate these terms. Both these techniques involve manipulation of the raw "azimuth data" as recorded by the spaceborne sensor and do not require any knowledge of the sensor's orbital geometry. The digital processor originally designed at JPL to decode the SIR-B data, uses clutterlock and autofocussing to estimate the form of the azimuth reference function[162]. However, Elachi argues that these techniques should only be used when the available orbital and attitude data for the satellite sensor in question is bad.

The algorithms developed in this thesis for azimuth correlation will use the orbital information directly.

3.5.2 AN ORBITAL GEOMETRY FOR SPACEBORNE SYNTHETIC APERTURE RADAR.

The predicted orbital trajectory (or "**ephemeris**") of a satellite is given with respect to an "**inertial reference frame**". This reference frame is defined to be stationary with respect to a rotating earth. It has as its origin the earth geocentre with the Z-axis along the rotational axis of the earth (positive north). The X-axis is defined to be in the direction of the vernal equinox. The Y-axis is orthogonal to the right hand system as defined by the X and Z axes directions[163].

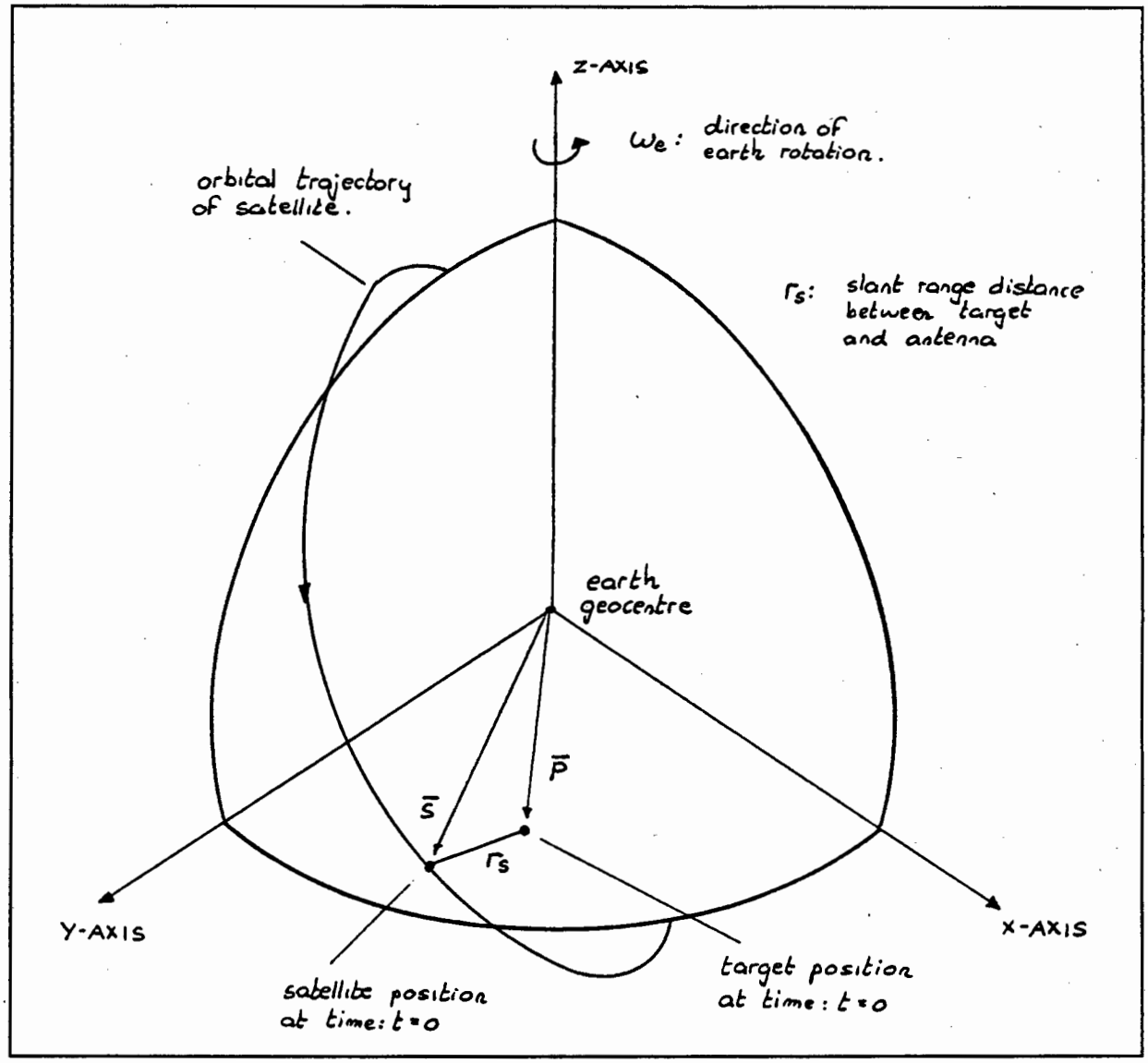

Figure 3-9: *Diagram showing the inertial coordinate system in which a specific target is to be located. (Adapted from Curlander)*

Figure 3-9 shows a simplified earth/satellite geometry in an inertial cartesian coordinate system. The earth is assumed to rotate at an angular velocity of ω_e radians per second within this coordinate system. S is defined to be the vector position of the satellite at time $t=0$ with respect to this inertial coordinate system. The slant range distance, r_s, to a point target, P, located in this target area is also shown.

3.5.3 GENERATING AN ACCURATE REFERENCE FUNCTION.

At a particular "azimuth time", defined for convenience to be $t=0$, the sidelooking Synthetic Aperture Radar platform occupies a certain position, S, in the inertial coordinate system shown in Figure 3-9. This inertial position can be measured fairly accurately by making use of measurements derived from satellite tracking stations and satellite orbital models (see Section 3.6.2). This position is usually included as a running variable with any raw radar data provided (see Table 3-3).

The real antenna beam is responsible for illuminating an area of the surface of the earth. The boundary of this target area is determined by the 3dB width of that antenna beam.

As explained in Section 2-17, the problem is to locate the doppler centroid position of a particular point target such that it lies as close as possible to the azimuth boresight of that antenna. In other words, the predicted target position at time t=0 should be as close as possible to the azimuth centre of the target area.

A suitable model can then be used to estimate the relative motion between the target and the antenna for the period of time that the target is located within this target area. Using this model, a doppler centroid frequency and doppler rate can be estimated for use in calculating an azimuth reference function.

In conclusion, it can be stated that the requirements for generating an accurate reference function are as follows:

a) A point target must be positioned (with respect to the antenna) such that at a particular time $t=0$ it is located on the measured direction of azimuth antenna boresight. (see Table 3-3).

b) A suitable model must be found to describe the relative motion of the target and antenna in three dimensional space, for the period of time during which the target is located within the target area.

3.6 THE ACCURATE POSITIONING OF A POINT TARGET WITH RESPECT TO THE SAR ANTENNA.

3.6.1 INTRODUCTION.

An accurate target placement technique, requiring no user interaction, has been proposed by Curlander[164]. In his paper Curlander describes how a target is located in inertial space by simply making use of the satellite ephemeris and the slant range distance from the satellite to the target in question. He assumes that an accurate model of the Earth geoid is available. A variation of the algorithm proposed by Curlander is now discussed.

3.6.2 AN ALGORITHM FOR ACCURATE TARGET POSITIONING.

The target positioning algorithm involves the following stages:

a) A plane is defined which passes through the satellite position, S, and includes the vector direction of the antenna azimuth boresight.

b) This plane intersects a model describing the earth geoid to form a locus of points.

c) The position on this locus, corresponding to the correct slant range between the antenna and target, gives the desired point target location in this inertial reference frame.

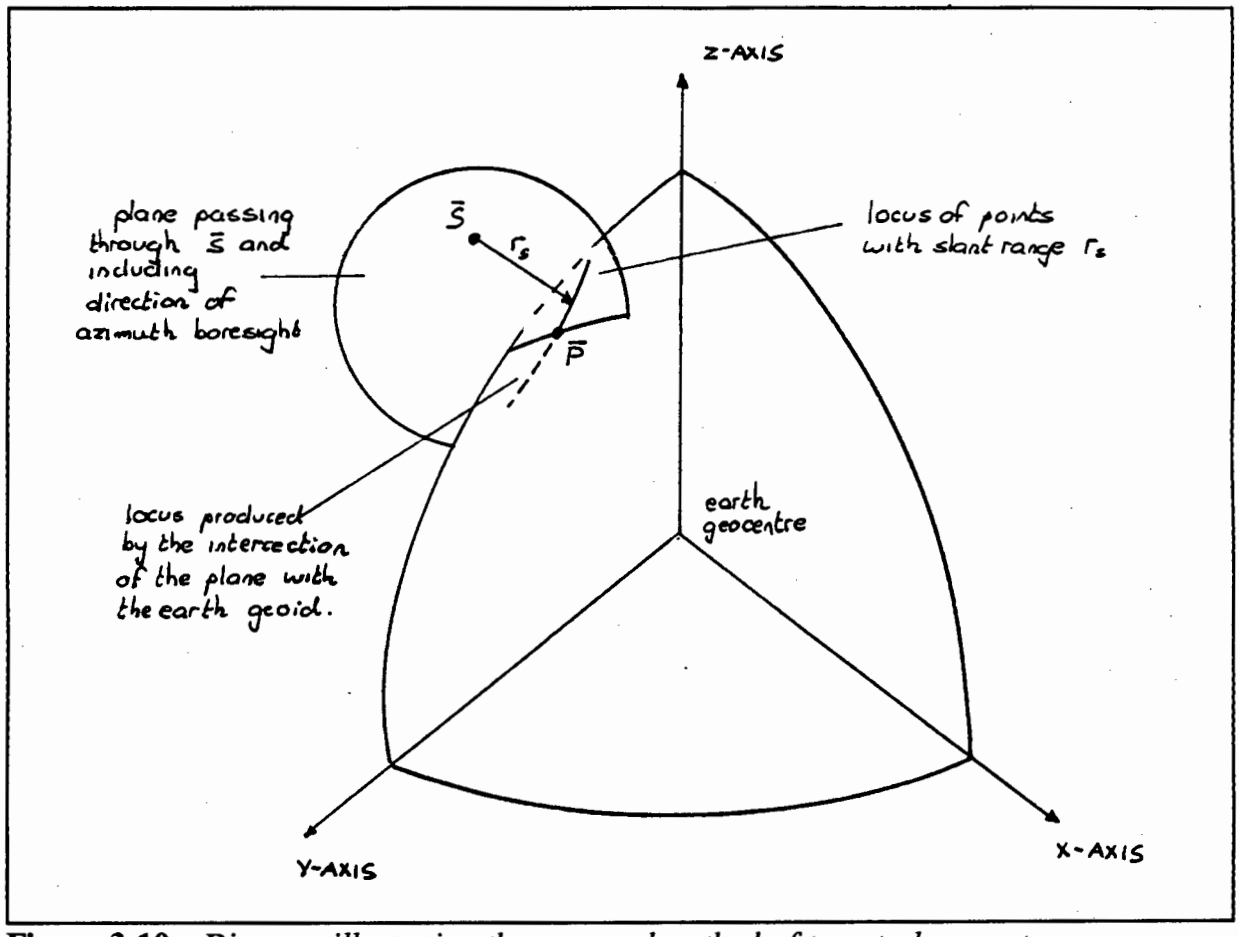

Figure 3-10: *Diagram illustrating the proposed method of target placement.*

The accuracy with which the target is placed with respect to the satellite depends on the accuracy with which the **satellite position** is known in inertial space, the **slant range distance**, and the accuracy of the **model** used to describe the earth geoid.

The ability to position this target so as to be coincident with the azimuth direction of maximum antenna power depends on the accuracy of the antenna boresight direction. These four variables will now be discussed in turn:

The Position (and Velocity) of a Satellite in Inertial Space.

Satellite position and velocity information obtained via ground tracking stations is used in orbital models to estimate a satellite's trajectory with respect to an inertial reference frame. This trajectory is then synchronised with the radar data recording system of the satellite in question[165]. The ephemeris can be calculated directly from this trajectory information.

In the case of the SIR-B data recording system the ephemeris information is updated every ten PRI's and included as "header information" in the raw data file. (An example of the type of information provided, is given in Table 3-3.) The ephemeris at the chosen azimuth time t=0 can be obtained by a simple extrapolation of the ephemeris data.

The Slant Range Distance (r_s).

The slant range distance can be estimated directly from the SAR data collection system independently of satellite geometry. The slant range to point targets located at the near edge of the target area at time t=0 is determined by the time delay from when pulse transmission took place to when the first sample of range data (corresponding to range array index [0]) is recorded. The time delay to points located further into the target area (larger range array index values) is given by the original time delay plus a suitable offset. The value of this offset can be calculated by multiplying the relevant range array index value by the sampling period of the range waveform. This method of slant range determination is inherently more accurate that any geometrical estimate[166].

Modelling the Earth Geoid:

Curlander limits his discussion to target placement for oceanic applications. The "25th degree harmonic model" is proposed for predicting sea level distance from the inertial

geocentre. This model predicts a surface height, accurate to better than 4 meters[167]. For calculations simply aimed at predicting an accurate reference function, an earth model of this accuracy is not required. The target placement algorithm proposed in this thesis uses the simpler geodal model.

For land based applications the height of the ground terrain above the predicted sea level height must also be included in any earth model. This height can only be obtained from topographic maps and, therefore, some prior knowledge is, required as to the approximate location of the target area on the earth's surface before an accurate estimate of point target position is made.

The solution to this problem is to produce a preliminary image of the target area based on the best estimates available at that time. This image can then be matched up (see article by Noack[168]) with topographic maps and the height of a point target calculated. This height is then superimposed on the earth model before reimplementing the target placement algorithm.

The Direction of Antenna Boresight:

The attitude of a spaceborne SAR sensor is usually given in terms of the attitude of the onboard radar antenna[169]. Therefore, the azimuth pointing direction of the antenna boresight can be established from this attitude data.

The attitude of a spaceborne antenna is estimated directly from sensors located on the satellite in question. For the proposed RADARSAT system, the attitude control system will be designed to "... maintain the spacecraft, pointing with the accuracy of better than $\pm 0.1^\circ$ about all three axes."[170] In the SIR-C system specialised PRF hopping techniques are proposed for the accurate measurement of antenna pointing direction[171]. No information was available at the time of writing on the accuracy of the SIR-B antenna attitude. However, the assumption is made that the attitude measurement displays the necessary accuracy.

Small misalignments between estimated target position and azimuth antenna boresight, that are in the order of a fraction of a degree, are not serious in terms of signal to noise ratio falloff. **Furthermore, the prediction of antenna attitude, beyond the accuracy required to prevent ambiguity, is not a requirement for target position prediction[172].**

3.6.3 A DISCUSSION OF THE TARGET POSITIONING ALGORITHM AS USED IN THE DECODING OF SIR-B DATA.

The position of zero time (t=0) was fixed at an arbitrary azimuth position (or column) in the raw SAR data matrix. Associated with this position were numerical values for the SIR-B antenna attitude, ephemeris, and slant range distance, as given in Table 3-3. The pointing direction in azimuth of the antenna boresight can be established from this attitude data. The information given in Table 3-3 indicates that the azimuth boresight direction lies in a plane having the shuttle (satellite) motion vector as its normal[173]. An average terrain height of 1000 meters for the target region was obtained by matching up an unfocussed SAR image of the region in question (Figure 3-8) with topographic maps. (see Appendix D2)

The above information was used as input variables to the target placement algorithm discussed in Section 3.6.2. A detailed description of the implementation of this algorithm is given in Appendix B2.

3.6.4 A SENSITIVITY ANALYSIS OF THE TARGET POSITIONING ALGORITHM.

The accuracy with which a target is placed depends on the accuracy with which the separate input variables are known. These variables will now be discussed in turn.

Ephemeris data:

The precision ephemeris as provided with JPL data[174] is accurate to "... 50 m along track and 30m radially and cross track. " This figure is typical of the accuracies expected for other proposed SAR system[175].

Slant range distance:

The accuracy with which the slant range distance can be established for a typical spaceborne SAR system is not known. The slant range distance as provided in the SIR-B menu tape (see Table 3-3) is quoted to an accuracy of ten meters. In the light of Curlander's article on pixel placement in the Seasat SAR case, this accuracy figure can be viewed with scepticism. Curlander estimated that for the Seasat data collection system an inaccuracy of less than 100 meters could be expected[176]. This somewhat conservative estimate of slant range accuracy can be assumed to be a worst case figure.

Earth model:

The geoidal earth model has a worst case inaccuracy of about 100 meters off the tip of Africa[177].

Curlander quotes a rule of thumb formula for the magnitude inaccuracy in target placement:

$$\Delta(M_e) = \frac{\Delta r}{\sin(\psi)}$$

where ψ is defined as the incident angle and Δr is defined as an uncertainty in range[178]. Since the radial error in the earth model and slant range can be expected to be no worse than 100 meters in any SAR system, a cumulative range error of 200 meters can be expected. Using the above equation a worst case magnitude range error of about 350 meters will occur in the estimate of target position.

However, local variations in earth terrain height have a much greater impact in target positioning error. In the Cradock region, in particular, the local variations in terrain height are of the order of one thousand meters (see topographic map included in Appendix D2). If only an average estimate of terrain height over the target area is used in the target location

algorithm††, it is obvious that range error caused by these local variations will dwarf any of the range error figures given above. Range error caused by slant range and geoidal errors can therefore be ignored in favour of the error caused by terrain fluctuations.

The effects of range error on the accuracy of the azimuth correlation process can be treated under the more general heading of "Depth of Focus" as is discussed in Section 3.10. In this section an equation is given for the change in one way range distance that can be tolerated before the azimuth correlation process begins to break down. This figure will be shown to be much larger than the local fluctuations in radial position caused by terrain variations over the target area. For this reason these variations can be ignored.

3.7 MODELLING THE RELATIVE MOTION BETWEEN THE SAR ANTENNA AND A POINT TARGET.

3.7.1 INTRODUCTION.

A suitable model is required to describe the motion of the target and antenna in three dimensional space, for the period of time during which the target is located within the target area. Using this model, a doppler centroid frequency and doppler rate can be calculated so as to estimate the form of the azimuth reference function.

Wu states that a two way phase deviation of 180 degrees from the actual azimuth waveform can be tolerated at the extrema of the reference function. A larger error will severely degrade the azimuth correlation of a point target response[179]. The peculiarities that exist in the geometry of the SAR system due to the curved orbit path and planetary motion make this specification very difficult to meet using some of the more simplistic models of target and

††Which is the case in all SAR processing algorithms that the author is aware of.

antenna motion described in the literature[180] [181]. A more accurate model is needed for the calculation of an azimuth reference function. Such a model is now described:

Wu point out that the "... coefficients of the quadratic function (azimuth function) are determined (only) by the relative motion vectors between the satellite and target."[182] This is illustrated in Figure 3-11. In this figure the vector V_s represents the instantaneous satellite velocity and the vector V_p the instantaneous target velocity at time t=0. The motion of the target and satellite can be modelled using these two directed velocity vectors for the short time duration required to generate the length of azimuth waveform required for azimuth processing. The relative one way radial distance, r, between target and satellite is simply given by the position of the target subtracted from the the position of the antenna, as a function of time. All position and motion vectors are given with respect to an inertial reference frame as defined in Section 3.5.2.

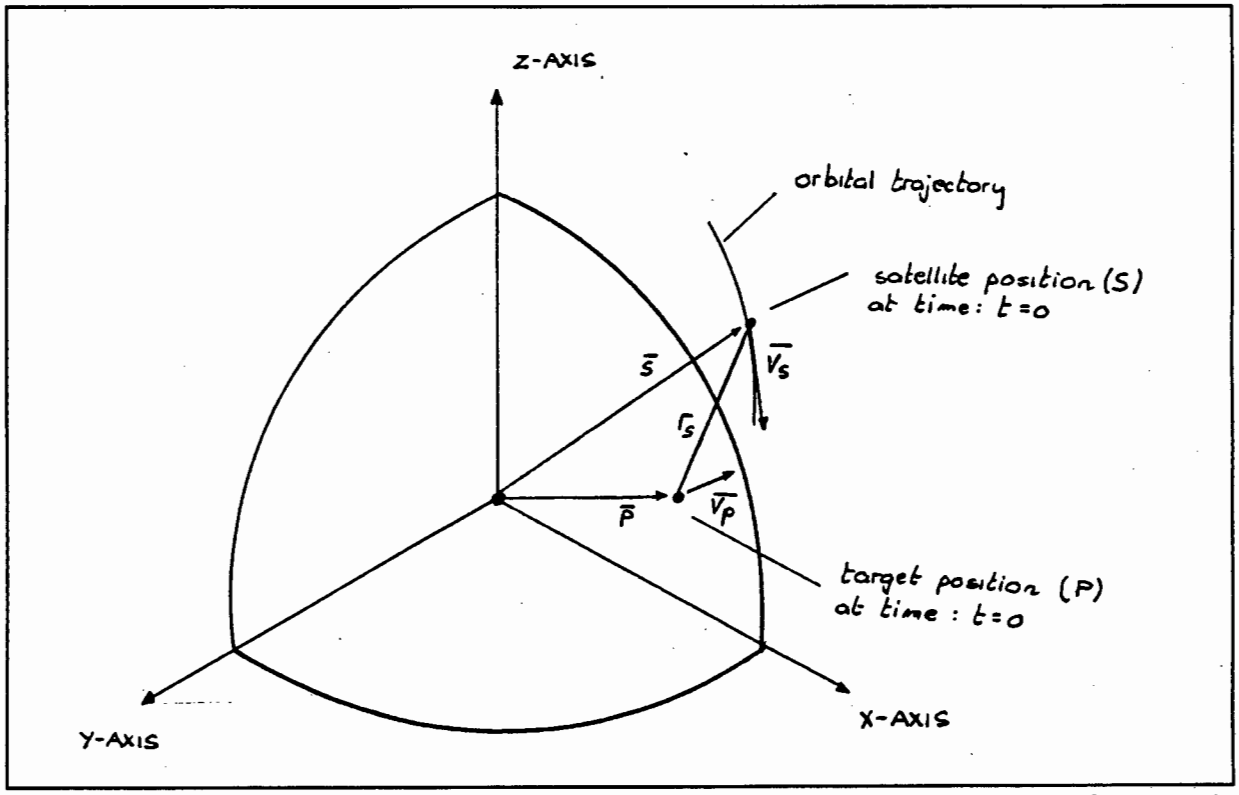

Figure 3-11: *The motion of the satellite (shuttle) and target expressed as directed vectors in 3D space (adapted from Wu)*

3.7.2 MODELLING THE MOTION OF THE SATELLITE AND TARGET AS TWO DIRECTED VELOCITY VECTORS.

The instantaneous velocity vector of a satellite can be obtained directly from the ephemeris data which is included with any raw radar data. This is discussed in Section 3.6.2. The instantaneous velocity component of target motion (with respect to this inertial coordinate system) arises as a direct result of the rotation of the earth.

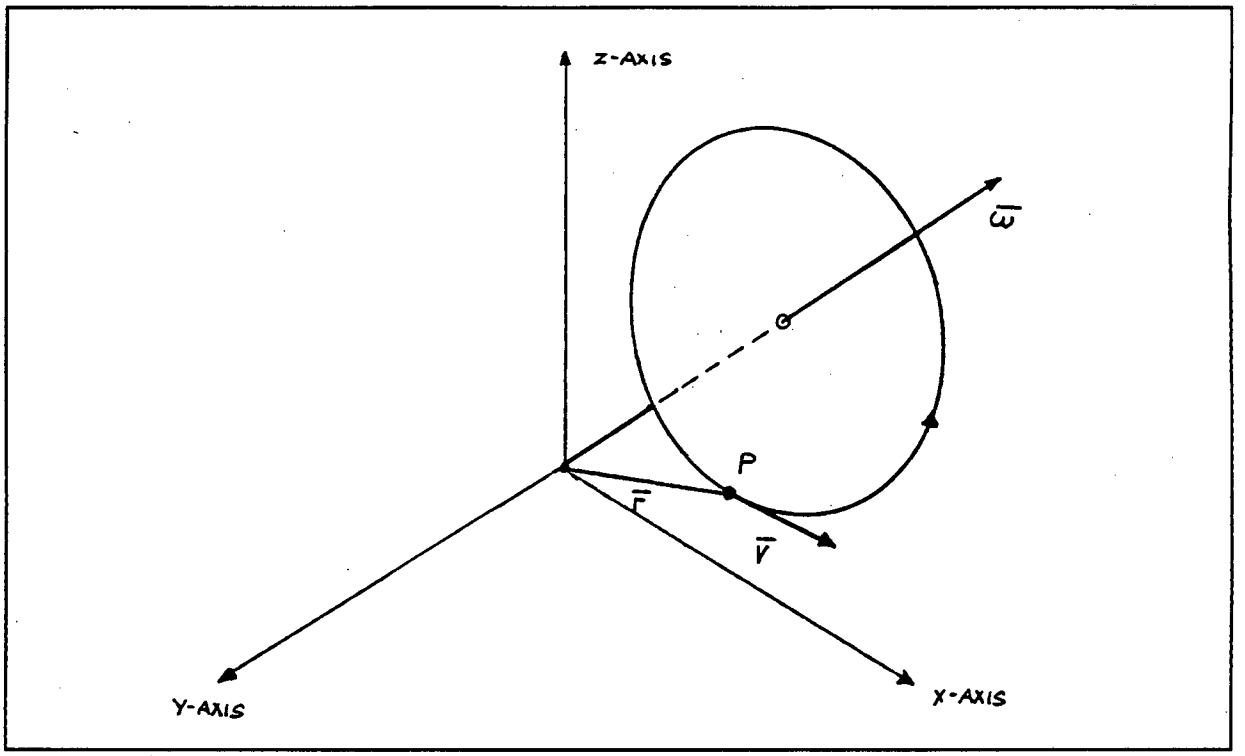

Figure 3-12: *Diagram showing the instantaneous vector velocity of a rotating point target (adapted from Meirovitch)*

The conversion of an angular velocity component of target motion to an instantaneous velocity vector can be done by making use of the "theorem of Coriolis"[183]. For pure rotational motion this theorem states that the instantaneous velocity is given by the cross product of a vector describing the angular velocity of the target with a vector describing the position of that target. This can be expressed mathematically as

$$\bar{v} = \bar{\omega} \times \bar{r}$$

The angular velocity vector, ω, is defined as a vector that is coincident with the instantaneous axis of rotation[184]. This is shown in Figure 3-12.

The rotation of the earth can be described as an angular velocity vector coincident with the z-axis of the inertial coordinate system, having as magnitude, the speed of earth rotation, expressed in radians. The instantaneous velocity of a target is then simply given by the cross product of this vector with the target position vector *P*. A more detailed description of this technique is given in Appendix B3.

3.7.3 AN ANALYSIS OF THE RELATIVE MOTION BETWEEN THE TARGET AND ANTENNA.

The motion of the target and antenna has now been modelled as two directed velocity vectors respectively. The generation of an azimuth reference function involves predicting the relative motion between target and antenna[185]. For this reason the antenna can be assumed to be fixed in space and the velocity of the target described as a directed three dimensional vector, V, equal to the vector sum of the target velocity vector, V_p, and satellite velocity vector, V_s.

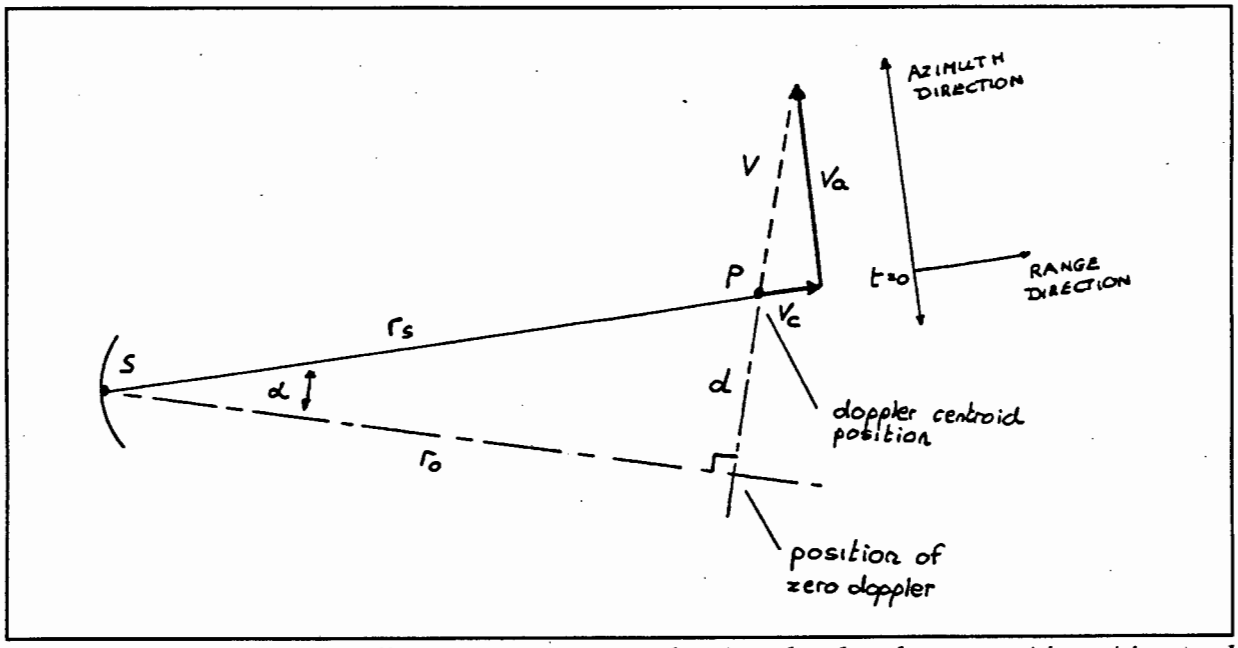

Figure 3-13: *Relative satellite/target geometry showing the doppler centroid position and target velocity* ***V*** *relative to an assumed stationary antenna.*

This "3D" geometry can be simplified to two dimensions by envisaging a plane passing through the satellite and target positions and containing the velocity vector, V. This plane is represented in Figure 3-13. An inspection of this figure reveals that there is no difference

between this geometry and the one described in Section 2-17 for the case of a simple sidelooking Synthetic Aperture Radar with a target illumination area that is offset from the zero doppler position. (see Figure 2-11 and Figure 2-12)

Point S is the position of an assumed stationary antenna. Point P is the target position at time t=0 (the doppler centroid position) and is removed a distance d away from the position of zero doppler. The slant range distance is given as r_s and the distance between the position of zero doppler and the antenna as r_o.

As is described in Section 2.17.2 the resultant velocity vector, V, can be resolved into an "along track" and "cross track" component of motion. The aspect angle, α, at the doppler centroid position is then simply given as the inverse tangent of along track velocity, V_c, over cross track velocity, V_a.

The cross track component of velocity shown in Figure 3-13 is due mainly to the rotation of the earth[186]. Since the azimuth antenna beam is usually orientated perpendicular to the satellite velocity vector, it is this velocity component that causes the target illumination area to be shifted away from the zero doppler position[187]. Both Tomiyasu and Barber suggest redirecting the antenna beam so as to illuminate this zero doppler position, in so doing removing this cross track component of relative velocity[188]. However, the discussions in Section 2.17.1 and Section 3.9.3 show that this cross track component of velocity can be accommodated fairly easily in digital azimuth processing.

3.8 COMPUTING AN AZIMUTH REFERENCE FUNCTION FOR THE SIR-B CASE.

3.8.1 INTRODUCTION.

The values of along track and cross track velocity, obtained using the model for relative motion, can be used to estimate the doppler centroid frequency and doppler rate. This is

discussed in detail in Appendix B4. Once the Doppler frequency and rate have been calculated an azimuth reference function can be determined.

3.8.2 ALIASING OF THE AZIMUTH OR DOPPLER WAVEFORM.

Based on the SIR-B SAR parameters in Table 3-1 and Table 3-2 an azimuth reference function is calculated. In Appendix B4 it is shown that for a target located at the range centre of the target area this reference function is equal to

$$f_a(t) = e^{j.2\pi\left(\frac{1}{2}f_r t^2 + f_d t\right)}$$

$$= e^{j.2\pi\left(\frac{(-1742)}{2}t^2 + (1568)t\right)}$$

The doppler centroid frequency of the above reference function is equal to 1568 Hertz. The azimuth sampling rate (or PRF) as used by the SIR-B system is given in Table 3-2 as 1463.8 Hertz. Since this sampling rate corresponds to a Nyquist frequency of 731.9 Hertz, the azimuth waveform as recorded by the SIR-B system is an alaised version of a spectrum located at a higher frequency. This aliasing occurs because of the large doppler component (doppler centroid frequency) introduced into the azimuth reference by the effects of earth rotation[189]. (see Section 3.7.3)

As is explained in Section 2.17.3 this aliasing does not present a problem in azimuth processing since a sampled version of the azimuth reference function will be aliased in exactly the same way.

3.8.3 A CHANGING DOPPLER CENTROID FREQUENCY.

The instantaneous Doppler frequency return of a point target located at the Doppler centroid position P is given by the doppler frequency of the azimuth waveform at time t=0. This instantaneous frequency has been defined previously as the Doppler centroid frequency, f_c. (see Section 2.17.1)

At time t=0 every point in the target area has associated with it an instantaneous Doppler frequency. The distribution of these Doppler values is described by authors such as Wehner[190] and Elachi. Elachi states that "... Points distributed on coaxial cones, with the flight line (of the shuttle) as the axis and the radar as the apex, provide identical Doppler shifts of the return echo... The intersection of these cones with a flat surface gives a family of hyperbolas. Objects on a specific hyperbola will provide equi-doppler returns."[191] This is illustrated in Figure 3-14.

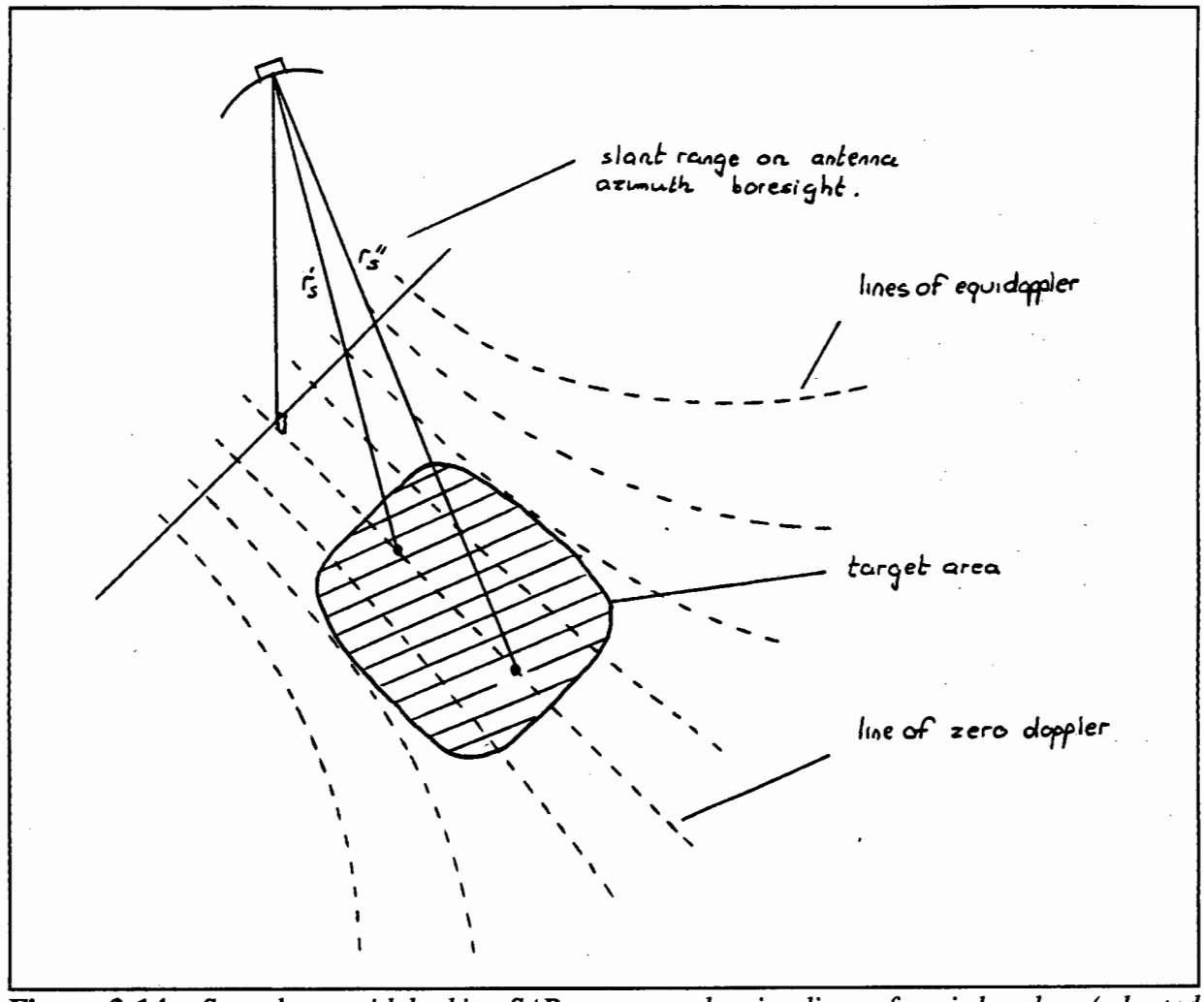

Figure 3-14: *Spaceborne sidelooking SAR geometry showing lines of equi-doppler. (adapted from Elachi)*

If the predicted azimuth boresight of the antenna is coaligned with the line of zero doppler it would be expected that points on this boresight with different slant range distance would have the same doppler centroid frequency associated with them. This is self evident from Figure 3-14.

The azimuth reference functions for a point target located at the near edge of the target area and one located at the centre of the target area are calculated in Appendix B4 for the SIR-B case. These reference functions are given respectively as:

$$f_a(t)' = e^{j.2\pi\left(\frac{(-1781)}{2}t^2 + (1493)t\right)}$$

and

$$f_a(t)'' = e^{j.2\pi\left(\frac{(-1742)}{2}t^2 + (1568)t\right)}$$

The Doppler centroid frequency associated with these two functions differs by a large amount. This is in contradiction to the argument given in the above paragraph.

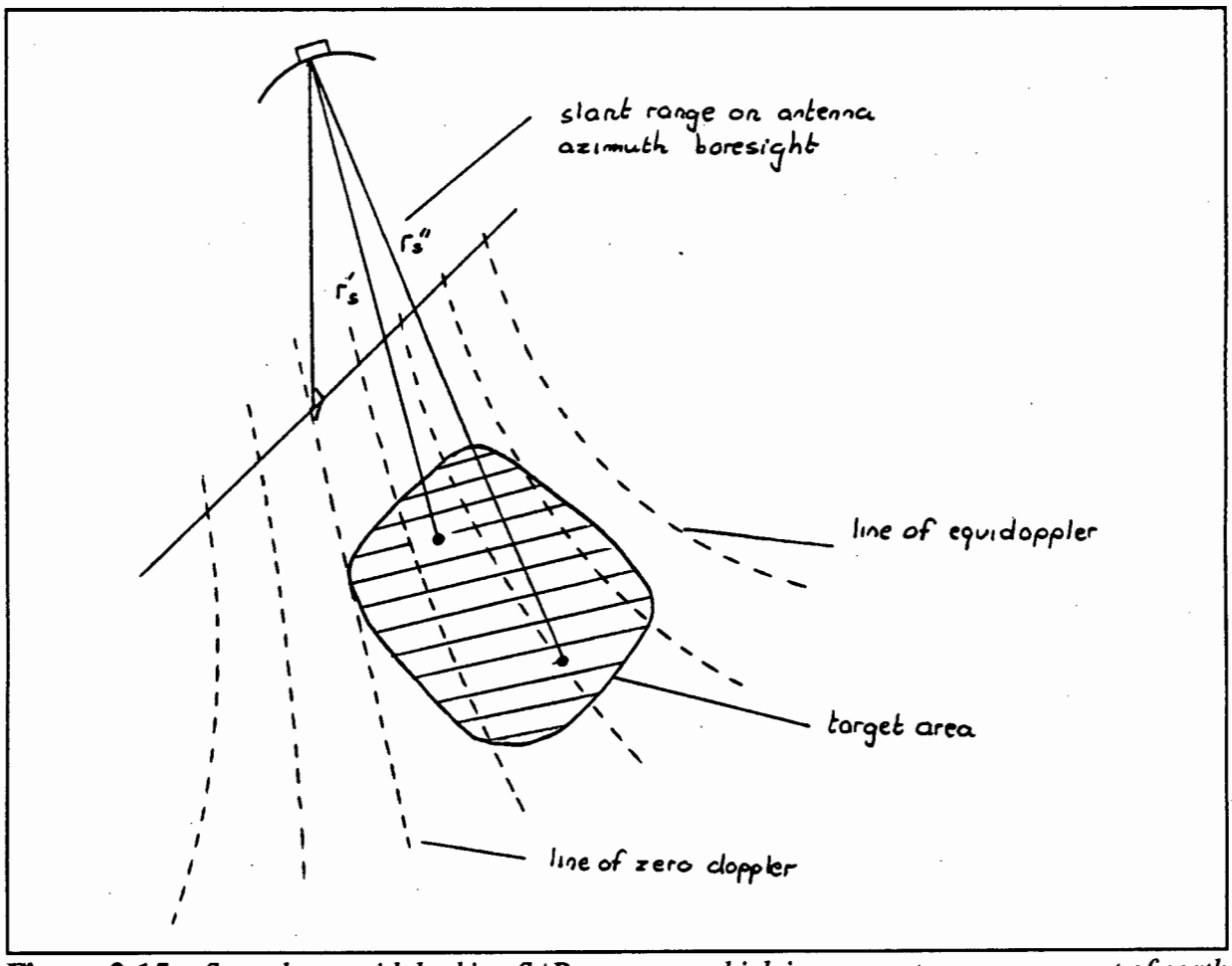

Figure 3-15: *Spaceborne sidelooking SAR geometry which incorporates a component of earth rotation. The lines of equi-doppler are shown.*

The problem arises because the effects of earth rotation have been ignored in the loci of equi-doppler sketched in Figure 3-14. The earth rotation produces an instantaneous vector component of target velocity (as calculated in Section 3.7.2) that must be included in any model of relative motion (or relative Doppler). As explained in Section 3.7.3 this vector component of target velocity has the effect of skewing the line of zero doppler away from the target area. This is shown graphically in Figure 3-15.

Points located on the azimuth boresight of the antenna are no longer situated on a locus of constant doppler. The doppler centroid frequency associated with these target positions will therefore vary with slant range distance[192]. The effect that this will have on azimuth processing is discussed in Section 3-10 under the heading of "Depth of Focus".

The effects of earth rotation on the location of the target area with respect to the lines of equi-doppler can be likened to the effects of a yaw error in antenna azimuth pointing direction as explained by Elachi[193]. In fact it is described in Section 3.7.3 how the introduction of an artificial yaw error can realign the target area with the locus of zero doppler.

3.9 AZIMUTH CORRELATION.

3.9.1 RESOLUTION IN AZIMUTH.

Resolution of a point target in azimuth is achieved by correlating the complex azimuth waveform

$$f_a(t) = e^{j.2\pi\left(\frac{1}{2}f_r t^2 + f_d t\right)}$$

with a reference function of the same form[194].

The result of correlating a single point target response in azimuth is shown in Appendix A7 to be

$$y_a(t) = \left| \beta'_a K . \frac{\sin(\pi \beta'_a t)}{\pi \beta'_a t} \right|$$

where β'_a is a numerical value equal to the range of frequencies (positive and negative) occupied by the length of azimuth signal used in azimuth correlation. In Section 2.11.2 the azimuth resolution (in time) was expressed directly in terms of this doppler bandwidth as

$$\delta_a = \frac{1}{2\beta_a} = \frac{1}{\beta'_a}$$

If the reference function covers a length of time, T_a, (symmetrical about t=0) the doppler frequency spread, β_a', is simply given as the product of the Doppler rate, f_d, and T_a. Using this figure for β_a', an azimuth resolution figure (in terms of time) can then be calculated. This time resolution, δ_{at}, can be converted to a spatial resolution, δ_a, simply by multiplying δ_{at} by the relative magnitude velocity, V, between the satellite and the target. This can be summarised as follows:

$$\delta_a = \frac{|\overline{V}|}{f_d . T_a} \qquad \textbf{(3-4)}$$

This method for calculating azimuth resolution is also described by Wu who states that "...Most of the reported work analyses the SAR resolution from a synthetic aperture point of view[195 196]. However, this model lacks the flexibility for incorporating such variations as curved sensor orbital flight path and a moving target surface... A more generalised approach is to analyze the problem in the Doppler frequency domain."[197] The azimuth resolution expressed in terms of Doppler bandwidth is also given by Kovaly in an identical form[198].

In Appendix B6 it is shown that for the SIR-B case, 256 samples of the predicted azimuth reference function need to be used to achieve an azimuth resolution that is compatible with the resolution of 21 meters in range. This requires that the azimuth reference function be

sampled with a period T symmetrically about zero to form an "**azimuth reference array**" of 256 points in length. The point target response is then correlated with this reference array.

The total Doppler bandwidth that is available for azimuth processing is limited by the 3dB azimuth beam width of the real antenna beam pattern (see Section 2.15). This bandwidth is usually a number of times greater than the bandwidth required to achieve the same resolution figure in azimuth as is obtained in range[199]. Separate azimuth reference functions can be generated that utilise separate subsections of the available bandwidth. These reference functions can be separately correlated with the point target response to form a number of images (or "**looks**")of that target[200]. These separate looks can be incoherently added to remove a degrading effect (specific to coherent imaging systems) known as speckle (or fading). This effect is described in detail by authors such as Elachi[201] and Li[202].

In the decoding of SIR-B data, only single look processing has been performed at this stage.

3.9.2 THE EFFECTS OF RANGE MIGRATION ON AZIMUTH CORRELATION

The equation for the correlated range waveform of a single point target response was derived in Section 3.3.5 to be

$$y_r(t') = \left\{ 2\beta_r K_o . \frac{\sin(\pi . 2\beta_r . (t' - D_n))}{\pi . 2\beta_r . (t' - D_n)} \right\} . e^{-j.\theta_n}$$

This function consists of a correlated envelope function modulated by a complex exponential term. The complex exponential term (or phase delay term) changes on a pulse to pulse basis as a function of azimuth time. A set of these complex phase terms makes up the discrete azimuth or Doppler waveform, which is discussed in Section 2.7

The envelope function is delayed by an amount directly proportional to the relative radial distance, r, between the antenna and target as a function of absolute time t. Therefore, the peak of this envelope function describes a locus through the range correlated SAR matrix[203]. A typical such locus is shown in Figure 3-16.

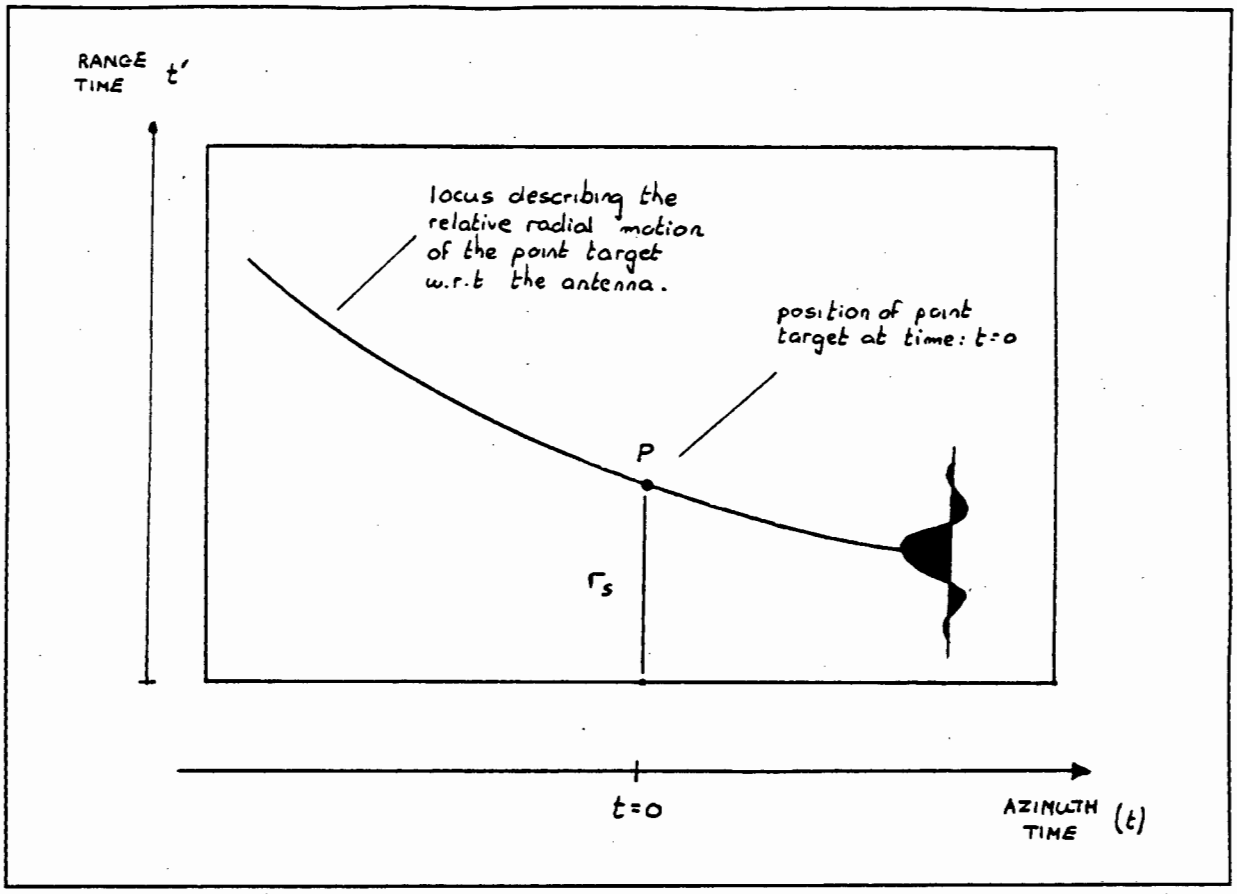

Figure 3-16: *The typical locus of a point target response as seen in the two dimensional SAR matrix.*

In this figure, r_s represents the radial distance to the point target, *P*, at time t=0. The direction of increasing azimuth time ($t=nT$) and increasing range time, t', is also shown. The locus, as generated by the SIR-B system, is shown for a single point target in Appendix C2.

This locus is generally known as the "**migration curve**" in the SAR literature. Azimuth correlation involves correlating an array containing the sampled reference function with an array containing samples of the doppler or azimuth waveform for a particular point target. However, the effects of migration cause the azimuth waveform to be spread over a number of rows in the SAR matrix. Efficient azimuth correlation require that the sampled azimuth waveform be confined to a single row of the SAR matrix[204]. For this reason the effects of migration must be corrected for. The correction techniques that were implemented in the azimuth processing of SIR-B data will now be discussed.

3.9.3 RANGE WALK CORRECTION.

Azimuth migration correction techniques are concerned with the component of target migration which occurs over the azimuth processing window shown in Figure 3.17. This processing window occupies an azimuth length equal to the length of the chosen reference function and is located symmetrically with respect to time t=0.

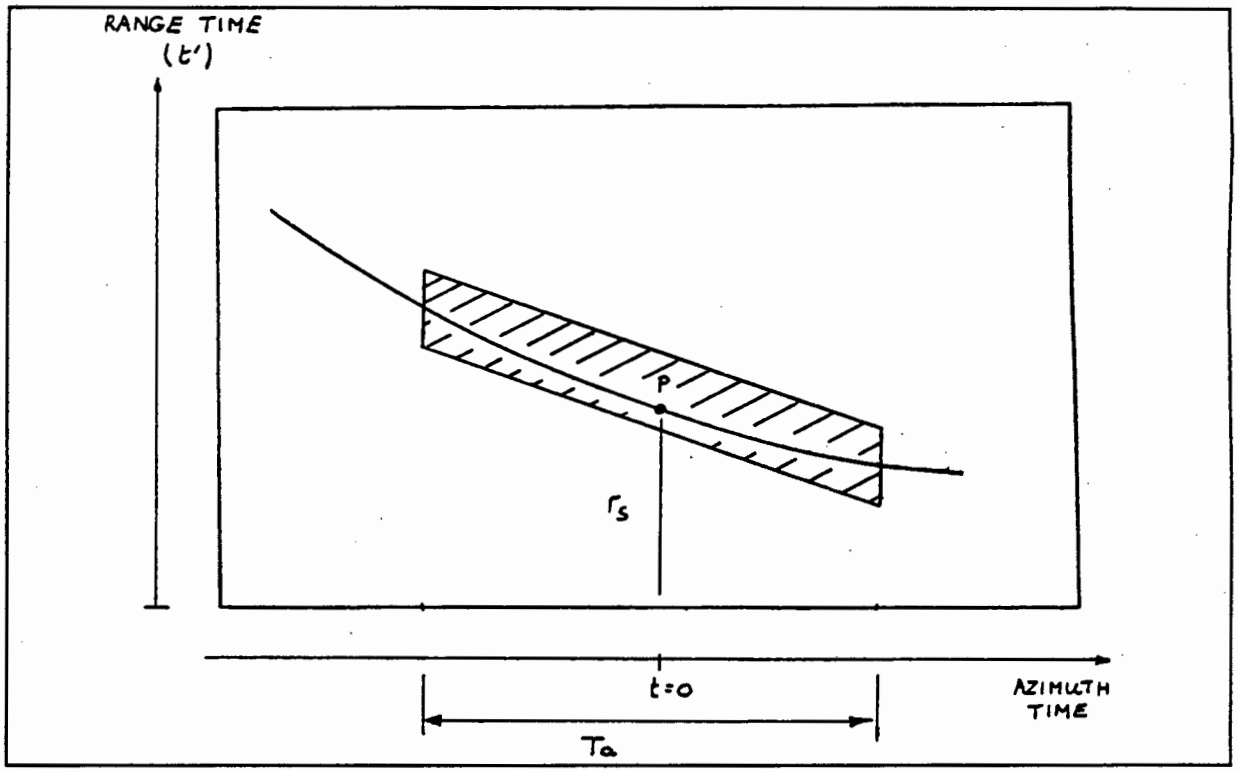

Figure 3-17: *Range migration over an azimuth processing window that is located symmetrically with respect to time t=0.*

The migration curve shown in Figure 3.17 can be split into two separate loci which are termed the **"range walk"** and **"range curvature"** components of relative radial motion[205]. The range walk is defined as the difference in one way radial distance (range) to a point target *P* at the left edge of the azimuth window relative to the right edge of this window[206]. Therefore, the range walk figure is dependent on the length of azimuth processing window used during correlation. The range curvature is then simply defined as the component of target motion not covered by the range walk component. This is shown in Figure 3-18.

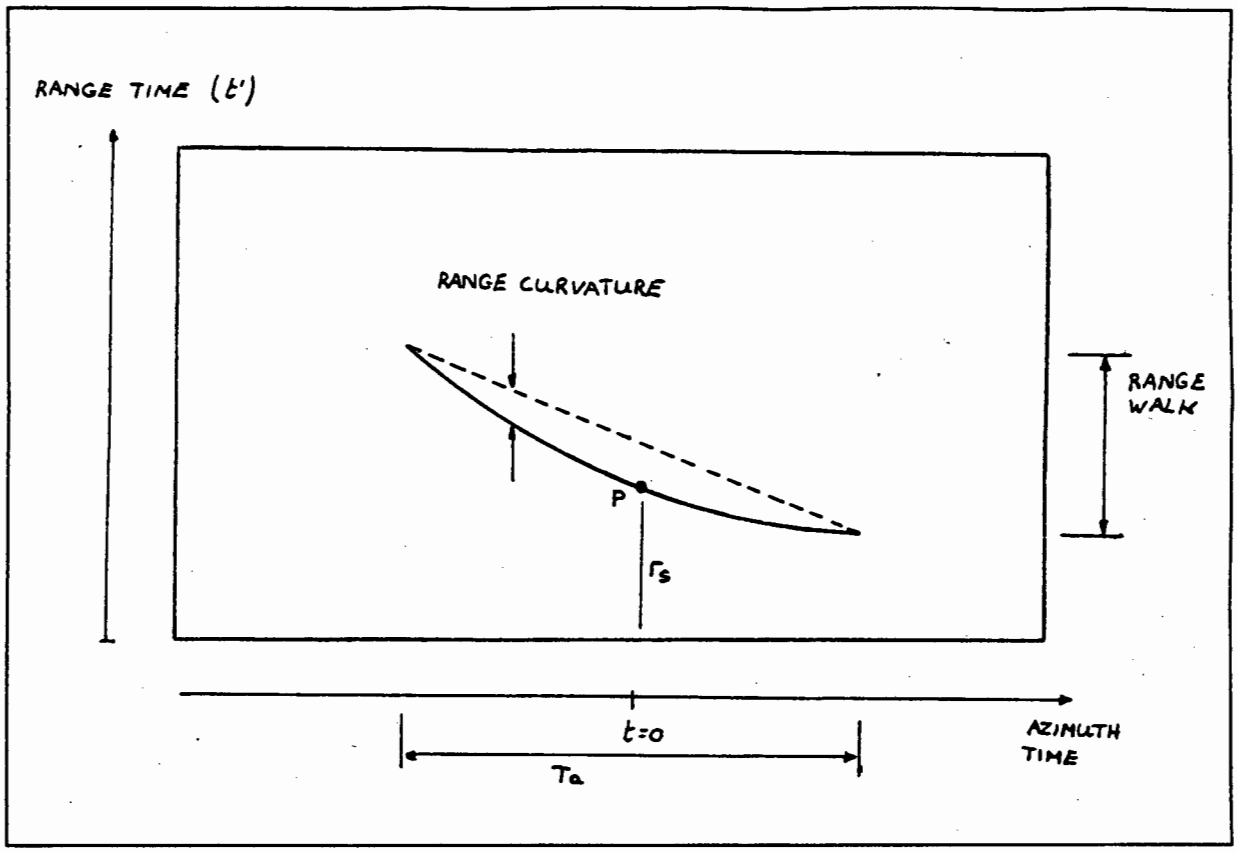

Figure 3-18: *Range walk and range curvature in a range correlated SAR matrix. (adapted from Wu)*

The range walk is caused by the cross track component of relative target motion and the range curvature by the along track component[207]. (see Section 3.7.3)

The migratory effects of range walk can be compensated for by a simple linear skewing of the locus describing the azimuth waveform over this azimuth processing window. Munson points out that the magnitude of range walk for all point targets in the target area can be considered constant when compared to the size of one range cell[208]. For this reason the effects of range walk can be corrected for all targets located in the SAR matrix by simply skewing the azimuth processing window of each point target by a radial amount equal to the total range walk component.

However, it is not necessary to skew each point target response in turn. If the full azimuth length of the SAR matrix is skewed by an amount equal to the range walk as measured from the left edge of the SAR matrix to the right edge, the range walk of all target loci contained within that matrix will be corrected for. This is a more efficient procedure in terms of

processing time and, therefore, is implemented before azimuth correlation of the SIR-B SAR matrix. A representation of the SAR matrix after skewing is shown in Figure 3-19.

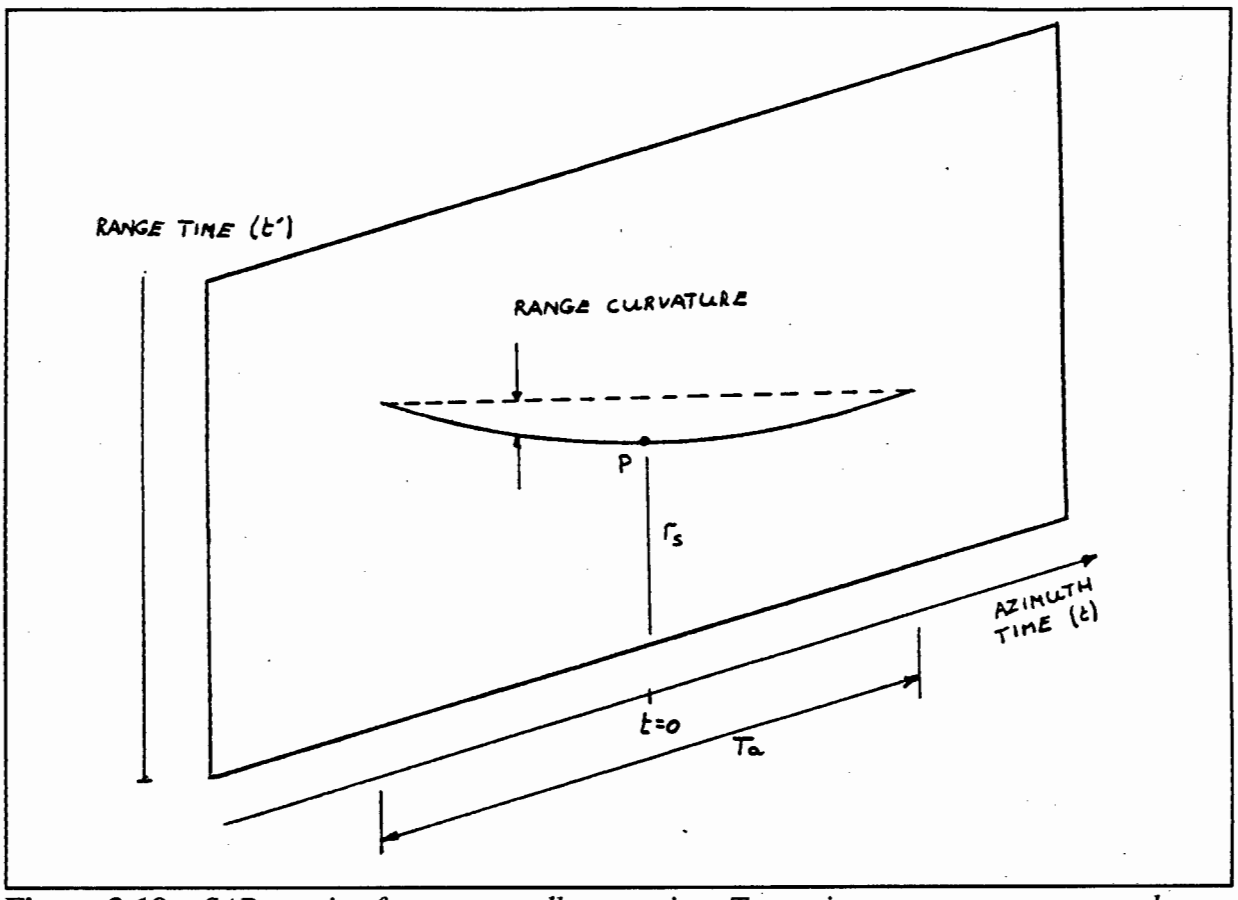

Figure 3-19: *SAR matrix after range walk correction. Two point target responses are shown.*

The uncorrected component of migration that remains is caused by range curvature. The magnitude of the curvature effect in Figure 3-19 is exaggerated and a more typical curve is shown for the SIR-B case in Appendix C2. This plot shows that range walk is the dominant feature.

3.9.4 RANGE WALK CORRECTION FOR THE SIR-B CASE.

The range correlated SIR-B SAR data matrix consists of range arrays containing 2492 complex samples. The azimuth array length is limited to 4096 samples. In Appendix B5 it is shown that each range sample (or bin) is separated by a radial distance, σ_r, equal to 4.94 meters and each azimuth bin is separated by an azimuth distance, σ_a, equal to 5.15 meters.

The range array covers a one way radial distance of 12306 meters and the azimuth array an azimuth distance of 21082 meters.

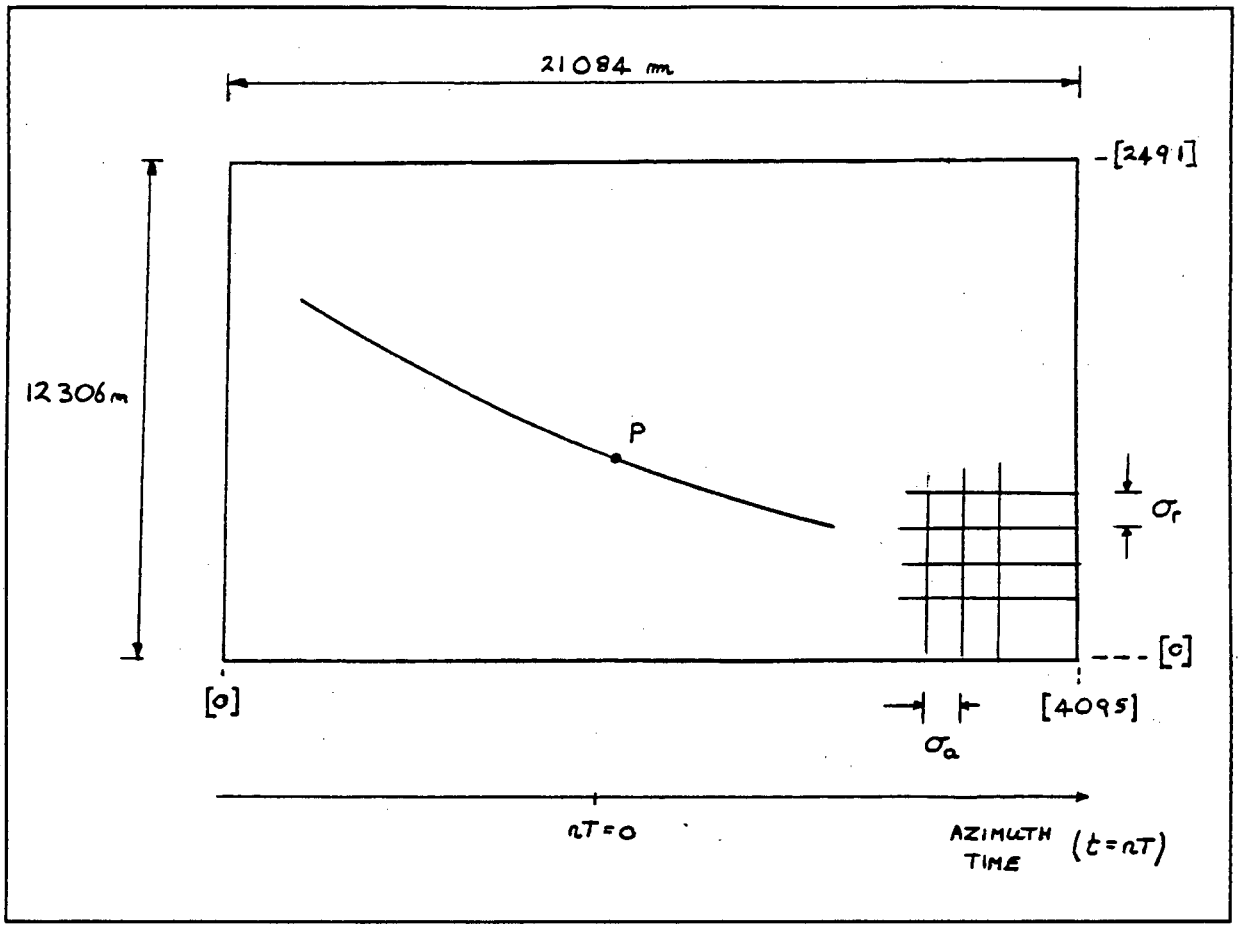

Figure 3-20: *The range correlated SAR data matrix as obtained in the decoding of SIR-B radar data. The range walk component is also shown.*

The range walk in the SIR-B case is measured over an azimuth processing window consisting of 256 sample points. In Appendix B5 it is shown that the range walk component for a target response at the near edge of the target area differs from that at the far edge by about 2.6 meters. This value is much smaller than the width of one range cell and for this reason only a single walk correction is necessary over the range extent of the SAR matrix†.

As is stated in the previous section it is more efficient to skew the full azimuth length (4096 points) of the SAR matrix by an amount equal to the range walk as measured from the left

†This confirms the statement made by Munson that the range walk does not differ appreciably over the radial extent of the target area. (see Section 3.9.3)

edge of the SAR matrix to the right edge. In Appendix B5 it is calculated that the walk over this distance (as measured for a target at the centre of the target area) is equal to 507.38 meters.

Range walk correction involves shifting sub arrays, of length $M.\sigma_a$, in azimuth so as to align the locus describing range walk into a straight line in the azimuth direction[209]. This procedure is illustrated in Figure 3-21. A sub array of azimuth data is shifted in memory every time the peak of the locus describing range walk leaves one range cell.

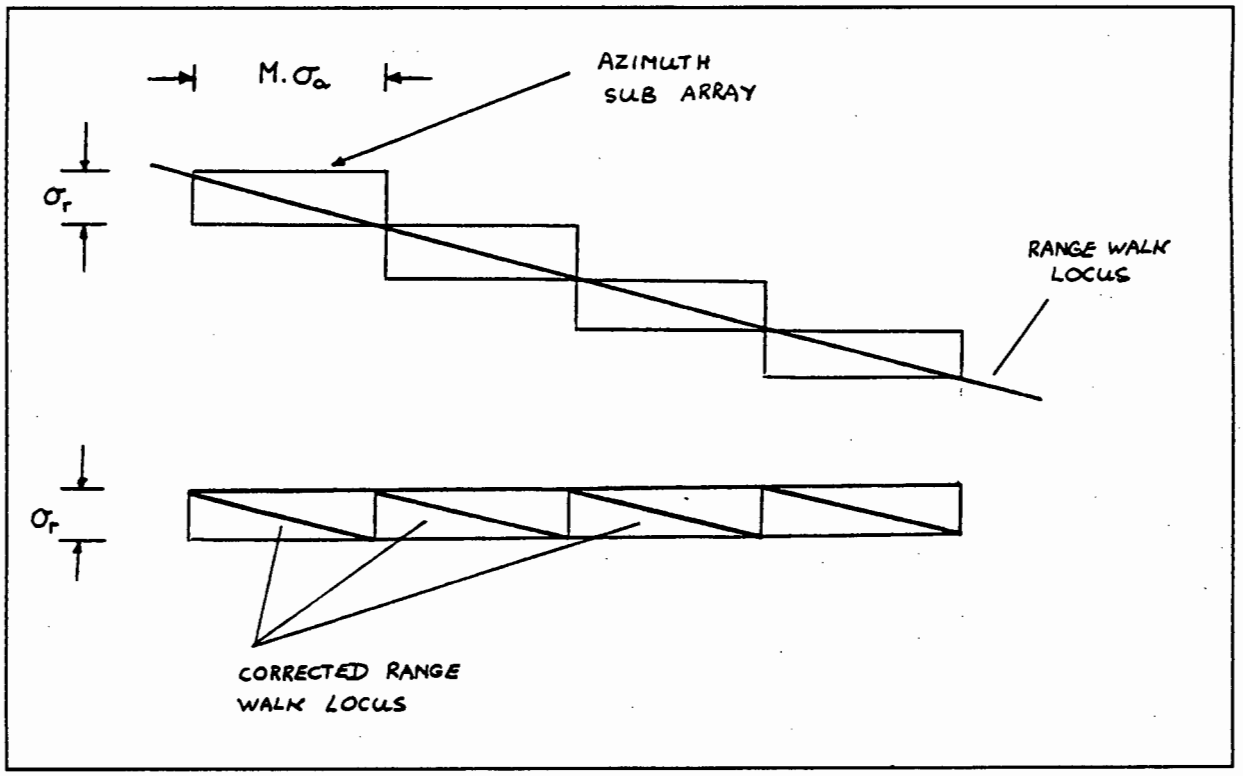

Figure 3-21: *Range walk correction by shifting sub arrays in azimuth.*

Although the range walk can be considered constant in one matrix of SAR data, it does change as a function of earth latitude. This has led Barber to argue that the above method of range walk correction is impractical since the length of azimuth sub array involved in walk correction will change for each new matrix that has to be processed[210]. However, the software design can be made flexible enough to cope with these changes in length of azimuth subarray with a negligible decrease in processing speed and increase in memory. Such a software design is described by Welsh[211] and is similar to the walk correction procedure used at JPL in the decoding of SAR data[212].

The piecewise correction of range walk shown in Figure 3.21 can cause problems. It can be calculated from Equation 3-3 that the 3dB width of the correlated range envelope covers a distance in range of approximately 12.5 meters. At the edge of each shifted sub array the centre of the range locus (and therefore the peak of the correlated range envelope) is removed a distance, σ_r, away from the centre in the adjoining section of sub array. This can be clearly seen from Figure 3-21.

Therefore, at each edge the sampled value will be located a distance, σ_r, away from the peak of the correlated range envelope. This scenario is sketched in Figure 3-22. Piecewise range walk correction has imposed an amplitude modulation on the azimuth waveform. For this particular case the amplitude modulation is not very severe and a typical modulating envelope is shown in Figure 3-23.

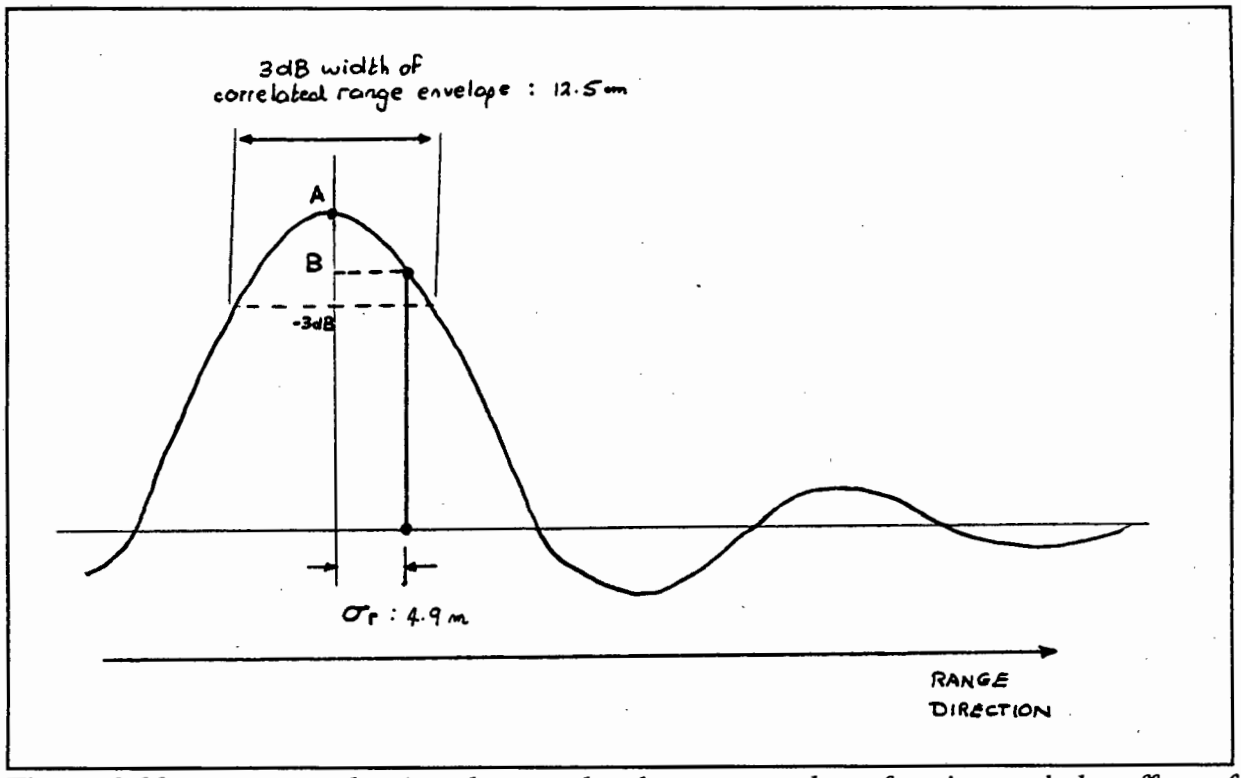

Figure 3-22: *Diagram showing the correlated range envelope function and the effect of sampling this envelope a distance, σ_r, away from the peak. (The SIR-B case)*

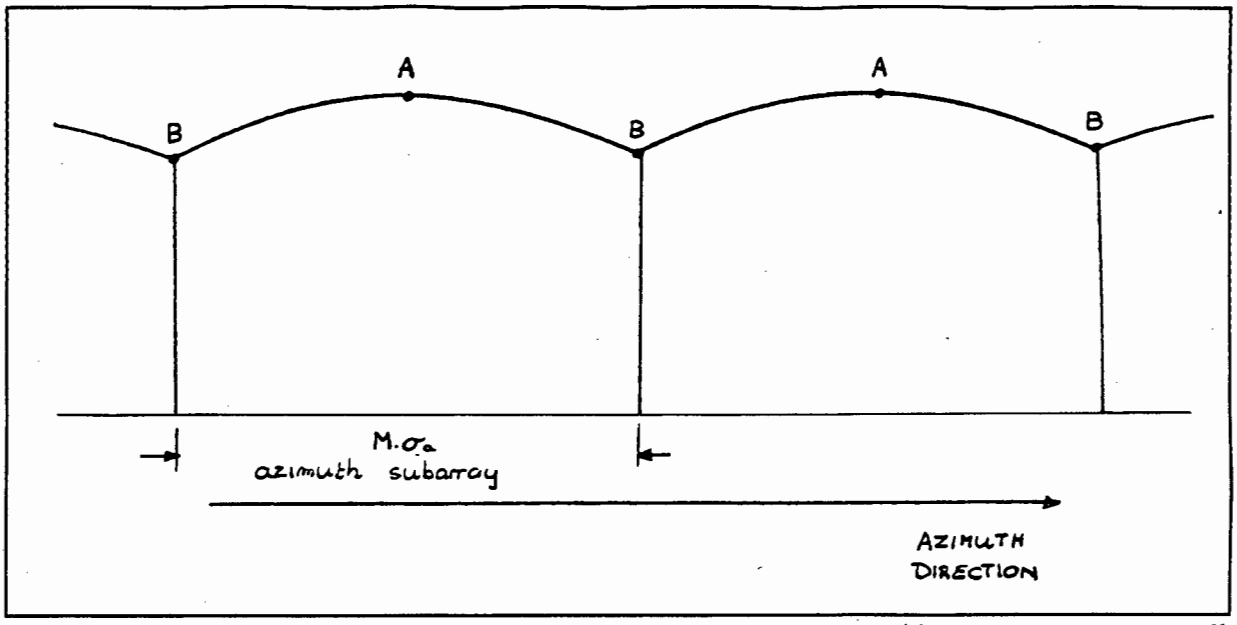

Figure 3-23: *Amplitude modulation of the azimuth waveform caused by piecewise range walk correction. (The SIR-B case)*

The reason for this relatively mild amplitude modulation effect lies in the fact that the range data was in fact interpolated by a factor of two. This procedure is described in detail in Section 3.3.3. In this section it was stated that there were certain speed advantages to be gained by retaining the finer sampling of the range waveform. The reason for this speed advantage will now be discussed.

Consider the case where no interpolation is used in the sampling of range data. The radial distance represented by one range bin would double from σ_r=4.94 meters to σ_r=9.88 meters. On performing piecewise range walk correction the amplitude modulation of the azimuth waveform would worsen to that shown in Figure 3.24. This amplitude modulation is severe and Barber describes in some detail the degrading effects that this might cause in the final SAR image[213]. In such cases the effects of modulation can be reduced by employing some form of local range interpolation at this stage. This usually involves fitting some form of cubic spline to a number of range samples in the vicinity of the required interpolation[214] [215]. However, this form of interpolation is described by Fitch as computationally expensive[216].

It is far more efficient to perform the required interpolation using FFT techniques during the range correlation process[217]. The only disadvantage of this method is that the memory requirements of the processor are obviously doubled. However, with the large onboard memory capacity of modern processors this difficulty falls away[218]. Therefore, this approach (as is also explained in Section 3.3.3) is the one adopted in the decoding of the SIR-B data.

(It can be argued that doubling the size of the range array results in the need to process twice as many azimuth arrays, thus nullifying the speed advantage mentioned. This is not true, since after the walk correction has taken place every second azimuth array can be discarded, thus cancelling the over sampling that was introduced in the range correlation process.)

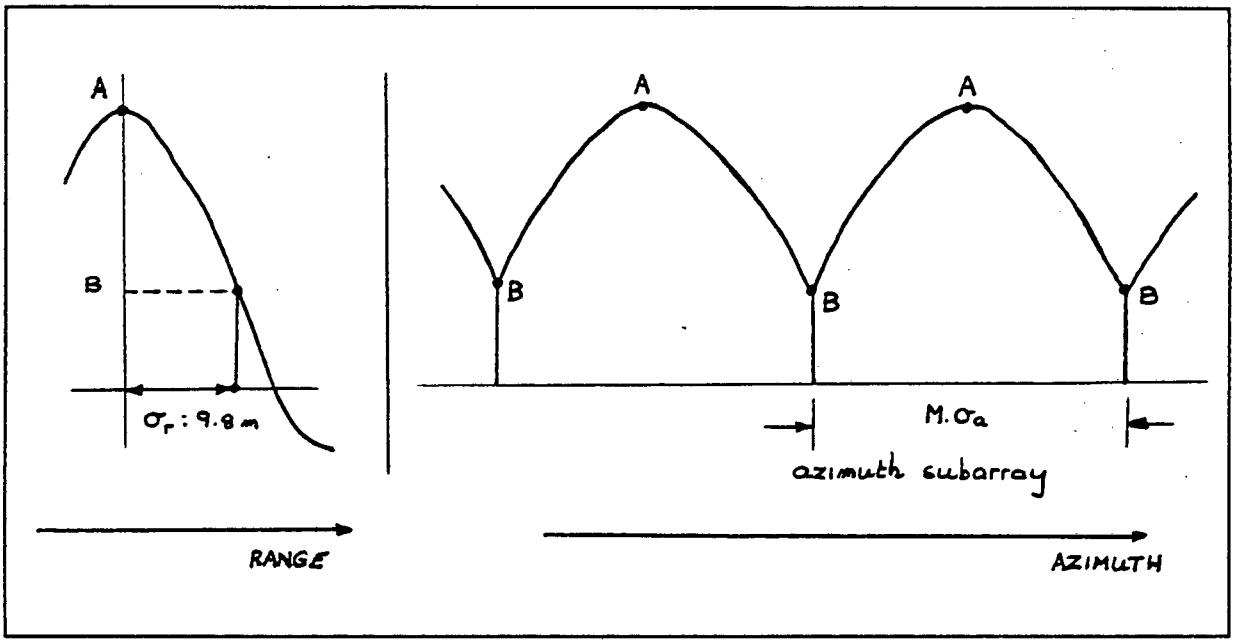

Figure 3-24: *Amplitude modulation of the azimuth waveform caused by a piecewise correction of range walk. No range interpolation has been implemented in this case.*

3.9.5 RANGE CURVATURE

The results of skewing the SAR matrix to correct for range walk is shown in Figure 3-19. The migration curve in azimuth would now be confined to one azimuth array if it were not

for the effects of range curvature. If a large enough length of azimuth waveform is processed, the curvature will cause the response in azimuth to be distributed over a length in range that exceeds the 3dB width of the correlated range envelope. This would result in an unacceptable fall off in azimuth signal power.

Range curvature cannot be corrected out as simply as is done in the case of range walk. A "parabolic" slewing of the SAR matrix such that a particular migration line falls within one azimuth array will cause other migration lines to be distorted even further. A simple solution to the problem of migration is to limit the length of azimuth processing window such that the curvature in one azimuth array does not exceed the 3dB width of the correlated range envelope[219]. This is shown diagrammatically in Figure 3-25.

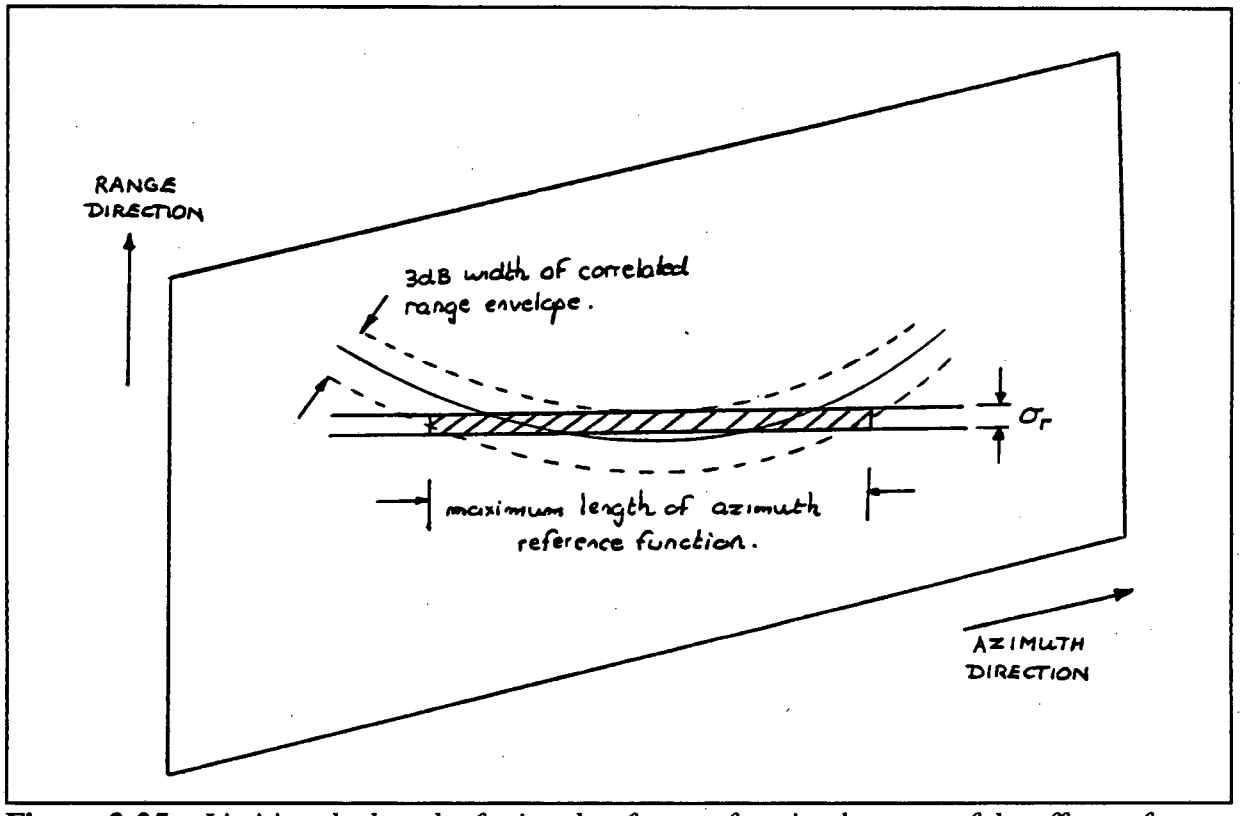

Figure 3-25: *Limiting the length of azimuth reference function because of the effects of range curvature.*

In the azimuth processing of SIR-B data an azimuth processing window consisting of 256 samples is required to obtain the desired resolution. It is shown in Appendix B5 that the maximum curvature over this length is less than 0.8 meters. This value is very small when

compared with the 3dB width of the correlated range envelope so the effects of curvature can be ignored.

If multiple look processing is attempted the effects of curvature cannot be ignored. Since the curvature is a quadratic function in azimuth, its effects become more noticeable the greater the total length of azimuth waveform that is processed. In such cases special curvature correction techniques must be performed. These techniques are discussed in detail by authors such as Fitch[220], Munson[221] and Barber[222].

3.10 DEPTH OF FOCUS

A requirement for efficient range correlation using the Fast Fourier Transform, is that the range reference function will correlate accurately with all target responses located within one range array (see Section 2.2).

In the same way, efficient azimuth correlation using the FFT requires that the azimuth reference function correlate accurately with all azimuth target responses contained within a particular azimuth array. This can be assumed to be the case over the azimuth length of one SAR matrix.

One complication that does arise during azimuth processing is that the azimuth waveform generated by a point target at one slant range is not the same as generated by a target located at another slant range. This is caused by changes in either the doppler centroid value, f_c, or the doppler rate, f_r.

It was shown in Section 3.8.3 that large changes take place in the value of the doppler centroid across the radial distance of the SAR matrix. If the same reference function is used to correlate targets located at different slant ranges there will be mismatch in the centroid value. Tomiyasu[223] and Raney[224] describe the effects of such a mismatch as a shift in the

observed target location in the fully processed SAR matrix. However, no deterioration occurs in the shape of the correlated point target response.

Changes in doppler rate can cause a breakdown of the correlation process and it is necessary to update the reference function at discrete intervals of slant range distance. The length of this interval, expressed as a one way radial distance, is usually termed the "**depth of focus**". A formula for the depth of focus is given by Elachi[225] as follows:

$$\Delta F = \frac{2\lambda_o r_s^2}{L_a^2}$$

ΔF: *The depth of focus expressed as a one way radial distance.*

λ_o: *The radar transmit frequency.*

r_s: *The slant range distance.*

L_a: *The synthetic aperture length.*

In Appendix B7 it is shown that for an azimuth processing window consisting of 256 azimuth samples the depth of focus is equal to about 19000 meters in range. The total distance covered by the SAR matrix in the range direction is only 12300 meters (see Appendix B5) so no updating of the azimuth reference function is required in the processing of SIR-B data.

3.11 A SENSITIVITY ANALYSIS OF THE AZIMUTH CORRELATION PROCESS.

An azimuth reference function (consisting of 256 samples) was generated for a target located at the range centre of the SAR matrix (see Appendix B4). This reference function was used to correlate the entire SIR-B, SAR matrix in azimuth.

Azimuth correlation is performed using the Fast Fourier Transform technique. The procedure is identical to the one used for range correlation (described in detail in Section 3.3.2) and is

not repeated. The point target response after range correlation, walk correction and azimuth correlation can be approximated by the following separable function

$$y_o(t,t') = \left\{ 2\beta_r K_r . \frac{\sin(2\pi\beta_r.(t'-D_n))}{2\pi\beta_r.(t'-D_n)} \right\} . \left\{ \left| \beta_a' K_a . \frac{\sin(\pi\beta_a' t)}{\pi\beta_a' t} \right| \right\} \qquad (3\text{-}5)$$

This function is made up of the range correlated envelope as a function of range time (Equation 3-2) multiplied by the correlated azimuth signal as a function of azimuth time (Equation 2-31). The two dependent variables, t' and t, represent range time and azimuth time respectively. This function is in the standard form of a two dimensional sinc function.

The accuracy of the correlation in azimuth is directly dependent on the accuracy with which the reference function mirrors the actual azimuth waveform generated by a point target. Factors which could influence the accurate prediction of the azimuth waveform are:

Errors in target placement:

The sensitivity of the target placement algorithm is discussed in detail in Section 3.6.4. The conclusion was reached that radial errors in position caused by inaccuracies in this algorithm would be dwarfed by radial error in earth height fluctuations over the target area. In turn these height variations were shown to be very small when compared with the depth of focus criterion discussed in Section 3.10

Errors in the model of motion:

An error in the prediction of the target or satellite velocity will have an accumulative error effect on the prediction of the azimuth reference function. This fact is self evident from Equation 2-24 and Equation 2-28.

The target velocity vector can be calculated to any desired accuracy. However, the prediction of satellite velocity is directly dependent on the accuracy of the orbital

models used to predict satellite motion. At the time of writing no information was available on this accuracy and no sensitivity analysis could be performed.

Errors in radar system parameters:

Equation 2-24 reveals that the accuracy of the predicted azimuth reference function is dependent on the accuracy with which the radar transmit frequency, f_o, is known. The reference function is also sampled before digital correlation and therefore the accuracy of the measured pulse repetition interval T is also of importance.

For the SIR-B system, the transmit frequency is known to a significance of 4 digits and the PRI to a significance of 5 digits (see Table 3-2). The effects of a unit variation in the least significant digit of these two variables on the output of the azimuth correlation process is shown in Figure 3-26 and Figure 3-27. Almost no degradation can be observed in the correlated responses.

The measured value of these radar system parameters will be known with less error in future spaceborne SAR missions. In the case of SIR-C, for example, these system parameters can be expected to be known to a significance of eight digits. (see Section 3.3.4)

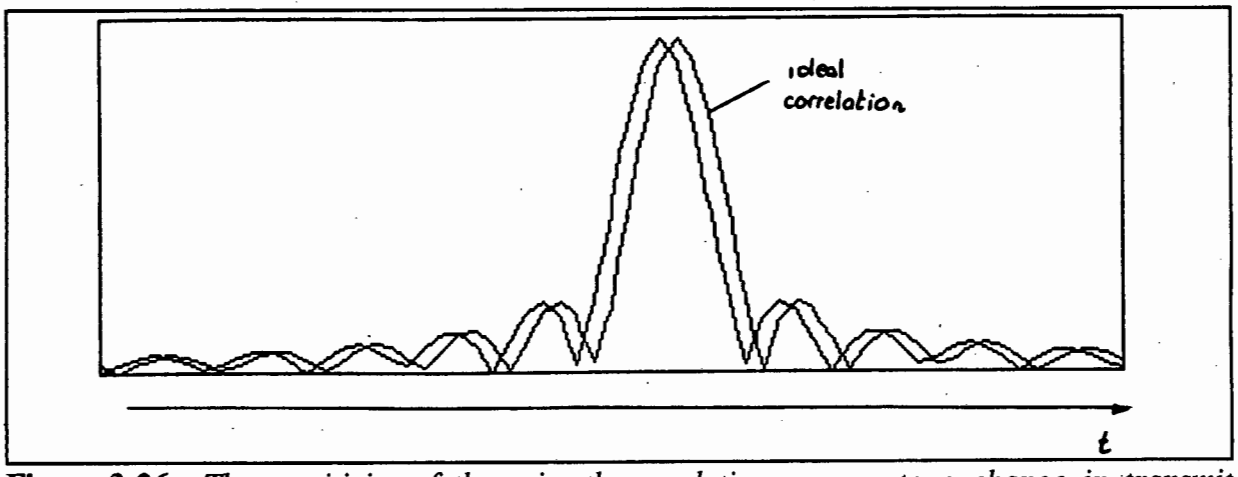

Figure 3-26: *The sensitivity of the azimuth correlation process to a change in transmit frequency, f_o. (The SIR-B case)*

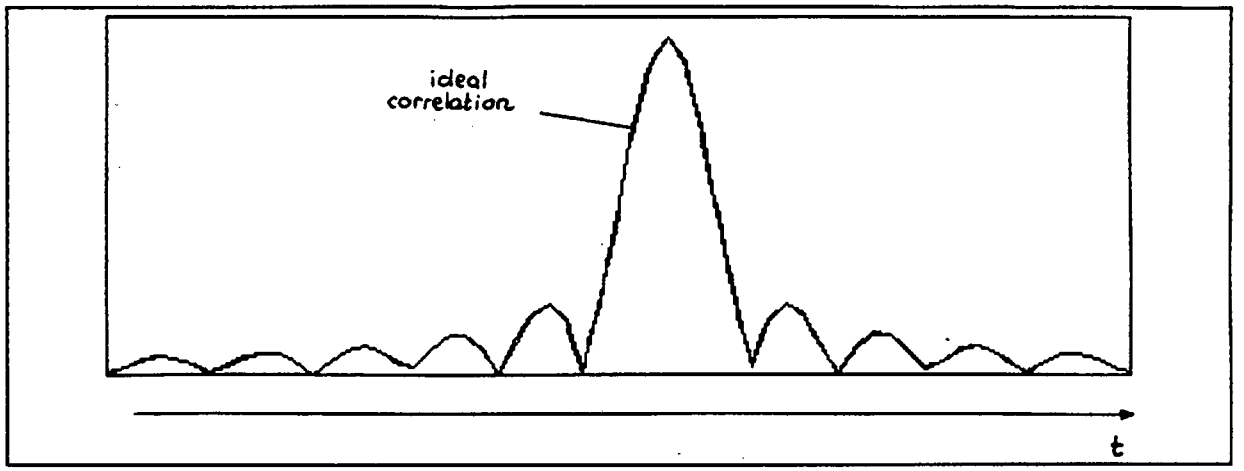

Figure 3-27: *The sensitivity of the azimuth correlation process to a change in azimuth sampling rate, T. (The SIR-B case)*

3.12 WINDOWING IN RANGE AND AZIMUTH

The correlated point target response is in the form of a two dimensional "sinc" function (Equation 3-5). This function has a characteristically high sidelobe level in both the range and azimuth directions. This can cause problems in target imaging. In the words of Rabiner: "For most (radar) systems (the) desirable main lobe of the filtered signal is accompanied by sidelobes of fairly high amplitude. This can be distressing when the radar is processing signals from several targets of differing cross section because the main lobe of the smaller target can be masked by the side lobe of the large target."[226]

Many SAR applications involve analyzing the magnitude of pixel reflectivity in the processed (correlated) SAR image[227]. Sidelobes caused by large target returns will adversely affect the reflectivity reading obtained from neighbouring pixels in the SAR image. Pictorial examples of this are given by Elachi[228] and Tomiyasu[229].

In the words of Rabiner: "At the cost of both range resolution and signal-to-noise ratio, the sidelobes can be reduced by windowing...This can be done... in the frequency domain by appropriate spectral weighting sandwiched between the forward and inverse FFT's."[230]

Windowing of the azimuth reference function was discussed in Section 2.15 (c). Artificial windowing in both the range and azimuth directions can be introduced either by windowing the appropriate reference function in the time domain[231] or by windowing in the frequency domain[232].

A wide variety of windows are discussed in the signal processing literature. Harris presents a paper in which most of these windows are discussed. In conclusion to his article he states that "...(The) Kaiser-Bessel... windows perform best in detection of nearby tones of significantly different amplitudes... The coefficients are easy to generate and the trade-off of sidelobe level as a function of time-bandwidth product is fairly simple[233]." For this reason the Kaiser-Bessel window has been chosen by the author for windowing in both range and azimuth. The implementation of this window and the image results obtained are discussed by Welsh[234].

3.13 A SYNTHETIC APERTURE RADAR IMAGE OF THE CRADOCK REGION.

The matrix of raw synthetic aperture radar data of the Cradock region was correlated in both the range and azimuth directions. Azimuth correlation is performed using a single azimuth reference function. This reference function is generated for a point target located at the range centre of the SAR matrix. No windowing has been implemented on either the range or azimuth reference functions.

A fully processed SAR image is shown below. This image covers a one way range distance of about 12000 meters and an azimuth distance about 21000 meters. The image consists of 2492 $\times$ 4096 pixels (or samples of terrain radar reflectivity). The resolution is range is about 21 meters and the resolution in azimuth about 24 meters.

The image area covering Buffelskop in the Gannahoek mountain range is enlarged for comparison with the unfocusses image of the same area. (see Section 3.4)

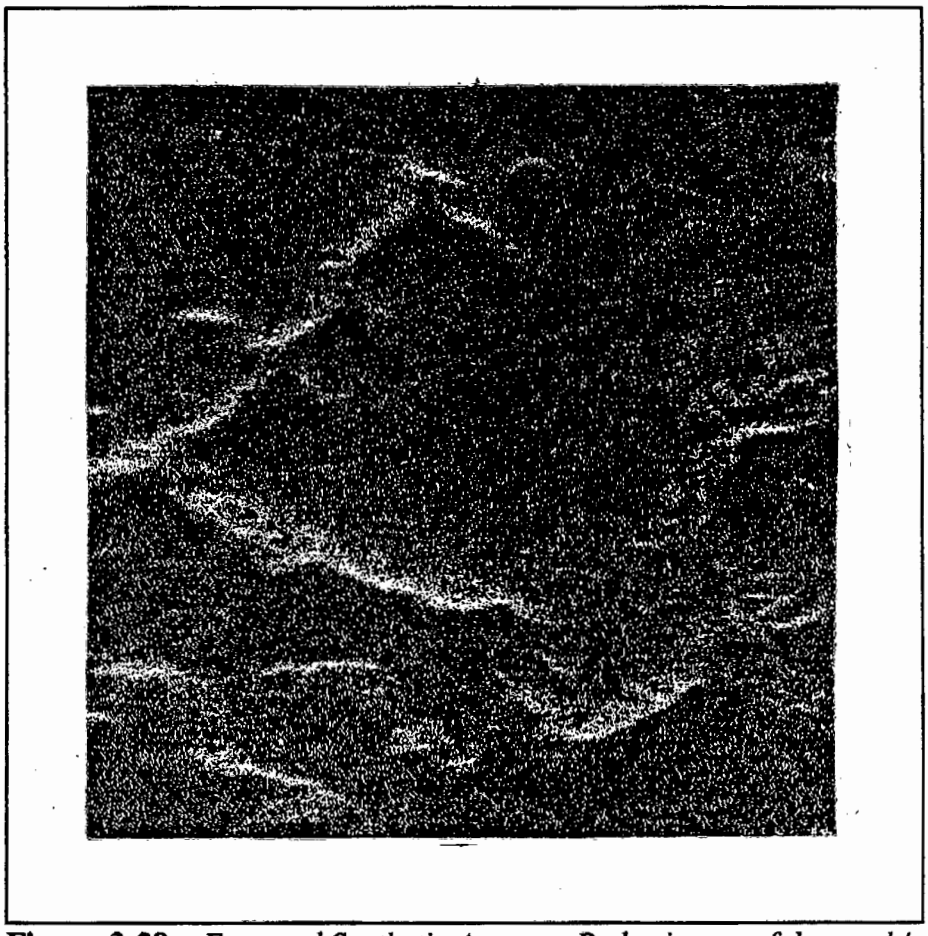

Figure 3-28: *Focussed Synthetic Aperture Radar image of the earth's surface. (The SIR-B experiment)*

This image can again be compared with the aerial and topographic maps included in Appendix D2.

A fully processed image of the Cradock region as obtained on the SAR processor at Jet Propulsion Laboratories was included with the raw radar data. A section of this image, covering the same area as shown in Figure 3-28 is included overleaf for comparison purposes.

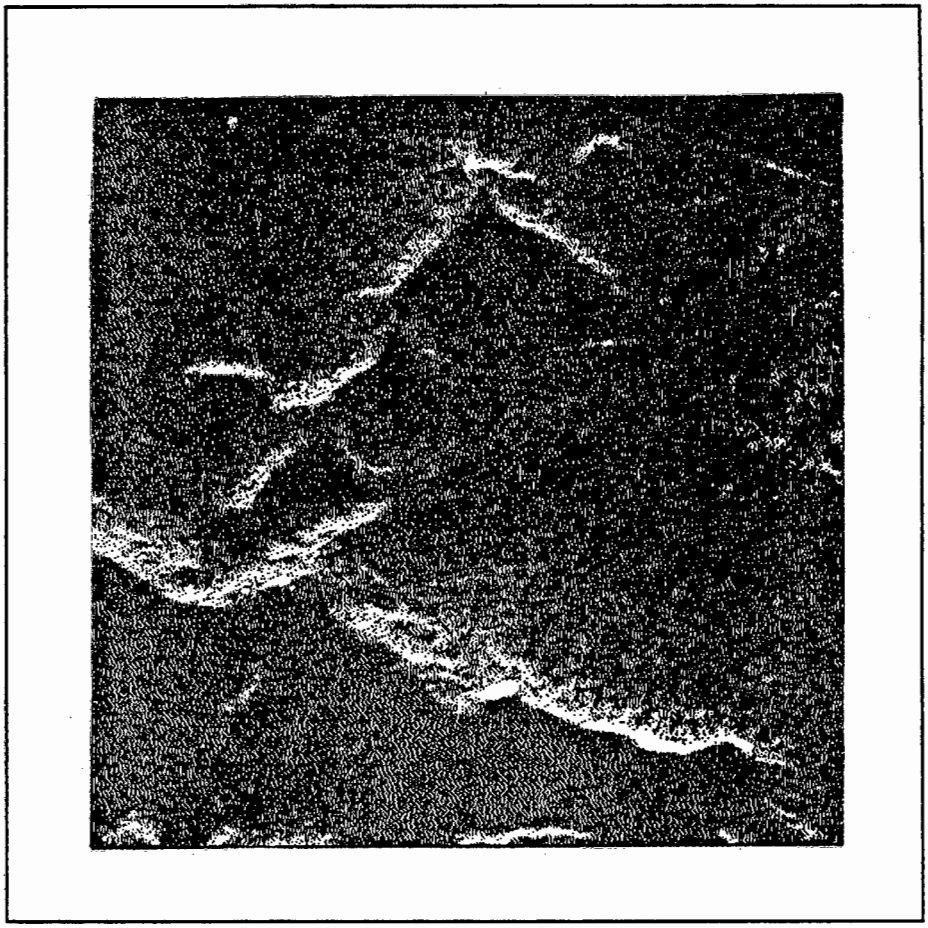

Figure 3-29: *Focussed Synthetic Aperture Radar image of the earth's surface, as provided by JPL. (The SIR-B experiment)*

A comparison of Figure 3-28 and Figure 3-29 reveals very little difference in resolution. However, the image obtained from JPL does displays a better signal to noise ratio. This is because their image is made up of four incoherently averaged "looks" of the same area. As mentioned in Section 3.9.1, Figure 3-28 is only a single look image and, therefore, the signal to noise ratio is poorer.

CHAPTER 4

CONCLUSIONS

It was shown in Chapter 2 that the theory of Synthetic Aperture Radar processing can be successfully treated as a signal processing problem. Complex ideas and terminology that are specific to radar imaging, can be treated in terms of fundamental signal processing theory.

The SAR azimuth waveform was shown to be a sampled version of the Doppler waveform generated by a moving target. The frequency spread contained within this sampled waveform is only dependent on the change in aspect angle through which the target is imaged by the radar. It is shown that standard discrete correlation techniques utilise this frequency spread to produce azimuth resolution of the imaged target.

It is also shown that the processing of a SAR data matrix can be approximated as two independent operations namely: correlation in range and correlation in azimuth. The range correlation process is well understood, but the process of azimuth correlation is generally treated in a confusing manner in the SAR literature. Discrete signal processing theory is used to put azimuth processing on a firm basis.

In Chapter 3, an algorithm design for the decoding of spaceborne SAR data is formulated. This design can accommodate data from a variety of spaceborne SAR systems, each with its own orbital geometry and system specifications. Automatic range correlation, range walk correction and azimuth correlation have been successfully designed into this software. The algorithms making up the software design have been shown to display the necessary insensitivity to numerical error in any predicted satellite orbital geometry and system values.

The algorithm design was implemented at UCT and tested on raw radar data that was recorded by the Shuttle Imaging Radar-B Experiment (SIR-B) over Cradock, South Africa. A radar image of this region was successfully obtained and is included in Chapter 3. This image compares favourably with a processed image of the same region, provided by Jet Propulsion Laboratories.

Further improvements, which were beyond the scope of this thesis, can be made. The target placement algorithm used in this thesis and discussed in Appendix B2 is specific to the data take over Cradock in that the antenna boresight is assumed to be perpendicular to the direction of flight. The earth geoidal model is also approximated as a sphere over the target area in question. A more general implementation of the target placement algorithm should conform to the basic algorithm described in Section 3.6.2.

Scope for further development lies in formulating a more general design that has the capacity to produce multiple look images of the area in question.

SAR images of the earth have been shown to be useful in a variety of applications such as terrain classification, vegetation classification, sea state monitoring and detection of ships. However, this requires a certain amount of image classification and feature extraction, which can be treated under the more general subject of image processing. Therefore, if SAR images are to be used for this application, study into the use of image processing techniques on SAR images is required.

REFERENCES

1. Brown, W.M. and Porcello, L.J., '*An Introduction To Synthetic Aperture Radar*', IEEE Spectrum, September 1969, p.52

2. Cutrona, L.J., Vivian, W.E., Leith, E.N. and Hall, G.O., '*A High Resolution Radar Combat-Surveillance System*', IRE Transactions on Military Electronics, Vol. MIL-5, No. 2, April 1961, p.127

3. Wu, C., Barkan, B., Karplus, W.J. and Caswell, D., '*SEASAT Synthetic-Aperture Radar Data Reduction Using Parallel Programmable Array Processors*', IEEE Transactions on Geoscience and Remote Sensing, Vol. GE-20, No. 3, July 1982, p.352

4. Noack, W., Popella, A., and Schreier, G., '*Knowledge-Based SAR Processing and Geocoding: The Elementary Components of the German Processing and Archiving Facility for High Throughput and High-Precision Processing of ERS-1 SAR Data*', IEEE Transactions on Geoscience and Remote Sensing, Vol. GE-25, No. 6, November 1987, 758-769

5. Ahmed, S., Warren, H.R., Symonds, M.D. and Cox, R.P., '*The Radarsat System*', IEEE Transactions on Geoscience and Remote Sensing, Vol. 28, No. 4, July 1990, 598-602

6. Munson, D.C. and Visentin, R.L. , '*A Signal Processing View of Strip-Mapping Synthetic Aperture Radar*', IEEE Transactions on Acoustics, Speech and Signal Processing, Vol. 37, No. 12, December 1989, 2131-2147.

7. Skolnik, M.I. , *Introduction to Radar Systems.* Tokyo: McGraw-Hill , 1980, 101-106

8. Wehner, D.R. , *High Resolution Radar.* Norwood MA: Artech House, 1987, p.73

9. Skolnik, M.R. , *Introduction to Radar Systems* , Tokyo: McGraw Hill , 1980, p.105 & (Figure 4-5)

10. Skolnik, M.I. , *Introduction to Radar Systems.* 2nd ed. Tokyo: McGraw-Hill, 1980, 359-366

11. Hovanessian, S.A. , *Introduction to Synthetic Array and Imaging Radars.* Dedham, MA: Artech House, 1980, p.95 (Figure 5-14)

12. Hovanessian, S.A., *Radar System Design and Analysis.* , Norwood, MA: Artech House, 1985, 4-12

13. Skolnik, M.I. , *Introduction to Radar Systems.* 2nd ed. Tokyo: McGraw-Hill, 1980, 223-235

14. Hovanessian, S.A. , *Radar System Design and Analysis.* , Norwood, MA: Artech House, 1984, 27-41

15. Skolnik, M.I., *Introduction to Radar Systems.* 2nd ed, Tokyo: McGraw-Hill, 1980, 33-52

16. Wehner, D.R. , *High Resolution Radar.* Norwood MA: Artech House, 1987, 72-73

17. Fitch, J.P. , *Synthetic Aperture Radar.* New York: Springer-Verlag, 1988, p28

18. Wu, C., Liu, K.Y. and Jin, M. , *'Modelling and a Correlation Algorithm for Spaceborne SAR Signals'* , IEEE Transactions on Aerospace and Electronic Systems , Vol. AES-18, No. 5, September 1982, 563-565

19. Kovaly, J.J. , *'Radar Techniques For Planetary Mapping With Orbiting Vehicle'*, Annals of the New York Academy of Sciences, Vol. 187, 25 January 1972 , p.155 (Figure 1)

20. Skolnik, M.I. , *Introduction to Radar Systems.* 2nd ed. Tokyo: McGraw-Hill, 1980, 369-375

21. Rihaczek, A.W. , *Principles of High-Resolution Radar.* Los Altos, California: Peninsula Publishing, 1985, 28-34

22. Wehner, D.R. , *High Resolution Radar.* Norwood, MA: Artech House, 1987, p.65

23. Rihaczek, A.W. , *Principles of High Resolution Radar.* Los Altos, California: Peninsula Publishing, 1985, p.32

24. Rihaczek, A.W. , *Principles of High Resolution Radar.* Los Altos, California: Peninsula Publishing, 1985, p.37 & p.472

25. Elachi, C. , *Spaceborne Radar Remote Sensing: Applications and Techniques.* New York: IEEE Press, 1987, p.56

26. Wehner, D.R. , *High Resolution Radar.* Norwood, MA: Artech House, 1987, p.280

27. Stremler, F.G. , *Introduction to Communication Systems.* 2nd ed. Reading, Massachusetts: Addison-Wesley, 1982, p.114

28. Stremler, F.G. , *Introduction to Communication Systems.* 2nd ed. Reading, Massachusetts: Addison-Wesley, 1982, p.88

29. Stremler, F.G. , *Introduction to Communication Systems.* 2nd ed. Reading, Massachusetts: Addison-Wesley , 1982, p.279 & p.280

30. Skolnik, M.I. , *Introduction to Radar Systems.* 2nd ed. Tokyo: McGraw-Hill, 1980, p.69

31. Skolnik, M.I. , *Introduction to Radar Systems.* 2nd ed. Tokyo: McGraw-Hill, 1980, p.70

32. Wehner, D.R. , *High Resolution Radar.* Norwood, MA: Artech House, 1987, p.50

33. Hovanessian, S.A. , *Introduction to Synthetic Array and Imaging Radars.* Dedham, MA: Artech House, 1980, p.15

34. Munson D.C. , Visentin R.L. , *'A Signal Processing View of Strip-Mapping Synthetic Aperture Radar'* , IEEE Transactions on Acoustics Speech and Signal Processing, Vol. 37, No. 12, December 1989, p.2146

35. Stremler, F.G. , *Introduction to Communication Systems.* 2nd ed. Reading, Massachusetts: Addison-Wesley, 1982, p.354

36. De Fatta, D.J., Lucas, J.G. and Hodgkiss, W.S., *Digital Signal Processing.* Singapore: John Wiley & Sons, 1988, 58-59 (Figure 2.21) & p.60

37. Rihaczek, A.W., *Principles of High Resolution Radar.* , Los Altos, California: Peninsula Publishing, 1985, p.162

38. Develet, J.A., *'Performance of a Synthetic-Aperture Mapping Radar System'*, IEEE Transactions on Aerospace and Navigational Electronics, Vol. ANE-11, No. 3, September 1964, p.174

39. Tomiyasu, K., *'Tutorial Review of Synthetic-Aperture Radar (SAR) with Applications to Imaging of the Ocean Surface'* , Proceedings of the IEEE , Vol. 66, No. 5, May 1978, p.567

40. Elachi, C., Bicknell, T., Rolando, L.J. and Wu, C., *'Spaceborne Synthetic-Aperture Imaging Radars: Applications, Techniques, and Technology'*, Proceedings of the IEEE, Vol. 70, No. 10. October 1982, p.1176

41. Hovanessian, S.A., *Introduction to Synthetic Array and Imaging Radars.* Dedham, MA: Artech House, 1980, p.46

42. Wehner, D.R., *High Resolution Radar.* Norwood, MA: Artech House, 1987, p.321

43. Chen, C. and Andrews, H.C., *'Target-Motion-Induced Radar Imaging'* , IEEE Transactions on Aerospace and Electronic Systems, Vol.AES-16, No. 1, January 1980, 2-14

44. van Zyl, M., *'Radar Signal Processing Lecture Notes'* , University of Cape Town: 1990, Lecture 2, p.3

45. Skolnik, M.I., *Introduction to Radar Systems.* 2nd ed. Tokyo: McGraw_Hill, 1980, p.103 (Figure 4.2)

46. Stremler, F.G., *Introduction to Communication Systems.* 2nd ed. Reading, Massachussets: Addison-Wesley, 1982, p.353

47. Tretter, S.A., *Introduction to Discrete-Time Signal Processing.* New York: John Wiley & Sons, 1976, 7-10

48. Skolnik, M.I., *Introduction to Radar Systems.* 2nd ed. Tokyo: McGraw-Hill, 1980, p412

49. Skolnik, M.I., *Introduction to Radar Systems.* 2nd ed. Tokyo: McGraw-Hill, 1980, p.414 (Figure 11.9)

50. Elachi, C., Spaceborne Radar Remote Sensing: Applications and Techniques. New York: IEEE Press, 1988, p.58

51. Hovanessian S.A. , *Introduction to Synthetic Array and Imaging Radars.* Dedham, MA: Artech House, 1980, 83-89

52. Rihaczek, A.W., *Principles of High_Resolution Radar.* Los Altos, California: Peninsula Publishing, 1985, p.469

53. Fitch, J.P., *Synthetic Aperture Radar.* New York: Springer-Verlag, 1988, p.51

54. Kovaly, J.J., *Synthetic Aperture Radar.* Dedham, Massachusetts: Artech House, 1976, (Introduction: p.ii)

55. Kovaly, J.J., *Synthetic Aperture Radar.* Dedham, Massachusetts: Artech House, 1976, (Introduction: p.vii)

56. Brown, W.M., *'Synthetic Aperture Radar'* , IEEE Transactions on Aerospace and Electronic Systems, Vol. AES-3, No. 2, March 1967, p.217

57. Hovanessian, S.A., *Introduction to Synthetic Array and Imaging Radars.* Dedham, MA: Artech House, 1980, p.24

58. Munson, D.C. and Visentin, R.L., *'A Signal Processing View of Strip-Mapping Synthetic Aperture Radar'* , IEEE Transactions on Acoustics, Speech, and Signal Processing, Vol. 37, No. 12, December 1989, p.2136

59. Rihaczek A.W. , *Principles of High Resolution Radar.* Los Altos, California: Peninsula Publishing, 1985, 226-233

60. Wu, C., Liu, K.Y. and Jin, M., *'Modeling and a Correlation Algorithm for Spaceborne SAR Signals'* , IEEE Transactions on Aerospace and Electronic Systems, Vol. AES-18, No. 5, September 1982, p.566

61. Stimson, G.W., *Introduction to Airborne Radar.* El Segundo, California: Hughes Aircraft Company, 1983, 527-539

62. Skolnik, M.I., *Introduction to Radar Systems.* 2nd ed. Tokyo: McGraw-Hill, 1980, 518-522

63. Tomiyasu, K., *'Tutorial Review of Synthetic-Aperture Radar (SAR) with Applications to Imaging of the Ocean Surface'* , Proceedings of the IEEE, Vol. 66, No. 5, May 1978

64. Cutrona, L.J., Vivian, W.E., Leith, E.N., and Hall, G.O., *'A High Resolution Radar Combat-Surveillance System'*, IRE Transactions on Military Electronics, Vol. MIL-5, No. 2, April 1961, p.127 & Figure 1

65. Hecht, E., *Optics.* 2nd ed. Reading, Massachusetts: Addison-Wesley, 1987, 397-399

66. Elachi, C., *Spaceborne Radar Remote Sensing: Applications and Techniques.* New York: IEEE Press, 1987, 53-55

67. Hecht, E., *Optics.* 2nd ed. Reading, Massachusetts: Addison-Wesley, 1987, 397-399

68. Stimson, G.W., *Introduction to Airborne Radar.* El Segundo, California: Hughes Aircraft Company, 1983, p.537

69. McCord, H.L., '*The Equivalence Among Three Approaches To Deriving Synthetic Array Patterns And Analyzing Processing Techniques*' , IRE Transactions on Military Electronics, Vol. MIL-6, No. 1, January 1962, 116-119

70. Stimson, G.W., *Introduction to Airborne Radar.* El Segundo, California: Hughes Aircraft Company, 1983, p.531

71. Elachi, C., *Spaceborne Radar Remote Sensing: Applications and Techniques.* New York: IEEE Press, 1987, p.74

72. Skolnik, M.I., *Introduction to Radar Systems.* 2nd ed. Tokyo: McGraw-Hill, 1980, 119-126

73. Elachi, C., *Spaceborne Radar Remote Sensing: Applications and Techniques.* New York: IEEE Press, 1987, p.61 (Figure 3-12)

74. Munson, D.C. and Visentin, R.L., '*A Signal Processing View of Strip-Mapping Synthetic Aperture Radar*', IEEE Transactions on Acoustics, Speech, and Signal Processing, Vol. 37, No. 12, December 1989, p.2137

75. Hovanessian, S.A., *Radar System Design and Analysis.* Norwood, MA: Artech House, 1984, p.29

76. Sherwin, S.M., *Monopulse Principles and Techniques.* Norwood MA: Artech House, p.13

77. Skolnik, M.I., *Introduction to Radar Systems.* Tokyo: McGraw-Hill, 1980, p.232

78. Cutrona, L.J. and Hall, G.O., '*A Comparison Of Techniques For Achieving Fine Azimuth Resolution*' , IRE Transactions on Military Electronics, Vol. MIL-6, No. 2, April 1962, p.120

79. Sherwin S.M. , *Monopulse Principles and Techniques.* Norwood MA: Artech House, p.205

80. Cutrona, L.J. and Hall, G.O., '*A Comparison Of Techniques For Achieving Fine Azimuth Resolution*' , IRE Transactions on Military Electronics, Vol. MIL-6, No. 2, April 1962, p.120 (Figure.1)

81. Hovanessian, S.A., *Introduction to Synthetic Array and Imaging Radars.* Dedham, MA: Artech House, 1980, p.46

82. Wehner, D.R., *High Resolution Radar.* Norwood, MA: Artech House, 1987, p.201

83. Kirk, J.C., *'A Discussion Of Digital Processing In Synthetic Aperture Radar',* IEEE Transactions on Aerospace and Electronic Systems, Vol. AES-11, No. 3, May 1975, p.332

84. Curlander, J.C., *'Performance of the SIR-B Digital Image Processing Subsystem'* , IEEE Transactions on Geoscience and Remote Sensing, Vol. GE-24, No. 4, July 1986, p.650

85. Skolnik, M.I., *Introduction to Radar Systems.* 2nd ed. Tokyo: McGraw-Hill, 1980, 254-258

86. Rihaczek, A.W., *Principles of High Resolution Radar.* Los Altos, California: Peninsula Publishing, 1985, p.77

87. Brigham, E.O., *The Fast Fourier Transform and its Applications.* Englewood Cliffs, New Jersey: Prentice-Hall, 1988, p.***

88. Dudgeon, D.E. and Mersereau, R.M., *Multidimensional Digital Signal Processing.* Englewood Cliffs, New Jersey: Prentice-Hall, 1984, p.299

89. Hovanessian, S.A., *Introduction to Synthetic Array and Imaging Radars.* Dedham, MA:, Artech House, 1980, p.48

90. Wehner, D.R., *High Resolution Radar.* Norwood, MA: Artech House, 1987, p.236

91. Ahmed, S., Warren, H.R., Symonds, M.D. and Cox, R.P., *'The Radarsat System'* , IEEE Transactions on Geoscience and Remote Sensing, Vol. 28, No. 4, July 1990, p.599 (Figure. 3)

92. Huneycutt, B.L., *'Innovative Operating Modes and Techniques For the Spaceborne Imaging Radar-C Instrument'* , IEEE Transactions on Geoscience and Remote Sensing, Vol. 28, No. 4, July 1990, p.606

93. Hovanessian, S.A., *Radar Systems Design and Analysis.* Norwood. MA, Artech House, 1984, p.29 & p.31 (Table 2-1)

94. Cutrona, L.J., Vivian, W.E., Leith, E.N. and Hall, G.O., *'A High Resolution Radar Combat Surveillance System'* , IRE Transactions on Military Electronics, Vol. MIL-5, No. 2, April 1961, p.128

95. Huneycutt, B.L., *'Innovative Operating Modes and Techniques For the Spaceborne Imaging Radar-C Instrument'* , IEEE Transactions on Geoscience and Remote Sensing, Vol. 28, No. 4, July 1990, p.606

96. Cutrona, L.J. and Hall, G.O., *'A Comparison Of Techniques For Achieving Fine Azimuth Resolution'* , IRE Transactions on Military Electronics, Vol. MIL-6, No. 2, April 1962, p.121

97. Munson, D.C. and Visentin, R.L., *'A Signal Processing View of Strip-Mapping Synthetic Aperture Radar'* , IEEE Transactions on Acoustics, Speech and Signal Processing, Vol. 37, No. 12, December 1989, p.2136

98. Ausherman, D.A., Kozma, A., Walker, J.L., Jones, H.M. and Poggio, E.C., *'Developments in Radar Imaging'* , IEEE Transactions on Aerospace and Electronic Systems, Vol. AES-20, No. 4, July 1984, p.380

99. Rihaczek, A.W., *Principles of High Resolution Radar.* Los Altos, California: Peninsula Publishing, 1985, p.55

100. Rihaczek, A.W., *Principles of High Resolution Radar.* Los Altos, California: Peninsula Publishing, 1985, p.167

101. Rihaczek, A.W., *Principles of High Resolution Radar.* Los Altos, California: Peninsula Publishing, 1985, p.227

102. Harger, R.O., *'An Optimum Design Of Ambiguity Function, Antenna Pattern, and Signal For Side-Looking Radars'* , IEEE Transactions on Military Electronics, Vol. MIL-9, Nos. 3 and 4 (July/October 1965) p.266

103. Harger, R.O., *'An Optimum Design Of Ambiguity Function, Antenna Pattern, and Signal For Side-Looking Radars'* , IEEE Transactions on Military Electronics, Vol. MIL-9, Nos. 3 and 4 (July/October 1965) p.266

104. Fitch, J.P., *Synthetic Aperture Radar.* New York: Springer-Verlag, 1988, p.51

105. Wu, C., Liu, K.Y. and Jin, M., *'Modeling and a Correlation Algorithm for Spaceborne SAR Signals'* , IEEE Transactions on Aerospace and Electronic Systems, Vol. AES-18, No. 5, September 1982, p.565

106. Hovanessian, S.A., *Introduction to Synthetic Array and Imaging Radars.* Dedham, MA: Artech House, 1980, p.83 (Figure 5-5)

107. Barber, B.C., *'Theory of Digital Imaging From Orbital Synthetic-Aperture Radar'* , INT. J. Remote Sensing, Vol. 6, No. 7, 1985, p.1037

108. Fitch, J.P., *Synthetic Aperture Radar.* New York: Springer-Verlag, 1988, 91-92

109. De Fatta, D.J., Lucas, J.G. and Hodgkiss, W.S., *Digital Signal Processing.* Singapore: John Wiley & Sons, 1988, p.204

110. Oppenheim, A.V. and Schafer, R.W., *Digital Signal Processing.* Prentice-Hall, 1975, p.241

111. Heimiller, R.C., *'Theory and Evaluation Of Gain Patterns Of Synthetic Arrays'* , IRE Transactions on Military Electronics, Vol. MIL-6, No. 2, April 1962, p.128

112. Harger, R.O., *'An Optimum Design Of Ambiguity Function, Antenna Pattern, and Signal For Side-Looking Radars'* , IEEE Transactions on Military Electronics, Vol. MIL-9, Nos. 3 and 4 (July/October 1965) p.264

113. Raney, R.K., *'Reconsideration of Azimuth Ambiguities in SAR'* , IEEE Transactions on Geoscience and Remote Sensing, Vol. GE-25, No. 6, November 1987, p.784 (Fig. 2)

114. Noack, W., Popella, A. and Schreier, G., *'Knowledge-Based SAR Processing and Geocoding: The Elementary Components of the German Processing and Archiving Facility for High Throughput and High Precision Processing of ERS-1 SAR Data'* , IEEE Transactions on Geoscience and Remote Sensing, Vol. GE-25, No. 6, November 1987, p.762 (Figure. 3)

115. Oppenheim, A.V. and Schafer, R.W., *Digital Signal Processing.* Prentice-Hall, 1975, p.26 (Figure 1.13)

116. Rihaczek, A.W., *Principles of High Resolution Radar.* Los Altos, California: Peninsula Publishing, 1985, 77-78

117. Raney, R.K., *'Reconsideration of Azimuth Ambiguities in SAR'* IEEE Transactions on Geoscience and Remote Sensing, Vol. GE-25, No. 6, November 1987, 783-787

118. Heimiller, R.C., *'Theory and Evaluation Of Gain Patterns Of Synthetic Arrays'* , IRE Transactions on Military Electronics, Vol. MIL-6, No. 2, April 1962, 122-129

119. Harger, R.O., *'An Optimum Design Of Ambiguity Function, Antenna Pattern, and Signal For Side-Looking Radars'* , IEEE Transactions on Military Electronics, Vol. MIL-9, Nos. 3 and 4 (July/October 1965) 264-278

120. Bayma, R.W. and McInnes, P.A., *'Aperture Size And Ambiguity Constraints For A Synthetic Aperture Radar'* , The Records of the IEEE 1975 International Radar Conference (21-23 April 1975), 499-504

121. Munson, D.C. and Visentin, R.L., *'A Signal Processing View of Strip-Mapping Synthetic Aperture Radar'*, IEEE Transactions on Acoustics, Speech and Signal Processing, Vol. 37, No. 12, December 1989, 2138-2139

122. Munson, D.C. and Visentin, R.L., *'A Signal Processing View of Strip-Mapping Synthetic Aperture Radar'* , IEEE Transactions on Acoustics, Speech, and Signal Processing, Vol. 37, No. 12, December 1989, p.2134

123. Curlander, J.C., *'Performance of the SIR-B Digital Image Processing Subsystem'* , IEEE Transactions on Geoscience and Remote Sensing, Vol. GE-24, No. 4, July 1986, 649-652

124. Wu, C., Barkan, B., Karplus, W.J. and Caswell, D., *'SEASAT Synthetic-Aperture Radar Data Reduction Using Parallel Programmable Array Processors'* , IEEE Transactions on Geoscience and Remote Sensing, Vol. GE-20, No. 3, July 1982, 352-357

125. Barber, B.C., *'Theory of Digital Imaging from Orbital Synthetic-Aperture Radar'* , INT. J. Remote Sensing, 1985, Vol. 6, No. 7, 1009-1057

126. Noack, W., Popella, A. and Schreier, G., *'Knowledge-Based SAR Processing and Geocoding: The Elementary Components of the German Processing and Archiving Facility for High Throughput and High-Precision Processing of ERS-1 SAR Data'* , IEEE Transactions on Geoscience and Remote Sensing, Vol. GE-25, No. 6, November 1987, 758-769

127. Noack, W., Popella, A. and Schreier, G., *'Knowledge-Based SAR Processing and Geocoding: The Elementary Components of the German Processing and Archiving Facility for High Throughput and High-Precision Processing of ERS-1 SAR Data'* , IEEE Transactions on Geoscience and Remote Sensing, Vol. GE-25, No. 6, November 1987, p.759

128. Welsh, S.D., (*Masters Thesis to be submitted*) , Department of Electrical Engineering, University of Cape Town, 1991

129. Cimino, J.B., Holt, B. and Richardson, A.H., *The Shuttle Imaging Radar B (SIR-B) Experimental Report.* Jet Propulsion Laboratory, California: NASA (JPL Pub. 88-2), 1988, p.1, p.141, p.174

130. Curlander, J.C., '*Performance of the SIR-B Digital Image Processing Subsystem*' , IEEE Transactions on Geoscience and Remote Sensing, Vol. GE-24, No. 4, July 1986, p.649

131. Cimino, J.B., Holt, B. and Richardson, A.H., *The Shuttle Imaging Radar B (SIR-B) Experimental Report.* Jet Propulsion Laboratory, California: NASA (JPL Pub. 88-2), 1988, p.6

132. Huneycutt, B.L., '*Innovative Operating Modes and Techniques For the Spaceborne Imaging Radar-C Instrument*' , IEEE Transactions on Geoscience and Remote Sensing, Vol. 28, No. 4, July 1990, 603-608

133. Ahmed, S., Warren, H.R., Symonds, M.D. and Cox, R.P., '*The Radarsat System*' , IEEE Transactions on Geoscience and REmote Sensing, Vol. 28, No. 4, July 1990, 598-602

134. Noack, W., Popella, A. and Schreier, G., '*Knowledge-Based SAR Processing and Geocoding: The Elementary Components of the German Processing and Archiving Facility for High Throughput and High-Precision Processing of ERS-1 SAR Data*' , IEEE Transactions on Geoscience and Remote Sensing, Vol. GE-25, No. 6, November 1987, 758-769

135. Wu, C., Liu, K.Y. and Jin, M., '*Modeling and a Correlation Algorithm for Spaceborne SAR Signals*' , IEEE Transactions on Aerospace and Electronic Systems, Vol. AES-18, No. 5, September 1982, p.564

136. Elachi, C., *Spaceborne Radar Remote Sensing: Applications and Techniques.* New York: IEEE Press, 1987, 91-96

137. Munson, D.C. and Visentin, R.L., '*A Signal Processing View of Strip-Mapping Synthetic Aperture Radar*' , Vol. 37, No. 12, December 1989, p.2134

138. Bergland, G.D., '*A guided tour of the fast Fourier transform*' , IEEE Spectrum, July 1969, 41-52

139. Roberts, R.A. and Mullis, C.T., *Digital Signal Processing.* Addison-Wesley, 1987, 130-139, 147-169

140. Barber, B.C., '*Theory of digital imaging from orbital synthetic-aperture radar*' , INT. J. Remote Sensing, 1985, Vol. 6, No. 7, p.1039

141. Rihaczek, A.W., *Principles of High-Resolution Radar.* Los Altos, California: Peninsula Publishing, 1985, p.232

142. Roberts R.A. and Mullis C.T. , *Digital Signal Processing.* Addison-Wesley, 1987, 130-139, p.130, p.134

143. Curlander, J.C., '*Performance of the SIR-B Digital Image Processing Subsystem*' , IEEE Transactions on Geoscience and Remote Sensing, Vol. GE-24, No. 4, July 1986, p.649

144. Barber, B.C., '*Theory of digital imaging from orbital synthetic-aperture radar*' , INT. J. Remote Sensing, 1985, Vol. 6, No. 7, p.1030

145. Wu, C., Barkan, B., Karplus, W.J. and Caswell, D., '*SEASAT Synthetic-Aperture Radar Data Reduction Using Parallel Programmable Array Processors*' , IEEE Transactions on Geoscience and Remote Sensing, Vol. GE-20, No. 3, July 1982, p.354

146. Bergland, G.D., '*A guided tour of the fast Fourier transform*' , IEEE Spectrum, July 1969, p.50

147. Bergland, G.D., '*A guided tour of the fast Fourier transform*' , IEEE Spectrum, July 1969, 48-49 & Figure 15 & Figure 16

148. Bracewell, R.N., *The Fourier Transform and Its Applications*. 2nd ed. New York: McGraw-Hill, 1978, 362-363

149. Oppenheim, A.V. and Willsky, A.S., *Signals and Systems*. Englewood Cliffs, New Jersey: Prentice-Hall, 1983, 329-333

150. Barber, B.C., '*Theory of digital imaging from orbital synthetic-aperture radar*' , INT. J. Remote Sensing, 1985, Vol. 6, No. 7, p.1039

151. Welsh, S.D., (*Masters Thesis to be submitted*) , Department of Electrical Engineering, University of Cape Town, 1991

152. Oppenheim, A.V. and Willsky, A.S., *Signals and Systems*. Englewood Cliffs, New Jersey: Prentice-Hall, 1983, 515-518

153. Barber, B.C., '*Theory of digital imaging from orbital synthetic-aperture radar*' , INT. J. Remote Sensing, 1985, Vol. 6, No. 7, p.1032

154. Huneycutt, B.L., '*Innovative Operating Modes and Techniques For the Spaceborne Imaging Radar-C Instrument*' , IEEE Transactions on Geoscience and Remote Sensing, Vol. 28, No. 4, July 1990, p.603 (Table I) & p.607

155. Elachi, C., *Spaceborne Radar Remote Sensing: Applications and Techniques*. New York: IEEE Press, 1987, p.56 & p.64

156. Stimson, G.W., *Introduction to Airborne Radar*. El Segundo, California: Hughes Aircraft Company, 1983, p.533

157. Cutrona, L.J. and Hall, G.O., '*A Comparison Of Techniques For Achieving Fine Azimuth Resolution*' , IRE Transactions on Military Electronics, Vol. MIL-6, No. 2, April 1962, p.120

158. Kovaly J.J. , *Synthetic Aperture Radar.* , Dedham, Massachusetts: Artech House, 1976, Introduction (p.v)

159. Welsh, S.D., (*Masters Thesis to be submitted*) , Department of Electrical Engineering, University of Cape Town, 1991

160. Li, F.K., Held, D.N., Curlander, J.C. and Wu, C., '*Doppler Parameter Estimation for Spaceborne Synthetic Aperture Radars*', IEEE Transactions on Geoscience and Remote Sensing, Vol. GE-23, No. 1, January 1985, 47-56

161. Elachi, C., Bicknell, T., Jordan, R.L. and Wu, C., '*Spaceborne Synthetic-Aperture Imaging Radars: Applications, Techniques, and Technology*' , Proceedings of the IEEE, Vol. 70, No. 10, October 1982, p.1189

162. Curlander, J.C., '*Performance of the SIR-B Digital Image Processing Subsystem*' , IEEE Transactions on Geoscience and Remote Sensing, Vol. GE-24, No. 4, July 1986, p.649

163. Curlander, J.C., '*Location of Spaceborne SAR Imagery*' , IEEE Transactions on Geoscience and Remote Sensing , Vol. GE-20, No. 3, July 1982, 359-360

164. Curlander, J.C., '*Location of Spaceborne SAR Imagery*' , IEEE Transactions on Geoscience and Remote Sensing , Vol. GE-20, No. 3, July 1982, 359-364

165. Curlander, J.C., '*Location of Spaceborne SAR Imagery*' , IEEE Transactions on Geoscience and Remote Sensing , Vol. GE-20, No. 3, July 1982, p.363

166. Curlander, J.C., '*Location of Spaceborne SAR Imagery*' , IEEE Transactions on Geoscience and Remote Sensing , Vol. GE-20, No. 3, July 1982, p.360

167. Curlander, J.C., '*Location of Spaceborne SAR Imagery*' , IEEE Transactions on Geoscience and Remote Sensing , Vol. GE-20, No. 3, July 1982, 359-360

168. Noack, W., Popella, A. and Schreier, G., '*Knowledge-Based SAR Processing and Geocoding: The Elementary Components of the German Processing and Archiving Facility for High Throughput and High-Precision Processing of ERS-1 SAR Data*', IEEE Transactions on Geoscience and Remote Sensing, Vol. GE-25, No. 6, November 1987, p.766

169. Elachi, C., *Spaceborne Radar Remote Sensing: Applications and Techniques.* New York: IEEE Press, 1987, p.104

170. Ahmed, S., Warren, H.R., Symonds, M.D. and Cox, R.P., '*The Radarsat System*', IEEE Transactions on Geoscience and Remote Sensing, Vol. 28, No. 4, July 1990

171. Huneycutt, B.L., '*Innovative Operating Modes and Techniques for the Spaceborne Imaging Radar-C Instrument*', IEEE Transactions on Geoscience and Remote Sensing, Vol. 28, No. 4, July 1990, p.605

172. Curlander, J.C., '*Location of Spaceborne SAR Imagery*' , IEEE Transactions on Geoscience and Remote Sensing , Vol. GE-20, No. 3, July 1982, p.359

173. Elachi, C., *Spaceborne Radar Remote Sensing: Applications and Techniques.* New York: IEEE Press, 1987, p.106 (Figure 4-19 & Figure 4-20)

174. Curlander, J.C., '*Location of Spaceborne SAR Imagery*' , IEEE Transactions on Geoscience and Remote Sensing , Vol. GE-20, No. 3, July 1982, p.363

175. Noack W. , Popella A. and Schreier G. , '*Knowledge-Based SAR Processing and Geocoding: The Elementary Components of the German Processing and Archiving Facility for High Throughput and High-Precision Processing of ERS-1 SAR Data*', IEEE Transactions on Geoscience and Remote Sensing, Vol. GE-25, No. 6, November 1987, p.764

176. Curlander, J.C., '*Location of Spaceborne SAR Imagery*' , IEEE Transactions on Geoscience and Remote Sensing , Vol. GE-20, No. 3, July 1982, p.363

177. Curlander, J.C., '*Location of Spaceborne SAR Imagery*' , IEEE Transactions on Geoscience and Remote Sensing , Vol. GE-20, No. 3, July 1982, p.360

178. Curlander, J.C., '*Location of Spaceborne SAR Imagery*' , IEEE Transactions on Geoscience and Remote Sensing , Vol. GE-20, No. 3, July 1982, p.363

179. Wu, C., Liu, K.Y. and Jin, M., '*Modeling and a Correlation Algorithm for Spaceborne SAR Signals*' , IEEE Transactions on Aerospace and Electronic Systems, Vol. AES-18, No. 5, September 1982, p.563 & p.566

180. Tomiyasu, K., '*Tutorial Review of Synthetic-Aperture Radar (SAR) with Applications to Imaging of the Ocean Surface*', Proceedings of the IEEE, Vol. 66, No. 5, May 1978, 565-566 & p.570

181. Elachi, C., *Spaceborne Radar Remote Sensing: Applications and Techniques.* , New York: IEEE Press, 1987, 130-131

182. Wu, C., Liu, K.Y. and Jin, M., '*Modeling and a Correlation Algorithm for Spaceborne SAR Signals*' , IEEE Transactions on Aerospace and Electronic Systems, Vol. AES-18, No. 5, September 1982, p.563 & p.566

183. Peschon, *Disciplines and Techniques of System Control.* New York: Blaisdell Publishing Company, 1965, p.394

184. Meirovitch, L., *Methods of Analytical Dynamics.* New York: McGraw-Hill, 1970, p.108

185. Ausherman, D.A., Kozma, A., Walker, J.L., Jones, H.M. and Poggio, E.C., '*Developments in Radar Imaging*', IEEE Transactions on Aerospace and Electronic Systems, Vol. AES-20, No. 4, July 1984, p.370

186. Munson, D.C. and Visentin, R.L., '*A Signal Processing View of Strip-Mapping Synthetic Aperture Radar*', IEEE Transactions on Acoustics, Speech and Signal Processing, Vol. 37, No. 12, December 1989, p.2138

187. Tomiyasu, K., '*Tutorial Review of Synthetic-Aperture Radar (SAR) with Applications to Imaging of the Ocean Surface*', Proceedings of the IEEE, Vol. 66, No. 5, May 1978, p.574

188. Barber, B.C., '*Theory of Digital Imaging from Orbital Synthetic-Aperture Radar.*', Int. J. Remote Sensing, Vol. 6, No. 7, 1985, p.1026

189. Elachi, C., *Spaceborne Radar Remote Sensing: Applications and Techniques.* New York: IEEE Press, 1987, p.106

190. Wehner, D.R., *High Resolution Radar.* Norwood, MA: Artech House, 1987, p.187

191. Elachi, C., Bicknell, T., Jordan, R.L. and Wu, C., '*Spaceborne Synthetic-Aperture Imaging Radars: Applications, Techniques, and Technology*', Proceedings of the IEEE, Vol. 70, No. 10, October 1982, p.1175 & Fig.1

192. Munson, D.C. and Visentin, R.L., '*A Signal Processing View of Strip-Mapping Synthetic Aperture Radar*', IEEE Transactions on Acoustics, Speech, and Signal Processing, Vol. 37,No. 12, December 1989, p.2139

193. Elachi, C., *Spaceborne Radar Remote Sensing: Applications and Techniques.* New York: IEEE Press, 1987, p.106 (Fig. 4-19)

194. Curlander, J.C., '*Performance of the SIR-B Digital Image Processing Subsystem*', IEEE Transactions on Geoscience and Remote Sensing, Vol. GE-24, No. 4, July 1986, p.649

195. Elachi, C., *Spaceborne Radar Remote Sensing: Applications and Techniques.* New York: IEEE Press, 1987, 72-73

196. Tomiyasu, K., '*Tutorial Review of Synthetic-Aperture Radar (SAR) with Applications to Imaging of the Ocean Surface*', Proceedings of the IEEE, Vol. 66, No. 5, May 1978, p.564

197. Wu, C., Liu, K.Y. and Jin, M., '*Modeling and a Correlation Algorithm for Spaceborne SAR Signals*', IEEE Transactions on Aerospace and Electronic Systems, Vol. AES-18, No. 5, September 1982, p.567

198. Kovaly, J.J., '*Radar Techniques For Planetary Mapping With Orbiting Vehicle*', Annals of the New York Academy of Sciences, Vol. 187, 25 January 1972, p.163

199. Curlander, J.C., '*Performance of the SIR-B Digital Image Processing Subsystem*', IEEE Transactions on Geoscience and Remote Sensing, Vol. GE-24, No. 4, July 1986, p.649-p.650

200. Fitch, J.P., *Synthetic Aperture Radar.* New York: Springer-Verlag, 1988, 67-69

201. Elachi, C., *Spaceborne Radar Remote Sensing: Applications and Techniques.* New York: IEEE Press, 1987, 66-71

202. Li, F.K. and Bryan, M.L., '*Tradeoffs Among Several Synthetic Aperture Radar Image Quality Parameters: Results of a User Survey Study*', Photogrammetric Engineering and Remote Sensing, Vol. 49, No. 6, June 1983, 792-793 & 795-801

203. Wu, C., Liu, K.Y. and Jin, M., '*Modeling and a Correlation Algorithm for Spaceborne SAR Signals*', IEEE Transactions on Aerospace and Electronic Systems, Vol. AES-18, No. 5, September 1982, p.565

204. Welsh, S.D., (*Masters thesis to be submitted*) , Department of Electrical Engineering, University of Cape Town, 1991

205. Wu, C., Barkan, B., Karplus, W.J. and Caswell, D., '*SEASAT Synthetic-Aperture Radar Data Reduction Using Parallel Programmable Array Processors*', IEEE Transactions on Geoscience and Remote Sensing, Vol. GE-20, No. 3, July 1982, p.352 (Fig. 1)

206. Elachi, C., Bicknell, T., Jordan, R.L. and Wu, C., '*Spaceborne Synthetic-Aperture Imaging Radars: Applications, Techniques, and Technology*', Proceedings of the IEEE, Vol. 70, No. 10, October 1982, p.1177

207. Munson, D.C. and Visentin, R.L., '*A Signal Processing View of Strip-Mapping Synthetic Aperture Radar*', IEEE Transactions on Acoustics, Speech, and Signal Processing, Vol. 37, No. 12, December 1989, p.2142

208. Munson, D.C. and Visentin, R.L., '*A Signal Processing View of Strip-Mapping Synthetic Aperture Radar*', IEEE Transactions on Acoustics, Speech, and Signal Processing, Vol. 37, No. 12, December 1989, p.2142

209. Barber, B.C., '*Theory of Digital Imaging from Orbital Synthetic-Aperture Radar*', Int. J. Remote Sensing, Vol. 6, No. 7, 1985, p.1052 & Figure 24.

210. Barber, B.C., '*Theory of Digital Imaging from Orbital Synthetic-Aperture Radar*', Int. J. Remote Sensing, Vol. 6, No. 7, 1985, p.1052 & Figure 24.

211. Welsh, S.D., (*Masters thesis to be submitted*), Department of Electrical Engineering, University of Cape Town, 1991

212. Cimino, J.B., Holt, B. and Richardson, A.H., *The Shuttle Imaging Radar B (SIR-B) Experimental Report.* Jet Propulsion Laboratory, California: NASA (JPL Pub. 88-2), 1988, p.50

213. Barber, B.C., '*Theory of Digital Imaging from Orbital Synthetic-Aperture Radar*', Int. J. Remote Sensing, Vol. 6, No. 7, 1985, p.1053 & Figure 26 & Figure 27

214. Cimino, J.B., Holt, B. and Richardson, A.H., *The Shuttle Imaging Radar B (SIR-B) Experimental Report.* Jet Propulsion Laboratory, California: NASA (JPL Pub. 88-2), 1988, p.50

215. Wu C. , Liu K.Y. and Jin M. , '*Modeling and a Correlation Algorithm for Spaceborne SAR Signals*', IEEE Transactions on Aerospace and Electronic Systems, Vol. AES-18, No. 5, September 1982, 569-570

216. Fitch, J.P., *Synthetic Aperture Radar.* New York: Springer-Verlag, 1988, 66-67

217. Barber, B.C., '*Theory of Digital Imaging from Orbital Synthetic-Aperture Radar*', Int. J. Remote Sensing, Vol. 6, No. 7, 1985, p.1048

218. Welsh, S.D., (*Masters thesis to be submitted*), Department of Electrical Engineering, University of Cape Town, 1991

219. Ausherman, D.A., Kozma, A., Walker, J.L., Jones, H.M. and Poggio, E.C., '*Developments in Radar Imaging*', IEEE Transactions on Aerospace and Electronic Systems, Vol. AES-20, No. 4, July 1984, p.364 & p.373

220. Fitch, J.P., *Synthetic Aperture Radar.* New York: Springer-Verlag, 1988, 67-69

221. Munson, D.C. and Visentin, R.L., '*A Signal Processing View of Strip-Mapping Synthetic Aperture Radar*', IEEE Transactions on Acoustics, Speech and Signal Processing, Vol. 37, No. 12, December 1989, 2142-2143

222. Barber, B.C., '*Theory of Digital Imaging from Orbital Synthetic-Aperture Radar*', Int. J. Remote Sensing, Vol. 6, No. 7, 1985, 1050-1053

223. Tomiyasu, K., '*Tutorial Review of Synthetic-Aperture Radar (SAR) with Applications to Imaging of the Ocean Surface*', Proceedings of the IEEE, Vol. 66, No. 5, May 1978, p.574 & (Table 1)

224. Raney, R.K., '*Synthetic Aperture Imaging Radar and Moving Targets*', IEEE Transactions on Aerospace and Electronic Systems, Vol. AES-7, No.3, May 1971, p.503

225. Elachi, C., *Spaceborne Radar Remote Sensing: Applications and Techniques.* New York: IEEE Press, 1988, p.108

226. Rabiner, L.R. and Gold, B., '*Theory and Applications of Digital Signal Processing*', Englewood Cliffs, New Jersey: Prentice-Hall, 1975, p.728

227. Noack, W., Popella, A. and Schreier, G., '*Knowledge-Based SAR Processing and Geocoding: The Elementary Components of the German Processing and Archiving Facility for High Throughput and High-Precision Processing of ERS-1 SAR Data*', IEEE Transactions on Geoscience and Remote Sensing, Vol. GE-25, No. 6, November 1987, 764-765

228. Elachi, C., *Spaceborne Radar Remote Sensing: Applications and Techniques.* New York: IEEE Press, 1987, p.38 (Fig. 2-37) & p.39 (Fig. 2-38)

229. Tomiyasu, K., '*Tutorial Review of Synthetic-Aperture Radar (SAR) with Applications to Imaging of the Ocean Surface*', Proceedings of the IEEE, Vol. 66, No. 5, May 1978, p.573 & (Fig. 15)

230. Rabiner, L.R. and Gold, B., '*Theory and Applications of Digital Signal Processing*', Englewood Cliffs, New Jersey: Prentice-Hall, 1975, p.728

231. Kirk, J.C., '*A Discussion Of Digital Processing in Synthetic Aperture Radar*', IEEE Transactions on Aerospace and Electronic Systems, Vol. AES-11, No. 3, May 1975, p.327

232. Barber, B.C., '*Theory of Digital Imaging from Orbital Synthetic-Aperture Radar*', Int. J. Remote Sensing, Vol. 6, No. 7, 1985, 1037-1038

233. Harris, F.J., '*On the Use of Windows for Harmonic Analysis with the Discrete Fourier Transform*', Proceedings of the IEEE, Vol. 66, No. 1, January 1978, p.82

234. Welsh, S.D., (*Masters thesis to be submitted*), Department of Electrical Engineering, University of Cape Town, 1991

BIBLIOGRAPHY.

Ahmed, S., Warren, H.R., Symonds, M.D. and Cox, R.P., *'The Radarsat System'* , IEEE Transactions on Geoscience and Remote Sensing, Vol. 28, No. 4, July 1990, 598-602

Ausherman, D.A., Kozma, A., Walker, J.L., Jones, H.M. and Poggio, E.C., *'Developments in Radar Imaging'* , IEEE Transactions on Aerospace and Electronic Systems, Vol. AES-20, No. 4, July 1984, 363-399

Barber, B.C., *'Theory of Digital Imaging from Orbital Synthetic-Aperture Radar'*, Int. J. Remote Sensing, Vol. 6, No. 7, 1985, 1009-1057

Bayma, R.W. and McInnes P.A., *'Aperture Size And Ambiguity Constraints For A Synthetic Aperture Radar'* , The Records of the IEEE 1975 International Radar Conference (21-23 April 1975), 499-504

Bergland, G.D., *'A guided tour of the fast Fourier tranform'* , IEEE Spectrum, July 1969, 41-52

Bracewell, R.N., *The Fourier Transform and Its Applications*. 2nd ed. New York: McGraw-Hill, 1978

Brigham, E.O., *The Fast Fourier Transform and its Applications*. Englewood Cliffs, New Jersey: Prentice-Hall, 1988

Brown, W.M. and Porcello, L.J., *'An Introduction To Synthetic Aperture Radar'*, IEEE Spectrum, September 1969, 52-62

Brown, W.M., *'Synthetic Aperture Radar'* , IEEE Transactions on Aerospace and Electronic Systems, Vol. AES-3, No. 2, March 1967, 217-229

Chen, C. and Andrews, H.C., *'Target-Motion-Induced Radar Imaging'* , IEEE Transactions on Aerospace and Electronic Systems, Vol.AES-16, No. 1, January 1980, 2-14

Cimino, J.B., Holt B. and Richardson A.H., *The Shuttle Imaging Radar B (SIR-B) Experimental Report.* Jet Propulsion Laboratory, California: NASA (JPL Pub. 88-2), 1988

Curlander, J.C., *'Performance of the SIR-B Digital Image Processing Subsystem'*, IEEE Transactions on Geoscience and Remote Sensing, Vol. GE-24, No. 4, July 1986, 649-652

Curlander, J.C., *'Location of Spaceborne SAR Imagery'* , IEEE Transactions on Geoscience and Remote Sensing , Vol. GE-20, No. 3, July 1982, 359-364

Cutrona, L.J., Vivian, W.E., Leith, E.N. and Hall, G.O., *'A High Resolution Radar Combat-Surveillance System'*, IRE Transactions on Military Electronics, Vol. MIL-5, No. 2, April 1961, 127-131

Cutrona, L.J. and Hall, G.O., *'A Comparison Of Techniques For Achieving Fine Azimuth Resolution'* , IRE Transactions on Military Electronics, Vol. MIL-6, No. 2, April 1962, 119-121

De Fatta, D.J., Lucas J.G. and Hodgkiss, W.S., *Digital Signal Processing.* Singapore: John Wiley & Sons, 1988

Develet, J.A., *'Performance of a Synthetic-Aperture Mapping Radar System'*, IEEE Transactions on Aerospace and Navigational Electronics, Vol. ANE-11, No. 3, September 1964, 173-179

Dudgeon, D.E., Mersereau R.M., *Multidimensional Digital Signal Processing.* Englewood Cliffs, New Jersey: Prentice-Hall, 1984,

Elachi, C., Bicknell, T., Jordan, R.L. and Wu, C., '*Spaceborne Synthetic-Aperture Imaging Radars: Applications, Techniques, and Technology*' , Proceedings of the IEEE, Vol. 70, No. 10, October 1982, 1174-1209

Elachi, C., *Spaceborne Radar Remote Sensing: Applications and Techniques.* New York: IEEE Press, 1987

Fitch, J.P., *Synthetic Aperture Radar.* New York: Springer-Verlag, 1988

Gaskill, J.D., *Linear Systems, Fourier Transforms, and Optics.* New York: John Wiley & Sons, 1978

Geckinli, N.C. and Yavuz, D., '*Some Novel Windows and a Concise Tutorial Comparison of Window Families*', IEEE Transactions on Acoustics, Speech, and Signal Processing, Vol. ASSP-26, No. 6, December 1978, 501-507

Harger, R.O., '*An Optimum Design Of Ambiguity Function, Antenna Pattern, and Signal For Side-Looking Radars*' , IEEE Transactions on Military Electronics, Vol. MIL-9, Nos. 3 and 4 (July/October 1965) 264-278

Harris, F.J., '*On the Use of Windows for Harmonic Analysis with the Discrete Fourier Transform*', Proceedings of the IEEE, Vol. 66, No. 1, January 1978, 51-83

Hecht, E., *Optics.* 2nd ed. Reading, Massachusetts: Addison-Wesley, 1987

Heimiller, R.C., '*Theory and Evaluation Of Gain Patterns Of Synthetic Arrays*' , IRE Transactions on Military Electronics, Vol. MIL-6, No. 2, April 1962, 122-129

Hovanessian, S.A., *Radar System Design and Analysis.* Norwood, MA: Artech House, 1984

Hovanessian, S.A., *Introduction to Synthetic Array and Imaging Radars.* Dedham, MA: Artech House, 1980

Huneycutt, B.L., '*Innovative Operating Modes and Techniques For the Spaceborne Imaging Radar-C Instrument*' , IEEE Tranactions on Geoscience and Remote Sensing, Vol. 28, No. 4, July 1990, 603-608

Jin, M.J., '*Optimal Doppler Centroid Estimation for SAR Data from a Quasi-Homogeneous Source*' , IEEE Transactions on Geoscience and Remote Sensing, Vol. GE-24, No. 6, November 1986, 1022-1025

Kirk, J.C., '*A Discussion Of Digital Processing in Synthetic Aperture Radar*', IEEE Transactions on Aerospace and Electronic Systems, Vol. AES-11, No. 3, May 1975, 326-337

Kovaly, J.J., *Synthetic Aperture Radar.* Dedham, Massachusetts: Artech House, 1976

Kovaly, J.J., '*Radar Techniques For Planetary Mapping With Orbiting Vehicle*', Annals of the New York Academy of Sciences, Vol. 187, 25 January 1972, 154-176

Lai, W.M., Rubin, D. and Kremple, E., *Introduction to Continuum Mechanics.* New York: Pergamon Press Inc, 1974

Li, F.K., Held, D.N., Curlander, J.C. and Wu, C., '*Doppler Parameter Estimation for Spaceborne Synthetic Aperture Radars*', IEEE Transactions on Geoscience and Remote Sensing, Vol. GE-23, No. 1, January 1985, 47-56

Li, F.K. and Bryan, M.L., '*Tradeoffs Among Several Synthetic Aperture Radar Image Quality Parameters: Results of a User Survey Study*', Photogrammetric Engineering and Remote Sensing, Vol. 49, No. 6, June 1983, 791-803

Madsen, S.N., '*Estimating the Doppler Centroid of SAR Data*' , IEEE Tranactions on Aerospace and Electronic Systems, Vol. AES-25, No. 2, March 1989, 134-140

McCord, H.L., '*The Equivalence Among Three Approaches To Deriving Synthetic Array Patterns And Analyzing Processing Techniques*' , IRE Transactions on Military Electronics, Vol. MIL-6, No. 1, January 1962, 116-119

Meirovitch, L., *Methods of Analytical Dynamics.* New York: McGraw-Hill, 1970

Munson, D.C. and Visentin, R.L., '*A Signal Processing View of Strip-Mapping Synthetic Aperture Radar*' , Vol. 37, No. 12, December 1989, 2131-2147

Noack, W., Popella, A. and Schreier, G., '*Knowledge-Based SAR Processing and Geocoding: The Elementary Components of the German Processing and Archiving Facility for High Throughput and High-Precision Processing of ERS-1 SAR Data*', IEEE Transactions on Geoscience and Remote Sensing, Vol. GE-25, No. 6, November 1987, 758-769

Oppenheim, A.V. & Willsky, A.S., *Signals and Systems.* Englewood Cliffs, New Jersey: Prentice-Hall, 1983

Oppenheim, A.V. and Schafer, R.W., *Digital Signal Processing.* Prentice-Hall, 1975

Peschon, *Disciplines and Techniques of System Control.* New York: Blaisdell Publishing Company, 1965

Rabiner, L.R. and Gold, B., '*Theory and Applications of Digital Signal Processing*', Englewood Cliffs, New Jersey: Prentice-Hall, 1975

Raney, R.K., '*Synthetic Aperture Imaging Radar and Moving Targets*', IEEE Transactions on Aerospace and Electronic Systems, Vol. AES-7, No.3, May 1971, 499-506

Raney, R.K., '*Reconsideration of Azimuth Ambiguities in SAR*' , IEEE Transactions on Geoscience and Remote Sensing, Vol. GE-25, No. 6, November 1987, 783-787

Rihaczek, A.W., *Principles of High_Resolution Radar.* Los Altos, California: Peninsula Publishing, 1985

Roberts, R.A. and Mullis, C.T., *Digital Signal Processing.* Addison-Wesley, 1987

Sherwin, S.M., *Monopulse Principles and Techniques.* Norwood MA: Artech House

Sherwin, C.W., Ruina, J.P. and Rawcliffe, R.D., '*Some Early Developments In Synthetic Aperture Radar Systems*', IRE Tranactions on Military Electronics, Vol. MIL-6, No. 2, April 1962, 111-115

Skolnik, M.I., *Introduction to Radar Systems.* 2nd ed. Tokyo: McGraw-Hill, 1980

Spiegel, M.R., *Mathematical Handbook of Formulas and Tables (Schaum's Outline Series).* New York: McGraw-Hill

Stimson, G.W., *Introduction to Airborne Radar.* El Segundo, California: Hughes Aircraft Company, 1983

Stremler, F.G., *Introduction to Communication Systems.* 2nd ed. Reading, Massachusetts: Addison-Wesley, 1982

Swokowski, E.W., *Calculus with Analytic Geometry.* 3rd ed. Boston, Massachusetts: Prindle Weber & Schmidt, 1984

Tomiyasu, K., '*Tutorial Review of Synthetic-Aperture Radar (SAR) with Applications to Imaging of the Ocean Surface*' , Proceedings of the IEEE, Vol. 66, No. 5, May 1978, 563-583

Tretter, S.A., *Introduction to Discrete-Time Signal Processing.* New York: John Wiley & Sons, 1976

Van Zyl, M.W., '*Radar Signal Processing Lecture Notes*' , University of Cape Town: 1990

Wehner, D.R., *High Resolution Radar.* Norwood, MA: Artech House, 1987

Welsh, S.D., (*Masters thesis to be submitted*) , Department of Electrical Engineering, University of Cape Town, 1991

Wu, C., Barkan, B., Karplus, W.J. and Caswell, D., '*SEASAT Synthetic-Aperture Radar Data Reduction Using Parallel Programmable Array Processors*', IEEE Transactions on Geoscience and Remote Sensing, Vol. GE-20, No. 3, July 1982, 352-357

Wu, C., Liu, K.Y. and Jin, M., '*Modeling and a Correlation Algorithm for Spaceborne SAR Signals*' , IEEE Tranactions on Aerospace and Electronic Systems, Vol. AES-18, No. 5, September 1982, 563-575

APPENDICES

APPENDIX A

APPENDIX A1

ANALOGUE IN-PHASE AND QUADRATURE DEMODULATION.

For a single radar return waveform we have the expression

$$h(t') = p(t'-D_n,\tau) \cdot \cos(2\pi f_o t' - \theta_n + \phi_n)$$

In-phase demodulation.

In-phase demodulation involves multiplying the radar return signal with a copy of the coherent oscillator waveform to produce the signal

$$p(t'-D_n,\tau) \cdot \cos(2\pi f_o t' - \theta_n + \phi_n) \cdot \cos(2\pi f_o t' + \phi_n)$$

Using a standard trigonometric identity

$$\cos(a).\cos(b) = \frac{1}{2} \cdot \cos(a+b) + \cos(a-b)$$

this equation can be rewritten as

$$p(t'-D_n,\tau) \cdot \left\{ \frac{1}{2} \cdot \cos(-\theta_n) + \frac{1}{2} \cdot \cos(4\pi f_o t + 2\phi_n - \theta_n) \right\}$$

Filtering out the high frequency terms using a Low Pass Filter this reduces to the following **In-phase** signal.

$$I(t') = \frac{1}{2} . p(t'-D_n,\tau) . \cos(\theta_n)$$

Quadrature demodulation.

Quadrature demodulation involves multiplying the radar return signal with a 90° phase shifted copy of the coherent oscillator waveform.

$$p(t'-D_n,\tau) . \cos(2\pi f_o t' - \theta_n + \phi_n) . \cos(2\pi f_o t' + \phi_n)$$

Using a standard trigonometric identity

$$\cos(a).\sin(b) = \frac{1}{2} . \cos(a+b) - \sin(a-b)$$

this equation is rewritten as

$$p(t'-D_n,\tau) . \left\{ -\frac{1}{2} . \sin(-\theta_n) + \frac{1}{2} . \sin(4\pi f_o t + 2\phi_n - \theta_n) \right\}$$

Filtering out the high frequency terms using a Low Pass Filter it reduces to the following "**Quadrature**" signal.

$$Q(t') = \frac{1}{2} . p(t'-D_n,\tau) . \sin(\theta_n)$$

APPENDIX A2

DIGITAL DEMODULATION OF A SAMPLED RETURN RADAR SIGNAL.

For a single return radar waveform we have that

$$h(t') = p(t'-D_n,\tau).\cos(2\pi f_o t' - \theta_n)$$

The Fourier transform of this signal can be written as the Fourier transform of the envelope $p(t'-D_n,\tau)$, convolved with the Fourier transform of the coherent carrier term.

$$\mathcal{F}[h(t',\tau)] = \mathcal{F}[p(t'-D_n,\tau)] \circledast \mathcal{F}[\cos(2\pi f_o t' + \theta_n)]$$

Using standard Fourier identities, the above equation is rewritten as

$$\mathcal{F}[h(t',\tau)] = \mathcal{F}[p(t',\tau)] \circledast$$

$$\left\{ \begin{array}{l} \dfrac{\cos(\theta_n)}{2}.[2\pi.\delta(2\pi f - 2\pi f_o) + 2\pi.\delta(2\pi f + 2\pi f_o)] + \\ \dfrac{\sin(\theta_n)}{2j}.[2\pi.\delta(2\pi f - 2\pi f_o) - 2\pi.\delta(2\pi f + 2\pi f_o)] \end{array} \right\}$$

Assuming that the Fourier transform of the envelope $p(t',\tau)$ is given by some function $P(2\pi f)$ and using the standard Fourier identity

$$\delta(2\pi f - 2\pi f_o) \circledast F(2\pi f)$$

$$= \frac{1}{2\pi} \cdot \int_{-\infty}^{\infty} F(\Omega).\delta(2\pi f - 2\pi f_o - \Omega)\, d\Omega$$

$$= \frac{1}{2\pi} . F(2\pi f - 2\pi f_o)$$

we get

$$\mathcal{F}[h(t',\tau)] = \frac{\cos(\theta_n)}{2} . \{P(2\pi f - 2\pi f_o) + P(2\pi f + 2\pi f_o\}$$

$$+ \frac{\sin(\theta_n)}{2j} . \{P(2\pi f - 2\pi f_o) - P(2\pi f + 2\pi f_o)\}$$

Removing the negative frequency components of this spectrum and performing a digital frequency shift to baseband (a simple translation of sampled array values), the following spectrum is obtained:

$$\frac{\cos(\theta_n)}{2} . P(2\pi f) + \frac{\sin(\theta_n)}{2j} . P(2\pi f)$$

The inverse Fourier transform of this produces a demodulated and complex signal called the **range waveform.** A set of these waveforms as recorded as a function of azimuth time, t, is written as a discrete set

$$f_r(t') = \sum_{n=-(\frac{N}{2}-1)}^{\frac{N}{2}} p(t'-D_n,\tau) . e^{-j.\theta_n}$$

where the phase delay θ_n is given as

$$\theta_n = 2\pi f_o D_n$$

APPENDIX A3

THE CORRELATION OF A COMPLEX CHIRP PULSE.

Rihaczek and Harger quote the following result for a chirp pulse of large time-bandwidth product:

$$\mathcal{F}\left[A(t).e^{j.\pi kt^2}\right] = \sqrt{\frac{1}{|k|}}.A\left(\frac{f}{k}\right).e^{-j.\frac{\pi f^2}{k} \pm j.\frac{\pi}{4}} \qquad \text{(A-1)}$$

Using this result the Fourier transform of

$$p(t',\tau) = e^{j.\pi a(t')^2}$$

is given as

$$P(f) = \sqrt{\frac{1}{|a|}}.e^{-j.\frac{\pi f^2}{a} \pm j.\frac{\pi}{4}} \qquad \text{(A-2)}$$

This signal is correlated with the best available estimate of that signal. This estimate, or reference function, will be termed $\underline{p(t',\tau)}$.

The correlation involves multiplying the Fourier transform of the chirp pulse with the conjugate of the Fourier transform of the reference function. Denoting the output of the correlation process as $y(t')$, the procedure can be written as

$$\begin{aligned} y(t) &= \mathcal{F}^{-1}\left[\mathcal{F}[p(t',\tau)].\left\{\mathcal{F}[\underline{p(t',\tau)}]\right\}^*\right] \\ &= \mathcal{F}^{-1}\left[P(f).\underline{P(f)^*}\right] \end{aligned}$$

Using Equation A-2 and assuming that the reference signal is exactly the same as the chirp waveform, the output from the correlation process can be rewritten as

$$y(t) = \mathcal{F}^{-1}\left\{\sqrt{\frac{1}{|a|}}.e^{j.\frac{\pi f^2}{a}}.e^{-j.\frac{\pi}{4}}\right\} \times \left\{\sqrt{\frac{1}{|a|}}.e^{j.\frac{\pi f^2}{a}}.e^{-j.\frac{\pi}{4}}\right\}^{\star}$$

Performing the indicated conjugation (which only involves changing the sign on the relevant exponentials) the exponentials cancel out to give

$$y(t) = \mathcal{F}^{-1}\begin{bmatrix} \frac{1}{|a|} & |f| \le f_{max} \\ 0 & elsewhere \end{bmatrix}$$

where f_{max} is defined to be the maximum frequency present in the chirp.

Substituting $K_o = 1/|a|$ and making use of the standard form

$$rect(\frac{x}{b}) = 1 \qquad -\frac{b}{2} < x \le \frac{b}{2}$$

$$= 0 \qquad elsewhere$$

$y(t)$ is rewritten as

$$y(t) = \mathcal{F}^{-1}\left[K_o . rect\left(\frac{f}{2\beta_r}\right)\right]$$

where β_r is equal in magnitude to f_{max} and represents the bandwidth of the correlated chirp pulse.

Finally, using the identity

$$\mathcal{F}\left[k.\frac{\sin(k\pi t)}{k\pi t}\right] = rect\left(\frac{f}{k}\right)$$

the result of correlation is

$$y(t) = 2\beta_r K_o.\frac{\sin(\pi.2\beta_r t)}{(\pi.2\beta_r t)}$$

To be noted from the above is that:

a) The correlation of a complex chirp waveform produces a purely real signal.

b) The real time signal is given as the inverse Fourier transform of a rect function whose width is governed by the frequency spread of the original chirp waveform.

c) The result of correlation is a time signal in the form of the classic "sinc" function with a first sidelobe whose magnitude is only 10dB down from the main lobe response. This time signal is sketched in Figure A1.

The 3dB resolution of this time signal is given by Equation 2-10 as

$$\delta_{rt} = \frac{1}{\beta_r}$$

If it is recognised that the frequency spread (positive and negative frequencies) of the original chirp signal is equal to twice the bandwidth β_r of the correlated signal this resolution can also be written as

$$\delta_{rt} = \frac{1}{2\beta_r'}$$

where β_r' is variable equal in value to this frequency spread: $2 \times f_{max}$.

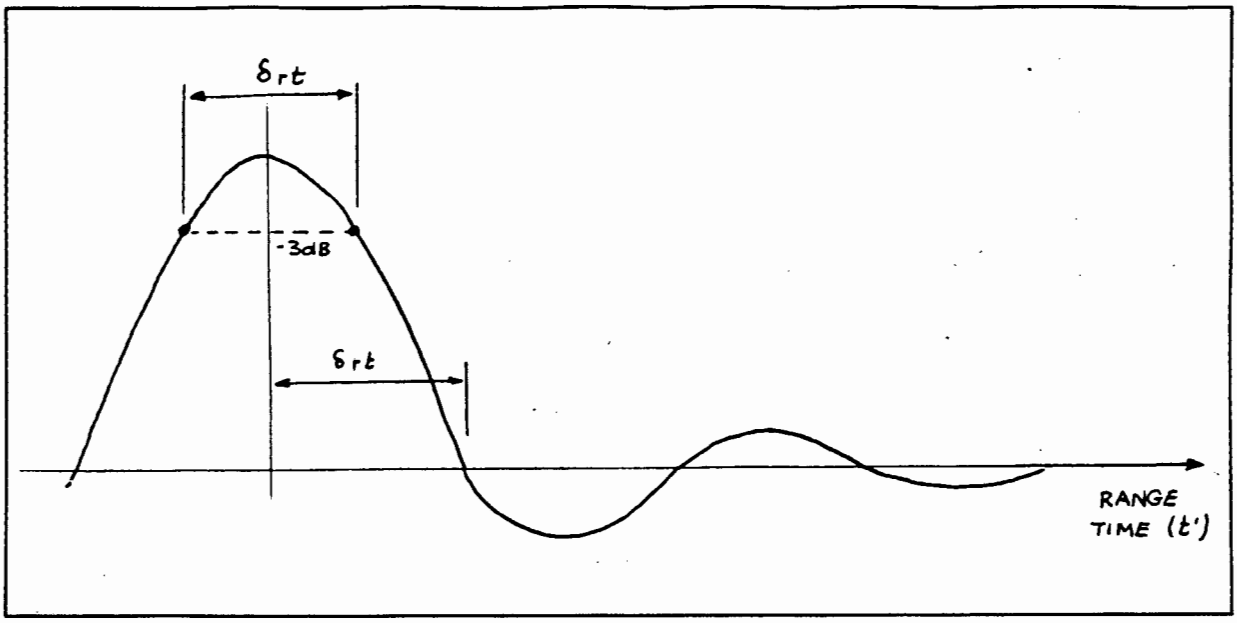

Figure A1: *A correlated chirp pulse.*

APPENDIX A4

A SMALL ANGLE APPROXIMATION TO RADIAL DISTANCE IN A SIDELOOKING SYNTHETIC APERTURE RADAR.

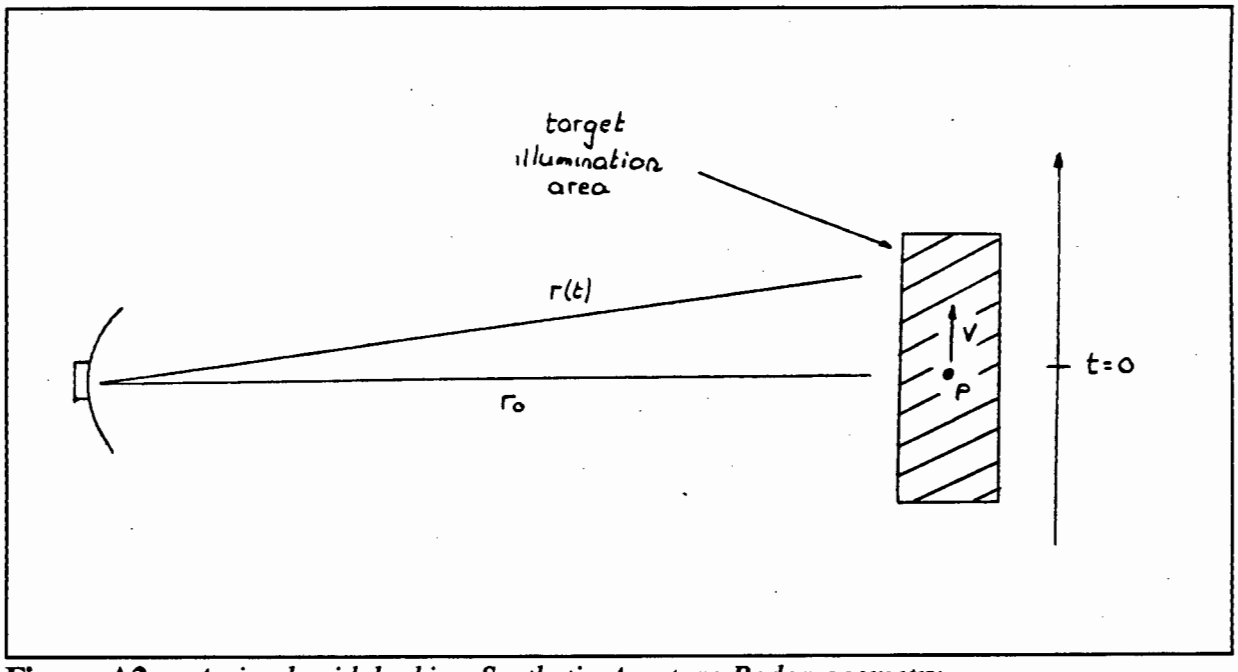

Figure A2: *A simple sidelooking Synthetic Aperture Radar geometry.*

A study of the simple SAR geometry shown in Figure A2 reveals that the relative radial distance between the target and the antenna is given as

$$r(t) = \left[r_o^2 + (Vt)^2\right]^{1/2}$$

A binomial approximation to the radial distance gives

$$r(t) = r_o + \frac{1}{2r_o}.(Vt)^2 + -\frac{1}{8r_o^3}.(Vt)^4 + \ldots$$

If only the first two terms of this approximation are kept, the following approximation to radial distance is obtained

$$r(t) = r_o + \frac{(Vt)^2}{2r_o}$$

APPENDIX A5

THE FREQUENCY SPECTRUM OF THE AZIMUTH WAVEFORM.

Rihaczek and Harger quote the following result for a chirp pulse of large time-bandwidth product:

$$\mathcal{F}\left[A(t).e^{j.\pi kt^2}\right] = \sqrt{\frac{1}{|k|}}.A\left(\frac{f}{k}\right).e^{-j.\frac{\pi f^2}{k} \pm j.\frac{\pi}{4}}$$

It is required to find the Fourier transform of

$$f_a(t) = B\left(\frac{Vt}{r_o}\right).e^{-j.2\pi\lambda_o\left(\frac{V^2t^2}{r_o}\right)}$$

The above equation can be rearranged as

$$f_a(t) = B\left(\frac{Vt}{r_o}\right).e^{-j.2\pi\lambda_o r_o\left(\frac{Vt}{r_o}\right)^2}$$

Making the substitutions

$$\zeta = \frac{Vt}{r_o}$$

and

$$k = -2\lambda_o r_o$$

the equation for the azimuth waveform reduces to the standard form

$$f_a = B(\zeta).e^{j.\pi k\zeta^2}$$

as given by Rihaczek for a chirp pulse.

The Fourier transform of this azimuth waveform can now be directly quoted as

$$\mathcal{F}[f_a(t)] = \sqrt{\frac{1}{|k|}}.B\left(\frac{f}{k}\right).e^{-j.\frac{\pi f^2}{k}-j.\frac{\pi}{4}}$$

Substituting for k and using the coordinate scaling theorem

$$\mathcal{F}[f(\alpha t)] = \frac{1}{|\alpha|}.F\left(\frac{f}{\alpha}\right)$$

the frequency spectrum of the azimuth waveform is finally

$$F_a(f) = \mathcal{F}[f_a(t)] = \sqrt{\frac{r_o}{2\lambda_o V^2}}.B\left(-\frac{\lambda_o}{2V}.f\right).e^{j.\frac{\pi}{2\lambda_o}.\left[\frac{r_o}{V^2}.f^2\right]}.e^{-j.\frac{\pi}{4}}$$

(A3)

APPENDIX A6

CORRELATION OF AN AZIMUTH WAVEFORM CENTRED AROUND THE ZERO DOPPLER POSITION.

The azimuth signal is given in Section 2-15 as

$$f_a(t) = B(\alpha(t)) \cdot e^{-j\frac{2\pi f_o}{c}\left[\frac{V^2 t^2}{r_o}\right]} \qquad -\alpha_{3dB} < t \leq \alpha_{3dB}$$

$$= 0 \qquad \textit{elsewhere}$$

with an aspect angle α equal to

$$\alpha = \frac{Vt}{r_o} .$$

This signal must be correlated with the best available estimate of that signal. This estimate, or reference signal, will be termed $\underline{f_a(t)}$.

The correlation involves multiplying the Fourier transform of the azimuth signal with the conjugate of the Fourier transform of the reference signal. Denoting the output of the azimuth correlation process as $y_a(t)$, the procedure can be written as

$$y_a(t) = \mathcal{F}^{-1}\left[\mathcal{F}[f_a(t)] \cdot \{\mathcal{F}[\underline{f_a(t)}]\}^* \right]$$

$$= \mathcal{F}^{-1}\left[F_a(f) \cdot \underline{F_a(f)^*} \right]$$

(The reference azimuth signal variable is underlined to indicate that it is only an estimate of the actual azimuth signal as received in the radar.)

Using Equation A-3 and assuming that the reference signal is exactly the same as the azimuth waveform, the output from the correlation process can be rewritten as

$$y_a(t) =$$

$$\mathcal{F}^{-1}\left[\begin{array}{l}\left\{\sqrt{\frac{r_o}{2\lambda_o V^2}}\cdot B\left(-\frac{\lambda_o}{2V}.f\right)\cdot e^{j.\frac{\pi}{2\lambda_o}.\left[\frac{r_o}{V^2}.f^2\right]}\cdot e^{-j.\frac{\pi}{4}}\right\} \\ \times\left\{\sqrt{\frac{r_o}{2\lambda_o V^2}}\cdot B\left(-\frac{\lambda_o}{2V}.f\right)\cdot e^{j.\frac{\pi}{2\lambda_o}.\left[\frac{r_o}{V^2}.f^2\right]}\cdot e^{-j.\frac{\pi}{4}}\right\}^{\star}\end{array}\right]$$

Performing the indicated conjugation (which only involves changing the sign on the relevant exponentials) the exponentials in the above equation cancel out to give a result

$$f_a(t) = \mathcal{F}^{-1}\left[\begin{array}{ll}\frac{r_o}{2\lambda_o V^2}\cdot B^2\left(-\frac{\lambda_o}{2V}.f\right) & -f_{3dB} < f \le f_{3dB} \\ 0 & elsewhere\end{array}\right]$$

If the beam pattern, B, can be approximated as a unity magnitude function over the frequency range of interest, the result after correlation is simplified to

$$f_a(t) = \mathcal{F}^{-1}\left[\begin{array}{ll}\frac{r_o}{2\lambda_o V^2} & -f_{3dB} < f \le f_{3dB} \\ 0 & elsewhere\end{array}\right]$$

Substituting $K_o = r_o/(2\lambda_o V^2)$ and making use of the standard form

$$rect\left(\frac{x}{b}\right) = 1 \qquad -\frac{b}{2} < x \leq \frac{b}{2}$$

$$= 0 \qquad \textit{elsewhere}$$

$y_a(t)$ can be rewritten as

$$y_a(t) = \mathcal{F}^{-1}\left[K_o \,.\, rect\left(\frac{f}{\beta_a'}\right)\right]$$

where β_a' is defined as a numerical value equal to the range of frequencies occupied by the azimuth waveform. In other words $\beta_a' = (f_{3dB} - (-f_{3dB}))$.

Finally using the identity

$$\mathcal{F}\left[k.\frac{\sin(k\pi t)}{k\pi t}\right] = rect\left(\frac{f}{k}\right)$$

the result of correlation is

$$y_a(t) = \beta_a' K_o . \frac{\sin(\pi \beta_a' t)}{(\pi \beta_a' t)}$$

To be noted from the above is that:

a) The correlation of a complex chirp waveform produces a purely real signal.

b) The real time signal is given as the inverse Fourier transform of a rect function whose width is governed by the frequency (or Doppler) spread of the original azimuth waveform.

c) The result of correlation is a time signal in the form of the classic "sinc" function with a first sidelobe whose magnitude is only 10dB down from the main lobe response.

To remove any constant and complex phase offset terms the absolute value of this result is taken. This gives

$$y_a(t) = \left| \beta_a' K_o \cdot \frac{\sin(\pi \beta_a' t)}{(\pi \beta_a' t)} \right|$$

This time signal is sketched in Figure A3.

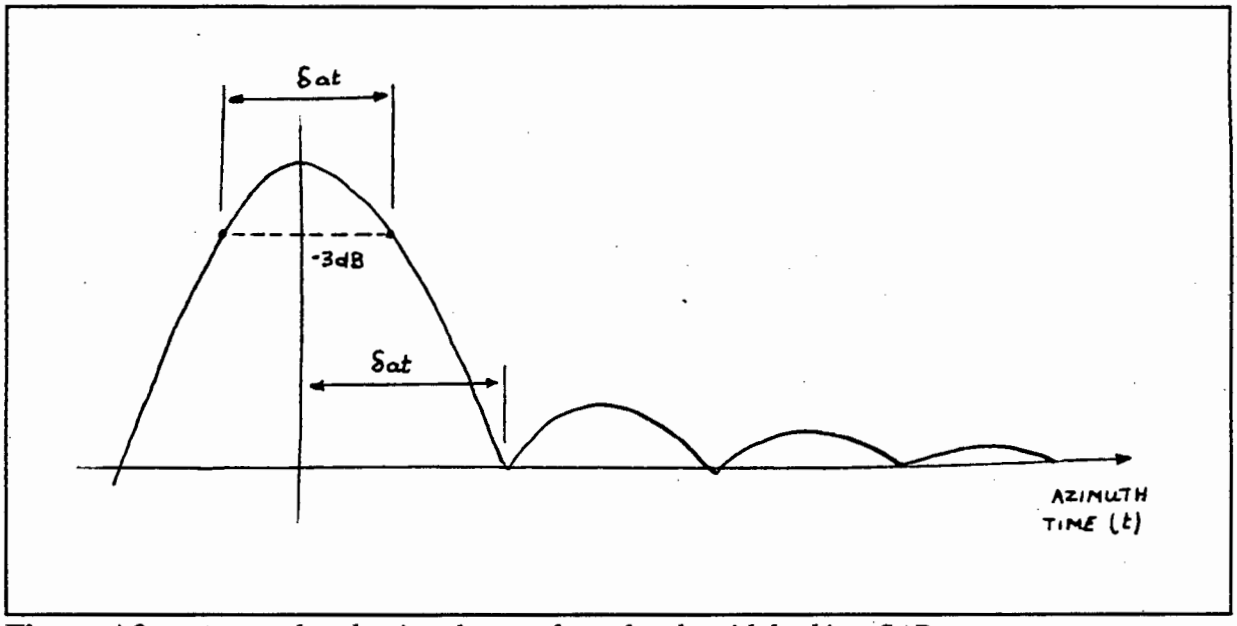

Figure A3: *A correlated azimuth waveform for the sidelooking SAR case.*

An inspection of this time signal reveals that the 3dB resolution is given as

$$\delta_{at} = \frac{1}{\beta_a}$$

where β_a is defined as the bandwidth of the correlated chirp. If it is recognised that the frequency or Doppler spread β_a' (positive and negative frequencies) of the original chirp

signal is equal to twice the bandwidth β_a of the correlated azimuth signal this resolution can also be written as

$$\delta_{at} = \frac{1}{2\beta_a'}$$

This result is consistent with Equation 2-10.

APPENDIX A7

A SMALL ANGLE APPROXIMATION TO RADIAL DISTANCE IN A SIDELOOKING SAR, WHERE THE TARGET ILLUMINATION AREA IS OFFSET FROM THE POSITION OF ZERO DOPPLER.

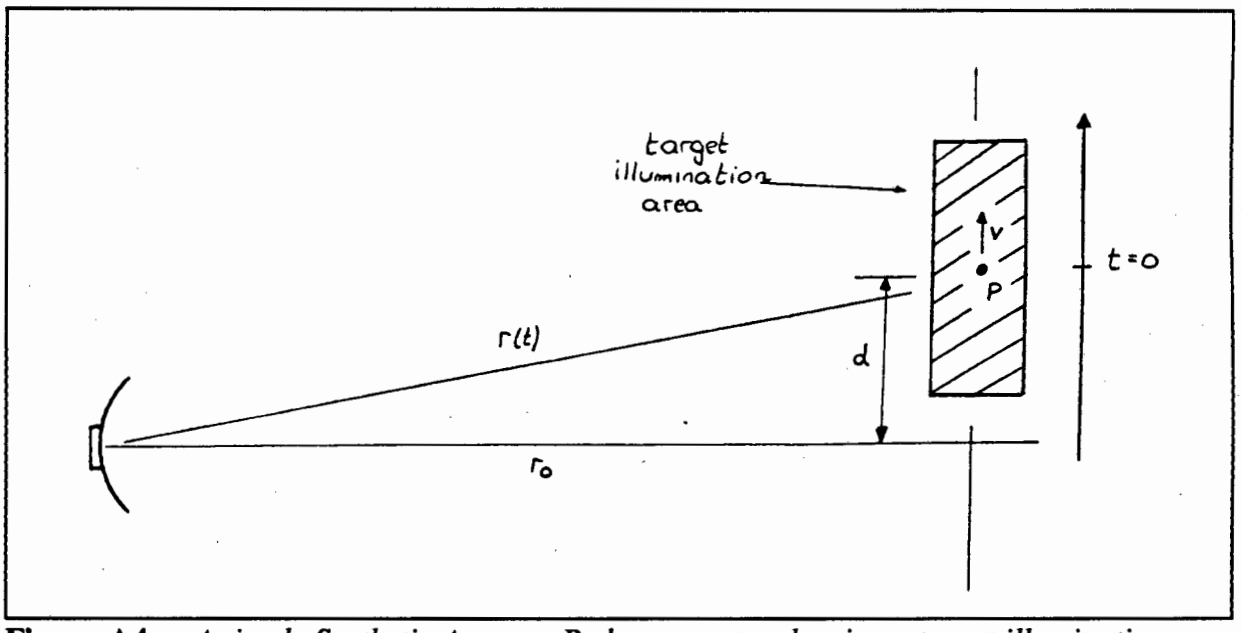

Figure A4: *A simple Synthetic Aperture Radar geometry showing a target illumination area offset from the zero doppler position.*

Figure A4 shows a target illumination area which has been offset from a symmetrical position around zero doppler. It is assumed that the centre of this illumination area is located at a perpendicular distance *d* away from the zero doppler line.

The relative radial distance between target and antenna as a function of time is given as

$$r(t) = [r_o^2 + (Vt + d)^2]^{1/2}$$

Using a two term binomial approximation to estimate this distance, we get

$$r(t) = r_o + \frac{1}{2r_o}.(Vt + d)^2$$

$$= r_o + \frac{d^2}{2r_o} + \frac{1}{2r_o}.(V^2t^2 + 2Vt.d)$$

APPENDIX A8

CORRELATION OF AN AZIMUTH WAVEFORM WHERE THAT WAVEFORM HAS BEEN OFFSET FROM THE ZERO DOPPLER POSITION.

For this case the azimuth signal $f_a(t)$ is

$$f_a(t) = B(\alpha(t)) \cdot e^{-j.\frac{2\pi f_o}{c}\left[\frac{V^2t^2}{r_o} + \frac{2dVt}{r_o}\right]} \qquad \alpha^L_{3dB} < t \leq \alpha^U_{3dB}$$

$$= 0 \qquad \textit{elsewhere}$$

with an aspect angle α equal to

$$\alpha = \frac{Vt + d}{r_o}$$

This signal must again be correlated with the best estimate of the azimuth waveform, namely $f_a(t)$. It can be proved (along much the same lines as the proof in Appendix A6) that the result of this correlation is

$$y_a(t) = \left| \beta'_a K. \frac{\sin(\pi \beta'_a t)}{\pi \beta'_a t} \cdot e^{-j.\frac{2\pi f_o}{c}\left[\frac{2dV}{r_o}\right]} \right|$$

where β_a' is again defined as a numerical value equal to the range of frequencies occupied by the azimuth waveform. In other words $\beta_a' = (f^L_{3dB} - (-f^U_{3dB}))$.

Taking the absolute value of this result and using the identity

$$|ab| = |a||b|$$

the result of correlation can be given as

$$y_a(t) = \left| \beta_a' K . \frac{\sin(\pi \beta_a' t)}{\pi \beta_a' t} \right| \left| e^{-j.\frac{2\pi f_o}{c}\left[\frac{2dVt}{r_o}\right]} \right|$$

$$= \left| \beta_a' K . \frac{\sin(\pi \beta_a' t)}{\pi \beta_a' t} \right|$$

This result demonstrates that a correlation of an azimuth waveform located at an offset frequency produces a result that is equivalent to correlating an azimuth reference centred on the zero doppler position, except for the presence of a modulating signal. On taking the absolute magnitude of this result, the carrier drops out to produce the same result as before.

From Appendix A6 the 3dB resolution of the correlated time signal is given by

$$\delta_{at} = \frac{1}{\beta_a'} = \frac{1}{2\beta_a}$$

APPENDIX B

APPENDIX B1

CALCULATIONS INVOLVING UNFOCUSED SYNTHETIC APERTURE RADAR PROCESSING.

The maximum synthetic aperture length over which simple coherent integration can be performed is given in Section 3.4 as

$$L_a = \sqrt{r_o \lambda_o}$$

$$= \sqrt{r_o \cdot \frac{c}{f_o}}$$

r_o: *The relative one way radial distance from the antenna to the zero doppler position of a point target.*

f_o: *The radar transmit frequency.*

c: *The speed of light.*

The slant range distance r_s (as given in Table 3-3) can be used as an approximation to r_o. Using this slant range distance and the radar transmit frequency given in Table 3-2 the maximum synthetic array length can be calculated to be about 230 meters.

The spatial azimuth resolution is given as

$$\delta_a = \frac{1}{2}\sqrt{r_o \lambda_o}$$

which for the SIR-B case corresponds to 115 meters.

The number of samples of the azimuth waveform that can be added coherently is given as: the distance L_a divided by the distance covered by the SAR antenna (with respect to a stationary point target in the target area of interest) in one PRI.

The SIR-B menu tape (Appendix C1) gives the velocity of the radar footprint on the ground as 7266.8 meters per second. The radar PRI (or *T*) is given in Table 3-2 as 1/1464 seconds. Using these two figures the distance covered within one PRI can be calculated to be about 5 meters. Therefore, the number of azimuth samples that can be added coherently is, therefore, about 46.

APPENDIX B2

AN ALGORITHM FOR ACCURATE TARGET POSITIONING.

INTRODUCTION.

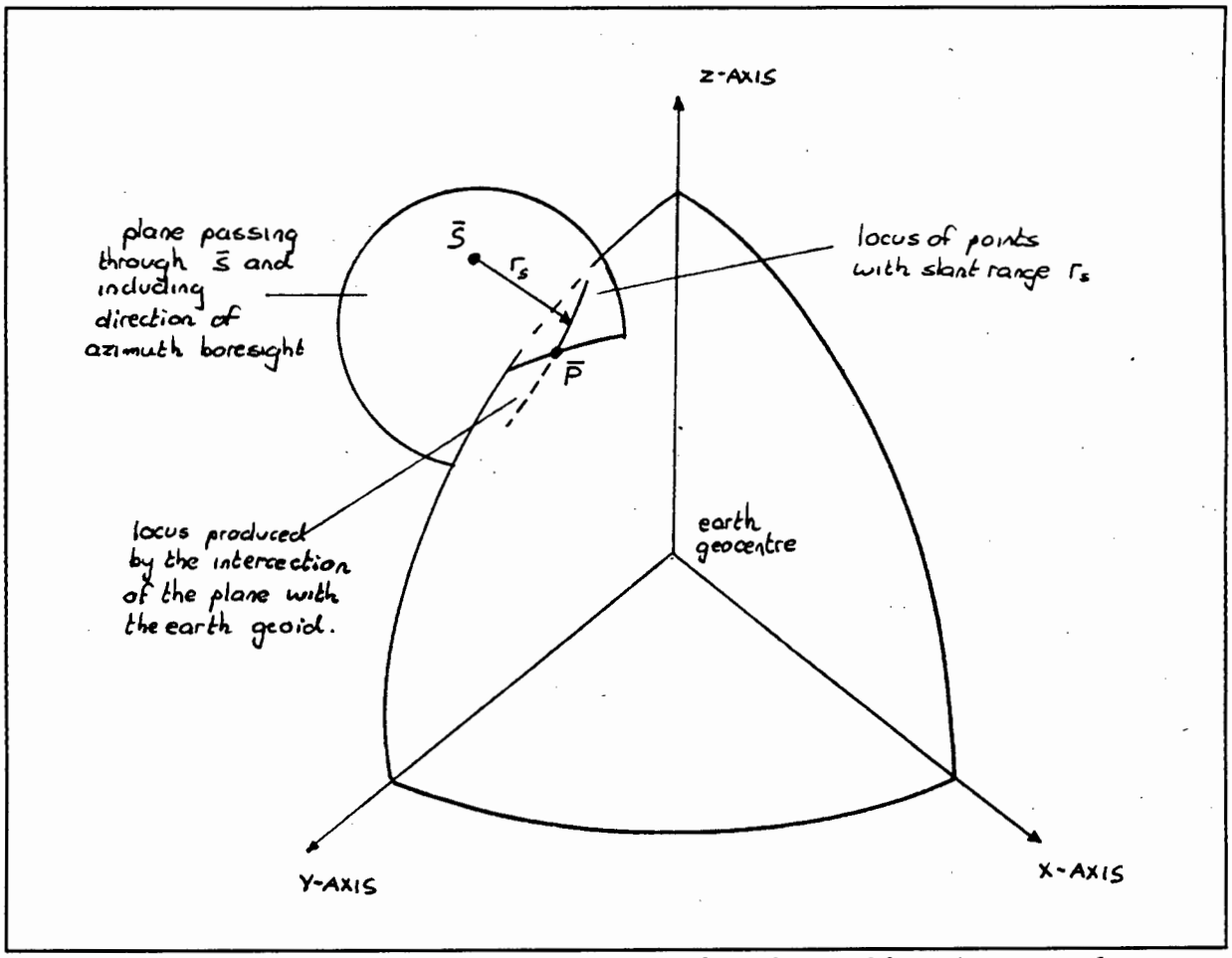

Figure B1: *A diagrammatical representation of the algorithm used for point target placement.*

The target positioning algorithm that is discussed in Section 3.5.4.2 involves the following stages:

a) A plane is defined which passes through the satellite position S and includes the vector direction of the estimated antenna boresight.

b) This plane intersects a model describing the earth geoid to form a locus of points.

c) The position on this locus, corresponding to the correct slant range distance r_s between the antenna and target, gives the desired point target location in an inertial reference frame.

The above steps are illustrated diagrammatically in Figure B1.

The version of this algorithm, used to locate point targets so as to decode the azimuth radar data taken in the Cradock region, is now discussed.

THE TARGET POSITIONING ALGORITHM AS USED IN THE DECODING OF SIR-B DATA.

Introduction:

An implementation of the target placement algorithm is simplified if it can be assumed that the satellite velocity vector V_s is a tangent to a spherical earth orbit as shown in Figure B2. This assumption can be made if the radial component of satellite velocity can be considered negligible.

Using the vector identity

$$comp_{\bar{b}}\bar{a} = \bar{a}.\frac{1}{|\bar{b}|}.\bar{b}$$

the component of satellite velocity as resolved in the radial direction S can be found as

$$\Delta h_s = \overline{V_s}.\frac{1}{|\bar{S}|}.\overline{V_s}$$

where Δh_s is defined as this radial component.

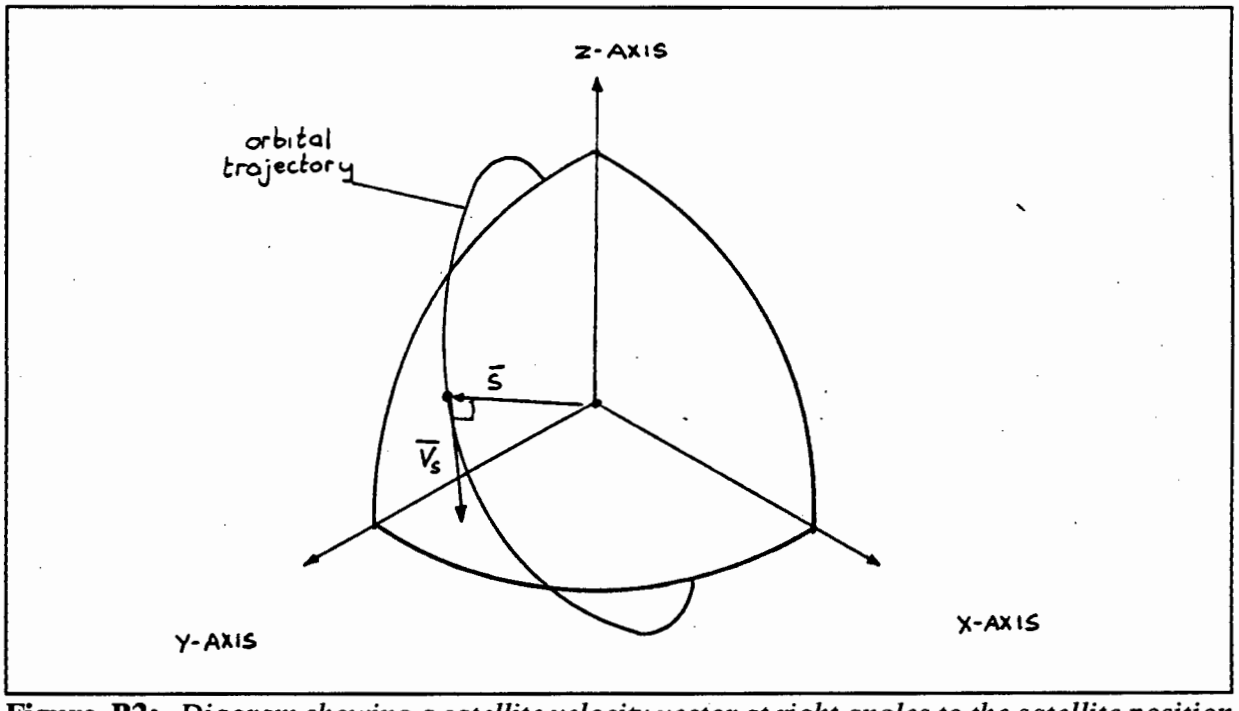

Figure B2: *Diagram showing a satellite velocity vector at right angles to the satellite position vector.*

For the SIR-B case this radial velocity can be calculated, using the data in Table 3-3, to be equal to about 1 meter per second. Given a magnitude satellite velocity of about 7800 meters per second, the angular offset between the actual velocity vector and a tangential vector at that point is about 0.007 degrees. For most applications this can be considered to be a negligible discrepancy.

If the radial component Δh_s is expressed as a vector component

$$\overline{\Delta h_s} = \frac{\bar{S}}{|\bar{S}|}.\Delta h_s$$

a tangential vector T_s to point P can be found by removing this component from the satellite velocity vector V_s as follows:

$$\overline{T_s} = \overline{V_s} - \overline{\Delta h_s}$$

This resultant vector also represents the tangential component of satellite motion.

Defining a plane of intersection:

A plane can now be defined that passes through the satellite position S and includes the vector direction of estimated antenna boresight. For the raw radar data take over the Cradock region the antenna boresight was located on a plane having as normal vector, the shuttle velocity vector, V_s. (see Section 3.6.4) For this special case, a plane can be defined that has as normal the tangential component of satellite velocity, T_s. A plane defined in this way will also pass through the centre of the earth. The equation for this plane, passing through a point P and having a normal vector T_s is given by

$$T_{s_1}.(x - P_1) + T_{s_2}.(y - P_2) + T_{s_3}.(z - P_3) = 0$$

The artificial error in beam pointing, introduced by the use of the tangential satellite velocity vector rather than the actual velocity vector, is in the order of 0.007 degrees (equal to the angular offset between T_s and V_s). This is a negligible figure in practice.

A coordinate transformation:

The plane intersects a model of the earth to form a locus of points as shown in Figure B1. Locating a point on this locus with the correct slant range from the antenna is a three dimensional problem. In this case it can, however, be simplified to two dimensions by setting up a temporary coordinate system as follows:

A z-axis is defined having the same direction as the tangential satellite velocity vector. An x-axis is defined having the same direction as the satellite position vector. The three unit vectors defining the orientation of this temporary coordinate system with respect to the inertial coordinate system can, therefore, be given as

$$e_x = \frac{\bar{S}}{|\bar{S}|}$$

$$e_z = \frac{\bar{T}_s}{|\bar{T}_s|} \qquad \textbf{(B-1)}$$

$$e_y = e_z \times e_x$$

The x-y plane of this coordinate system passes through the satellite position *P* and (as a result of defining the z-axis in a direction tangent to a spherical orbit) the earth origin. If the z-axis is suppressed, the earth/satellite geometry can be expressed in two dimensions as shown in Figure B3.

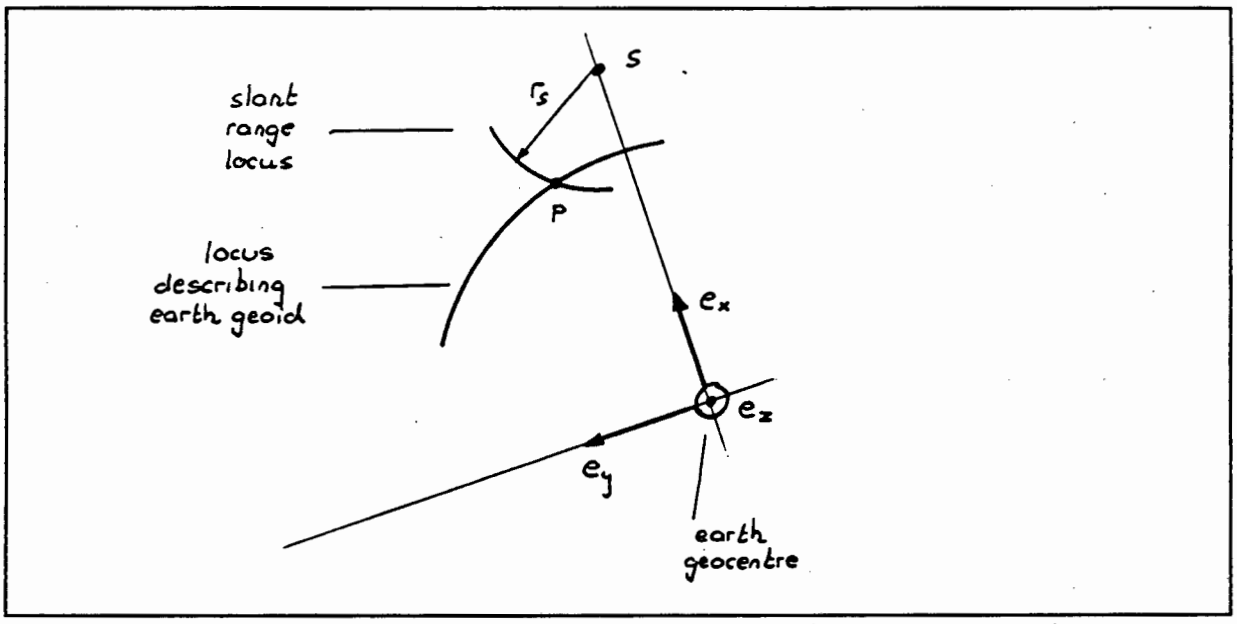

Figure B3: *The earth/satellite geometry expressed in terms of a temporary coordinate system.*

The problem now reduces to finding the x and y coordinates of the intercept between the slant range locus and the locus describing the earth geoid.

Locating a point target:

An unfocussed SAR image (Section 3.4) of the target area can be matched up with topographic maps. The geoidal sea level radius, r_e, and average terrain height, h_t, was then estimated using these maps.

Using the above information the locus problem reduces to that of finding the intercept between slant range and a curve of radius: $(r_e + h_t)$.

This problem is one of simple trigonometry as shown in Figure B4. Referring to this figure, point *C* is located at the earth origin, point *S* is located on the x-axis of this new coordinate system and corresponds to the position of the satellite. The distance *CS* is equal to the radial distance of the satellite from the earth origin (in other words $|\bar{S}|$). The distance *PC* represents the distance between the point target and the centre of the earth. *PS* corresponds the slant range distance r_s.

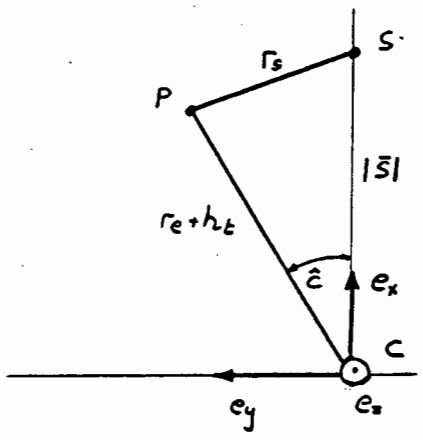

Figure B4: *Intersection of loci expressed as a two dimensional trigonometric problem.*

Using the trigonometric "Law of Cosines"

$$c^2 = a^2 + b^2 - 2ab.\cos(\hat{C})$$

angle C can be found as

$$\hat{C} = \cos^{-1}\left[\frac{|\bar{S}|^2 + (r_e + h_t)^2 - r_s}{2|\bar{S}| \,.\, (r_e + h_t)^2}\right]$$

Position P in this new coordinate system is then given by simple trigonometry as

$$\bar{P} = \begin{bmatrix} (r_e + h_t) \,.\, \cos(\hat{C}) \\ (r_e + h_t) \,.\, \sin(\hat{C}) \\ 0 \end{bmatrix}$$

The vector position of point P must now be found in terms of the inertial coordinate system. This can be done by means of a matrix transformation

$$\bar{P} = [M] \,.\, \bar{P'}$$

(The position vector P, as expressed in terms of the temporary coordinate system, is the indexed variable in the above equation).

The matrix $[M]$ must have as its columns, the unit vectors which define the temporary coordinate system in terms of the inertial coordinate system. These three unit vectors $\{e_x, e_y, e_z\}$ are given in Equation B-1, allowing the transformation matrix to be expressed as

$$[M] = \begin{bmatrix} e_{x_1} & e_{y_1} & e_{z_1} \\ e_{x_2} & e_{y_2} & e_{z_2} \\ e_{x_3} & e_{y_3} & e_{z_3} \end{bmatrix}$$

TARGET PLACEMENT FOR THE SIR-B CASE.

Target placement for the SIR-B case is implemented in a Mathcad spreadsheet in Appendix C1. The input parameters to this spreadsheet are as follows:

a) The slant range, r_s, satellite position, S, and satellite velocity, V_s. These parameters are obtained directly from Table 3-3.

b) The average radius of the target area. This is estimated from an unfocused SAR image and topographic maps of the area.

Target positions at the near edge, far edge and centre of the target area were calculated by a suitable modification of the slant range input parameter. The slant range to the near edge of the target area for the SIR-B case is 272670 meters. The slant range to the far edge of the target area is simply given as this slant range plus the one way radial distance covered by the SAR matrix in range. In Appendix B5 this extra one way radial distance is calculated to be equal to 12306 meters.

The following target positions were obtained:

Near edge:

$$r_s = 272670\,m \quad : \quad \overline{P} = \begin{bmatrix} +0.155\times10^6\,m \\ -5.399\times10^6\,m \\ -3.382\times10^6\,m \end{bmatrix}$$

Centre:

$$r_s = 278823\,m \quad : \quad \overline{P} = \begin{bmatrix} +0.146\times10^6\,m \\ -5.396\times10^6\,m \\ -3.388\times10^6\,m \end{bmatrix}$$

Far edge:

$$r_s = 284976\,m \quad : \quad \overline{P} = \begin{bmatrix} +0.138\times10^6\,m \\ -5.393\times10^6\,m \\ -3.393\times10^6\,m \end{bmatrix}$$

APPENDIX B3

A MODEL OF THE RELATIVE MOTION BETWEEN TARGET AND ANTENNA.

INTRODUCTION

In Section 3.7 it is described how the relative radial motion between target and antenna can be predicted if the instantaneous velocity and position of the target and antenna are known at a particular time t=0. The satellite ephemeris data is calculated from the known orbital trajectory (see Section 3.7.2). The target position is calculated using the target placement algorithm described in Appendix B2. The instantaneous target velocity is predicted by making use of the theorem of Coriolis. In Section 3.7.2 this theorem was stated mathematically as

$$\bar{v} = \bar{\omega} \times \bar{r}$$

where ω is the angular velocity vector describing the rotation of the target and r is the vector position of that target.

The geometry describing an earth located target is shown in Figure B5. The angular velocity vector ω_e describes the rotation of the earth. This vector has a magnitude equal to the rotational speed of the earth in radians per second. The direction of this vector is coincident with the z-axis of the inertial coordinate system. The vector position of the target is simply the vector P. Therefore, the instantaneous velocity of the target can therefore be expressed as

$$\overline{V_p} = \overline{\omega_e} \times \overline{P}$$

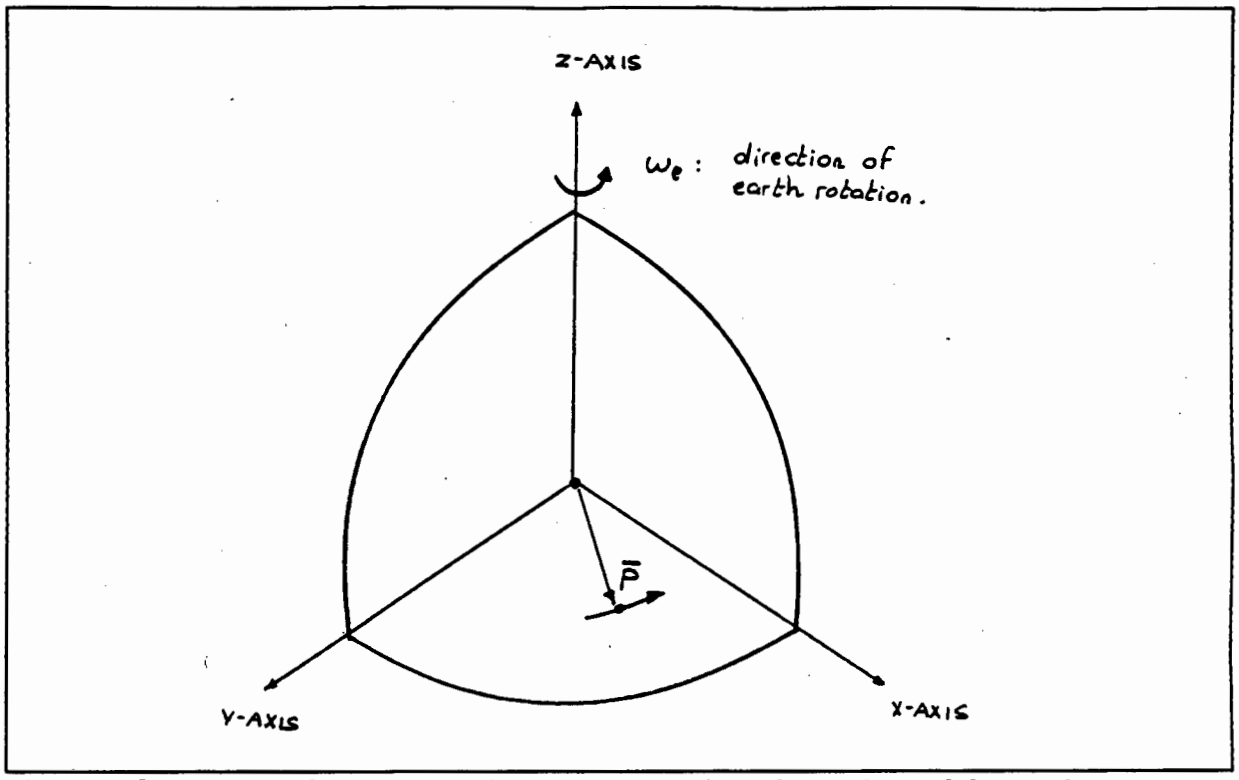

Figure B5: *The angular velocity of a target located on the surface of the earth.*

RESULTS FOR THE SIR-B CASE.

The modelling of the relative motion between target and antenna is implemented in a Mathcad spreadsheet included in Appendix C2. As explained in Section 3.7 this model requires as input, the satellite position and velocity and target position and velocity at time t=0.

Values for relative along track velocity, V_a, cross track velocity, V_c, and magnitude velocity, are obtained for a target located at the near edge, centre, and far edge of the target area. The results obtained are as follows:

Near edge:

$$r_s = 272670\,m \quad : \quad \begin{aligned} V_c &= -175.09\,m/s \\ V_a &= 7532.29\,m/s \\ |\bar{V}| &= 7534.32\,m/s \end{aligned}$$

Centre:

$$r_s = 278823\,m \quad : \quad \begin{aligned} V_c &= -183.28\,m/s \\ V_a &= +7532.50\,m/s \\ |\bar{V}| &= +7534.73\,m/s \end{aligned}$$

Far edge:

$$r_s = 272670\,m \quad : \quad \begin{aligned} V_c &= -175.09\,m/s \\ V_a &= 7532.29\,m/s \\ |\bar{V}| &= 7534.32\,m/s \end{aligned}$$

APPENDIX B4

CALCULATING THE AZIMUTH REFERENCE FUNCTION.

INTRODUCTION.

The relative satellite/ target geometry shown in Section 3.7.3 is repeated in Figure B6.

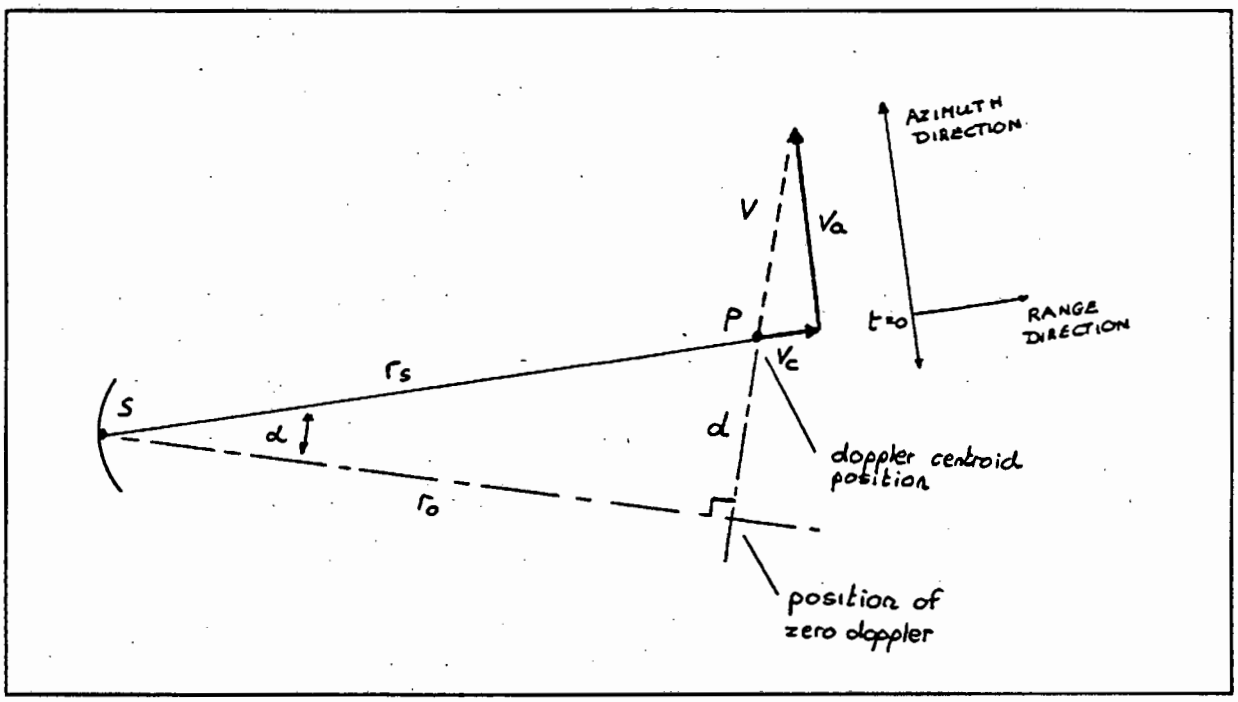

Figure B6: *Relative satellite/ target geometry showing the doppler centroid position and target velocity V relative to an assumed stationary antenna.*

Point *S* is the position of an assumed stationary antenna. Point *P* is given as the Doppler centroid position (the target position at time t=0). This Doppler centroid position is removed a distance *d* away from the position of zero Doppler. The slant range distance is given as r_s. The distance between the position of zero doppler and the antenna is given as r_o.

The aspect angle, α, at the Doppler centroid position is given as

$$\alpha = \tan^{-1}\left(\frac{V_c}{V_a}\right)$$

Using this aspect angle, simple trigonometry can be used to predict values for r_o and d.

In Section 2.17.1 equations are given for the Doppler centroid and Doppler rate in terms of the above variables. These equations are repeated as follows

$$f_c = \frac{-2f_o}{c} \cdot \frac{Vd}{r_o}$$

and

$$f_r = \frac{-2f_o}{c} \cdot \frac{V^2}{r_o}$$

The variable V refers to the relative magnitude velocity of the target with respect to the antenna at time t=0.

The values for Doppler centroid frequency and Doppler rate can be substituted directly into the azimuth reference function given in Equation 2-28 as

$$f_a(t) = e^{j.2\pi\left(\frac{1}{2}f_r t^2 + f_d t\right)}$$

RESULTS FOR THE SIR-B CASE.

The above calculations and substitutions are implemented in a Mathcad spreadsheet included in Appendix C2. For a target located at the near edge, centre, and far edge of the target area, these results can be summarised as follows:

Near edge:

$$r_s = 272670\,m \quad : \quad \alpha = -0.0232\,rads,\ d = -6337\,m,\ r_o = 272.6 \times 10^3\,m$$

Centre:

$$r_s = 272670\,m \quad : \quad \alpha = -0.0243\,rads,\ d = -6782\,m,\ r_o = 278.7 \times 10^3\,m$$

Far edge:

$$r_s = 272670\,m \quad : \quad \alpha = -0.0253\,rads,\ d = -7209\,m,\ r_o = 284.9 \times 10^3\,m$$

Using the above information and the relative magnitude velocity of the target at time t=0 (as calculated in Appendix B3), values can be calculated for the Doppler centroid frequency and Doppler rate.

Near edge:

$$r_s = 272670\,m \quad : \quad f_c = 1493\,Hz,\ f_r = -1781\,Hz/s$$

Centre:

$$r_s = 272670\,m \quad : \quad f_c = 1568\,Hz,\ f_r = -1742\,Hz/s$$

Far edge:

$$r_s = 272670\,m \quad : \quad \begin{matrix} f_c = 1631\,Hz \\ f_r = -1705\,Hz/s \end{matrix}$$

A simple substitution of these quantities into Equation 2-28 will give the desired azimuth reference function.

APPENDIX B5

RANGE MIGRATION CALCULATIONS.

INTRODUCTION.

The typical migration curve for a correlated point target is shown in Figure B7.

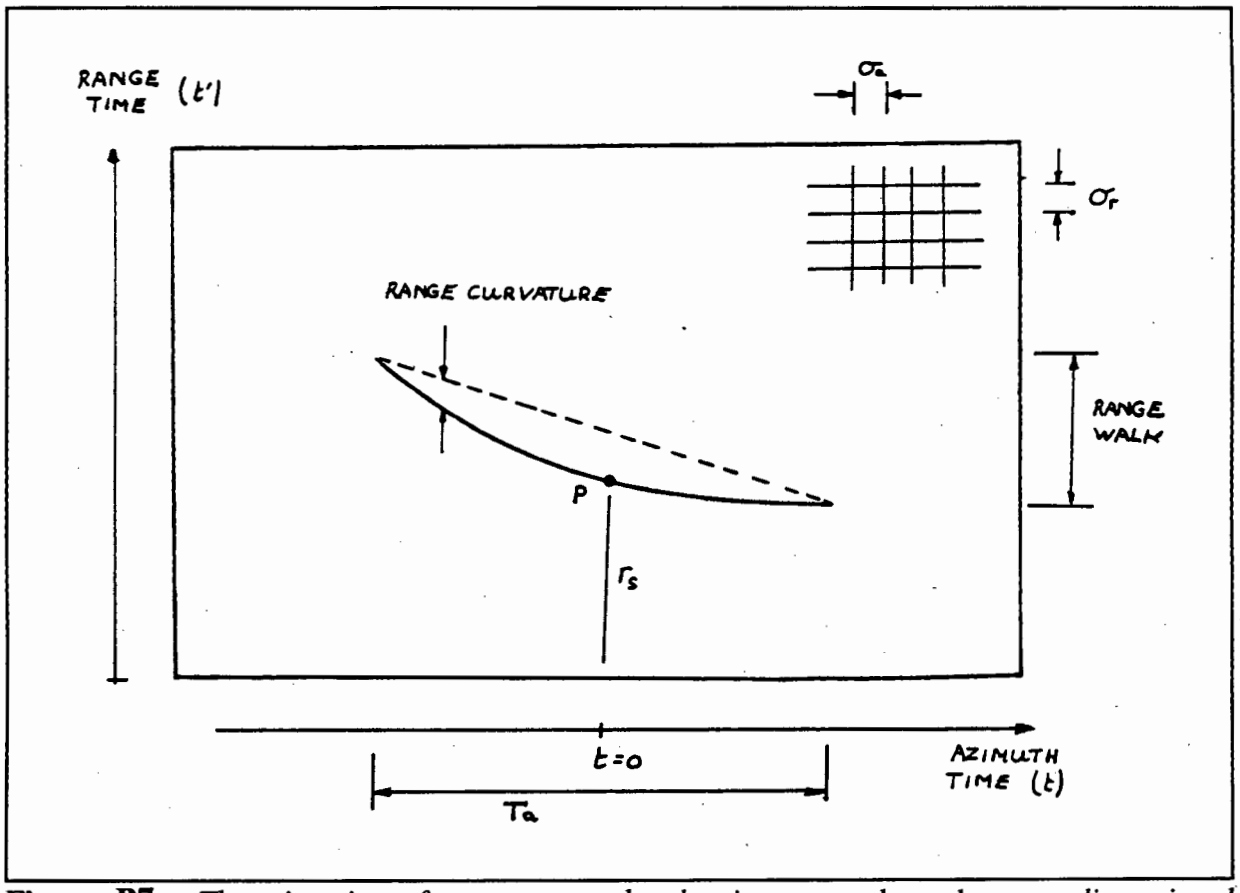

Figure B7: *The migration of a range correlated point target through a two dimensional matrix of SAR data.*

The one way range distance between two range bins is given as

$$\sigma_r = \frac{c.dt}{2}$$

where c is the speed of light and dt is the sampling rate of the radar receiver. The spatial distance between two bins in azimuth is given as the relative magnitude velocity of the target with respect an antenna multiplied by the radar PRI or

$$\sigma_a = |\bar{V}|.T$$

The radial extent of the SAR matrix in the range direction is given as σ_r multiplied by the number of range samples. The total azimuth distance is given by σ_a multiplied by the number of azimuth samples.

The range walk, *RW*, is defined as the one way radial distance covered by the migration curve of a point target over the extent of the azimuth processing window. The range curvature is defined as the component of migration that is left after the removal of range walk.

RESULTS FOR THE SIR-B CASE.

The SIR-B receiver sampling rate is given in Table 3-2 as 30.355 MHz. Using this value the radial distance between two range bins can be calculated to be equal to 4.94 meters. The length of range array used in processing was set at 2492 samples (see Section 3.3.2). The distance covered by the SAR matrix in the range direction is, therefore, 12306 meters.

The relative magnitude velocity of the target with respect to the antenna was calculated in Appendix B3 to be about 7534 meters per second. The radar PRF is given in Table 3-2 as 1463.8 Hz. Using these two values the spatial distance between two azimuth bins can be calculated to be 5.15 meters. The SAR matrix was limited in size to 4096 samples in the azimuth direction. Therefore, a spatial azimuth distance of 21082 meters is covered.

The length of azimuth reference function was limited to 256 samples (see Section 3.9.1). The range walk, *RW*, and maximum range curvature, *RC*, over this distance is calculated in the

Mathcad spreadsheet included in Appendix C2. The results for a point target located at the near edge, centre, and far edge of the target area is given below:

Near edge:

$$r_s = 272670\,m \quad : \quad \begin{matrix} RW = 30.49\,m \\ RC = 0.789\,m \end{matrix}$$

Centre:

$$r_s = 272670\,m \quad : \quad \begin{matrix} RW = 31.92\,m \\ RC = 0.772\,m \end{matrix}$$

Far edge:

$$r_s = 272670\,m \quad : \quad \begin{matrix} RW = 33.19\,m \\ RC = 0.755\,m \end{matrix}$$

To improve the efficiency of azimuth processing (see Section 3.9.3) the full azimuth length of the two dimensional SAR matrix is corrected for range walk. The amount of range walk was calculated, for a point target located at the centre of the swath, to be 507.38 meters over this length. This calculation was again performed in the MCAD spreadsheet included in Appendic C2.

APPENDIX B6

AZIMUTH RESOLUTION.

INTRODUCTION.

It was shown in Section 2.11.2 that the azimuth resolution (in time) is given as

$$\delta_{at} = \frac{1}{2\beta_a} = \frac{1}{\beta'_a}$$

where β'_a is equal to the total frequency spread of the azimuth waveform. This frequency spread is given simply as the product of the Doppler rate, f_r, and the length of time, T_a, represented by the azimuth processing window.

The spatial azimuth resolution, δ_a, is given as the product of the time resolution and the magnitude component of the relative velocity between antenna and target. In summary the spatial azimuth resolution can be obtained as follows

$$\delta_a = \frac{|\bar{V}|}{f_d . T_a} \qquad \textbf{(B-2)}$$

RESULTS FOR THE SIR-B CASE.

Azimuth processing was performed with an azimuth reference function consisting of 256 azimuth samples. The PRF used is given in Table 3-2 as 1436.8 Hz. For a target located at the centre of the swath the relative magnitude velocity is given in Appendix B3 as 7534 meters per second. The Doppler rate f_r is given in Appendix B4 as -1742 Hertz per second.

Using these values in Equation B-2 gives a spatial azimuth resolution of 24.28 meters. This resolution figure is compatible with the resolution in range.

APPENDIX B7

A DEPTH OF FOCUS CALCULATION FOR THE SIR-B CASE.

In Section 3.11 a formula is given for the depth of focus as follows:

$$\Delta F = \frac{2\lambda_o r_s^2}{L_a^2}$$

ΔF: *The depth of focus expressed as a one way radial distance.*

λ_o: *The radar transmit frequency.*

r_s: *The slant range distance.*

L_a: *The synthetic aperture length.*

In the processing of azimuth SIR-B data an azimuth processing window consisting of 256 azimuth samples was correlated. The synthetic aperture length can be calculated as follows:

$$L_a = 256 \times \frac{1}{PRF} . |\bar{V}|$$

The PRF is given in Table 3-2 as 1436.8 Hz. For a target located at the centre of the swath the relative magnitude velocity is given in Appendix B3 as 7534 meters per second. Therefore, the synthetic aperture length is calculated to be equal to 1342 meters.

The depth of focus is then calculated to be about 19000 meters.

APPENDIX B8

SHIFT IN RADIAL TARGET LOCATION DUE TO DOPPLER MODULATION EFFECTS ON THE TRANSMITTED RANGE CHIRP.

In Section 2-10 it was pointed out that the continuous Doppler modulation of the chirp envelope of a received radar pulse causes a shift in the observed radial position of the target after correlation. This offset in range time was given as:

$$t_o = -\frac{\tau f_d}{\beta_r'}$$

τ: *The time duration of a single radar pulse.*

f_d: *The Doppler frequency at the instant of target observation.*

β_r': *The bandwidth of the transmitted radar waveform.*

Table 3-2 gives the time duration of the radar pulse, as used in the SIR-B experiment, as 30.4μs. The bandwidth of this pulse is 12MHz. Appendix B4 gives a maximum Doppler frequency of about 1600 Hz over the target area.

Using these values in the above equation the offset in range time is calculated to be in the order of 4 nanoseconds. This corresponds to a one way range distance of about 1.2 meters. This offset is negligible when compared to the 3dB width of the correlated range envelope and can be ignored in processing.

APPENDIX C

APPENDIX C1

A MATHCAD SPREADSHEET FOR TARGET PLACEMENT.

TARGET PLACEMENT ALGORITHM.

The position of a target relative to a satellite is placed in a 3D inertial frame.

It is assumed that the position and velocity of the satellite, the slant range distance and the average radius of the earth over the target area is known.

DESCRIPTION OF VARIABLES:

S: Satellite position vector.
Vs: Satellite velocity vector.

Re: Average radius of the target area.
hs: The radial component of satellite velocity.
Ts: The tangential component of satellite velocity.

ωe: The angular velocity vector describing earth rotation.

SECTION 1:

The position of a target in the inertial reference frame is calculated.

Part 1:

The known parameters are defined.

--- The position and velocity of the satellite, in the inertial reference frame, is given ---

$$S := \begin{bmatrix} 282.499 \cdot 10^{3} \\ -5637.355 \cdot 10^{3} \\ -3419.207 \cdot 10^{3} \end{bmatrix} \qquad V_s := \begin{bmatrix} 4763.469 \\ 3359.391 \\ -5143.152 \end{bmatrix}$$

--- The slant range from satellite to target is given ---

$$r_s := (272.67 + 6.153) \cdot 10^{3}$$

--- The average radius of the target area (including the additive effect of terrain height) is given ---

$$R_e := (6372.07 + 1) \cdot 10^{3}$$

Part 2:

A tangential velocity vector is found for the satellite in question.

--- The radial component of satellite velocity is calculated ---

$$h_s := V_s \cdot \frac{1}{|S|} \cdot S \qquad h_s = -1.0460378688$$

--- This velocity vector is removed from the satellite
velocity vector to obtain the tangential velocity vector. ---

$$\delta h_s := \frac{S}{|S|} \cdot h_s$$

$$T_s := V_s - \delta h_s$$

Part 3:

The equation of a plane having as unit normal the tangential satellite velocity and passing through the earth origin is calculated.

A new 3D coordinate system is defined having the above plane as its xy plane. Using the slant range distance and the distance of the target area from the centre of the earth the targets position is calculated in this new coordinate system

---

--- The orthogonal unit vectors describing the orientation of this new 3D coordinate system are now defined. ---

$$e_x := \frac{S}{|S|} \qquad e_z := \frac{T_s}{|T_s|} \qquad e_y := e_z \times e_x$$

--- A transformation matrix is created to transform points from this new coordinate system back into the inertial coordinate system. ---

$$M^{\langle 1 \rangle} := e_x \qquad M^{\langle 2 \rangle} := e_y \qquad M^{\langle 3 \rangle} := e_z$$

$$M = \begin{bmatrix} 0.0428075207 & -0.7890897939 & 0.6127844754 \\ -0.8542373268 & 0.2891692087 & 0.4320413848 \\ -0.5181178492 & -0.5419579927 & -0.6616913393 \end{bmatrix}$$

--- A locus lying in the x-y plane of this new coordinate system and having as origin the antenna position and a radius equal to the slant range distance will intercept the model for the earth. This intercept point will give the target position in this coordinate system. ---

$$\theta_c := \operatorname{acos}\left[\frac{r_s^2 - (|S|)^2 - R_e^2}{-\left[2 \cdot R_e \cdot |S|\right]}\right]$$

$$P := \begin{bmatrix} R_e \cdot \cos(\theta_c) \\ R_e \cdot \sin(\theta_c) \\ 0 \end{bmatrix} \qquad P = \begin{bmatrix} 6.3710569526 \cdot 10^6 \\ 1.6017032254 \cdot 10^5 \\ 0 \end{bmatrix}$$

Part 3:

The position of the target is found in the inertial reference frame by a coordinate transformation.

$$P := M \cdot P \qquad P = \begin{bmatrix} 1.4634038528 \cdot 10^5 \\ -5.3960783348 \cdot 10^6 \\ -3.3877639116 \cdot 10^6 \end{bmatrix}$$

==========

Section 2:

The parameters necessary for modelling the satellite geometry using the coriolis approximation are generated and stored to data files. These data files are then read and used in a simulation program.

==========

Part 1:

The target position and rotational vector is defined and stored to disk for use by a coriolis approximate simulation.

--- The target rotational vector is calculated. ---

$$\omega_e := \begin{bmatrix} 0 \\ 0 \\ \dfrac{2 \cdot \pi}{24 \cdot 60 \cdot 60} \end{bmatrix}$$

--- The target rotational vector and position is stored to disk. ---

$$\text{WRITEPRN}(\text{TP}_{\text{PRN}}) := P \qquad \text{WRITEPRN}(\text{TW}_{\text{PRN}}) := \omega_e$$

Part 2:

The satellite position and motion vector is stored to disk for use in a simulation program.

--- The satellite position, rotation and velocity vector is stored to disk. ---

$$\text{WRITEPRN}(\text{SP}_{\text{PRN}}) := S \qquad \text{WRITEPRN}(\text{SV}_{\text{PRN}}) := V_s$$

Part 3:

The slant range is stored to disk.

$$\text{WRITE}(\text{RS}_{\text{DAT}}) := r_s$$

==========

APPENDIX C2

A MATHCAD SPREADSHEET FOR CALCULATING THE AZIMUTH REFERENCE FUNCTION AND MIGRATION CURVES FROM A MODEL OF THE RELATIVE TARGET/ ANTENNA MOTION.

A MODEL OF THE RELATIVE MOTION BETWEEN TARGET AND ANTENNA.

The motion of the satellite and target is approximated as two velocity vectors respectively.

The satellite velocity vector is obtained from the ephemeris data. The target velocity vector is obtained by means of the theorem of Coriolis.

Using these estimates of position and velocity the relative motion is modelled as a function of time.

A cross track and along track velocity component is calculated from which the Doppler centroid and rate can be estimated for use in an azimuth reference function.

A plot of range migration is obtained. The range walk component is corrected to leave only the locus of range curvature. The magnitude of this curvature is calculated.

DESCRIPTION OF VARIABLES:

S: Satellite position vector.
Vs: Satellite velocity vector.
P: Target position vector.
Vp: Target velocity vector.

c: Speed of light.
fo: Radar transmit frequency.
PRF: Pulse repetition frequency.
δt: Azimuth sampling period (PRI).

ωe: The angular velocity vector describing earth rotation.

R: The relative displacement between the target and the antenna.

V: The vector component of relative motion between target and antenna.
Vc: Cross track velocity.
Va: Along track velocity.

α: Aspect angle.
d: Distance between the zero Doppler position and the Doppler centroid position.
ro: Distance from the antenna to the zero Doppler position.

fc: Doppler centroid position.
fr: Doppler rate.

RW: The range walk.

==========

Part 1:

The radar system parameters are defined.

$c := 2.9979 \cdot 10^{8}$ --- speed of light ---

$f_o := 1282 \cdot 10^{6}$ --- transmit frequency ---

$PRF := 1463.8$ --- pulse repetition frequency ---

$\delta t := \left\lfloor \frac{1}{PRF} \right\rfloor \cdot 1$ --- azimuth sampling period ---

$SAMPLES := 256$ --- number of azimuth samples ---

$T := \frac{SAMPLES}{2}$

$n := 1 \,..\, SAMPLES$

Part 2:

The satellite position and velocity vector is read from disk. The slant range is also read from disk.

$S := READPRN\begin{bmatrix} SP \\ PRN \end{bmatrix}$

$$S = \begin{bmatrix} 5 \\ 2.82499 \cdot 10 \\ 6 \\ -5.637355 \cdot 10 \\ 6 \\ -3.419207 \cdot 10 \end{bmatrix}$$

$V_s := READPRN\begin{bmatrix} SV \\ PRN \end{bmatrix}$

$$V_s = \begin{bmatrix} 3 \\ 4.763469 \cdot 10 \\ 3 \\ 3.359391 \cdot 10 \\ 3 \\ -5.143152 \cdot 10 \end{bmatrix}$$

$r_s := READ\begin{bmatrix} RS \\ DAT \end{bmatrix}$

$$r_s = 2.78823 \cdot 10^5$$

Part 3:

The target position and rotational vector is read from disk.

The instantaneous velocity of the target is calculated using the Coriolis approximation.

$P := READPRN\begin{bmatrix} TP \\ PRN \end{bmatrix}$

$$P = \begin{bmatrix} 5 \\ 1.46340385 \cdot 10 \\ 6 \\ -5.39607833 \cdot 10 \\ 6 \\ -3.38776391 \cdot 10 \end{bmatrix}$$

$\omega_e := READPRN\begin{bmatrix} TW \\ PRN \end{bmatrix}$

$$\omega_e = \begin{bmatrix} 0 \\ 0 \\ -5 \\ 7.27220522 \cdot 10 \end{bmatrix}$$

--- Coriolis approximation used to obtain
target velocity. ---

$V_p := \omega_e \times P$

$$V_p = \begin{bmatrix} 392.41389016 \\ 10.64217313 \\ 0 \end{bmatrix}$$

Part 4:

The relative position and velocity vector is calculated for the target/ satellite geometry.

$R := P - S$ --- The relative displacement vector is calculated. ---

$V := V_p - V_s$ --- The relative vector component of motion is calculated. ---

$|V| = 7.53473649 \cdot 10^{3}$ --- The magnitude of relative velocity at time t=0. ---

---

Part 5:

The along track and cross track components of relative velocity is calculated at time t=0. (The satellite is assumed to be stationary.)

--- A unit radial vector is defined. This vector has as direction a line passing through the satellite position and target position at time t=0. ---

$$r_u := \frac{R}{|R|}$$

--- The cross track component of velocity is calculated. ---

$V_c := V \cdot r_u$ $\qquad V_c = -183.27597839$

--- The along track component of velocity is calculated. ---

$V_a := \sqrt{(|V|)^2 - V_c^2}$ $\qquad V_a = 7.53250715 \cdot 10^3$

--- The aspect angle at time t=0 is calculated. ---

$\alpha := \operatorname{atan}\left[\frac{V_c}{V_a}\right]$ $\qquad \alpha = -0.02432654$

--- The distance between the zero doppler position and the doppler centroid position. ---

$d := r_s \cdot \sin(\alpha)$ $\qquad d = -6.78212943 \cdot 10^3$

--- The distance from the antenna to the zero doppler position is calculated. ---

$r_o := r_s \cdot \cos(\alpha)$ $\qquad r_o = 2.78740503 \cdot 10^5$

--- Using these parameters the doppler centroid and doppler rate can be calculated. ---

$f_c := \left[\frac{-2 \cdot f_o}{c}\right] \cdot \left[\frac{|V| \cdot d}{r_o}\right]$ $\qquad f_c = 1.56795986 \cdot 10^3$

$$f_r := \left[\frac{-2 \cdot f_o}{c}\right] \cdot \left[\frac{(|V|)^2}{r_o}\right} \qquad f_r = -1.74195502 \cdot 10^3$$

--- The azimuth reference function is calculated. ---

$$azim_n := e^{j \cdot 2 \cdot \pi \cdot \left[\frac{1}{2} \cdot f_r \cdot (-T \cdot \delta t + n \cdot \delta t)^2 + f_c \cdot (-T \cdot \delta t + n \cdot \delta t)\right]}$$

--- The In-phase amd Quadrature components of this azimuth reference function are plotted. ---

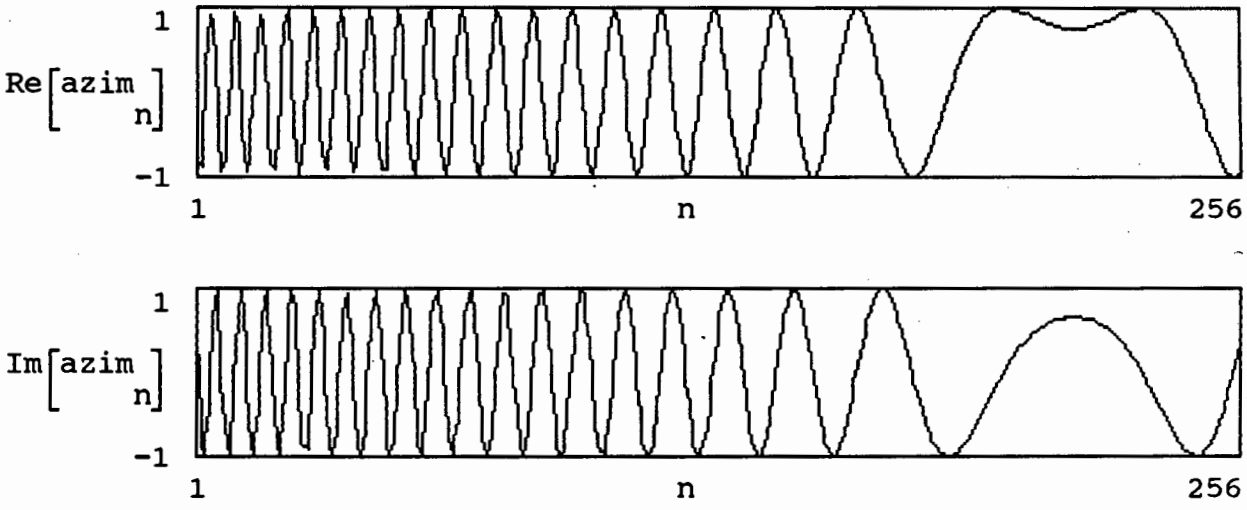

Part 5:

The range migration locus is plotted. The total amount of range walk is calculated over this azimuth length. A migration curve is also plotted.

--- The relative radial distance (one way) as a function of time ---

$$r_n := ((|R + V \cdot (-T \cdot \delta t + n \cdot \delta t)|) - |R|)$$

--- The locus of range migration (radial distance as a function of azimuth time). ---

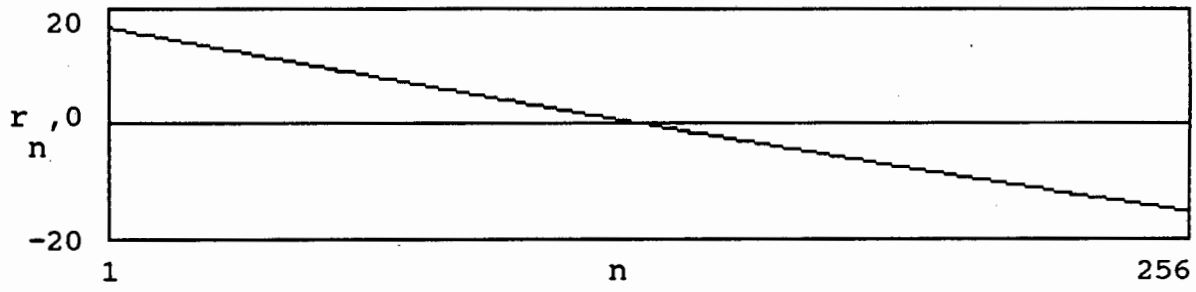

--- The total amount of range walk (in meters), over the azimuth window shown above, is calculated. ---

$$RW := \begin{bmatrix} r_{SAMPLES} - r_1 \end{bmatrix} \qquad |RW| = 31.91523462$$

--- The range curvature is calculated by removing the range walk ---

$$Grad := \frac{RW}{SAMPLES - 1}$$

--- The slope of the range walk line in units of δt. ---

$$y_n := r_n - \left[Grad \cdot n + \left[r_1 - Grad \right] \right]$$

--- The range walk is corrected. ---

--- A plot of the locus for range curvature is shown. ---

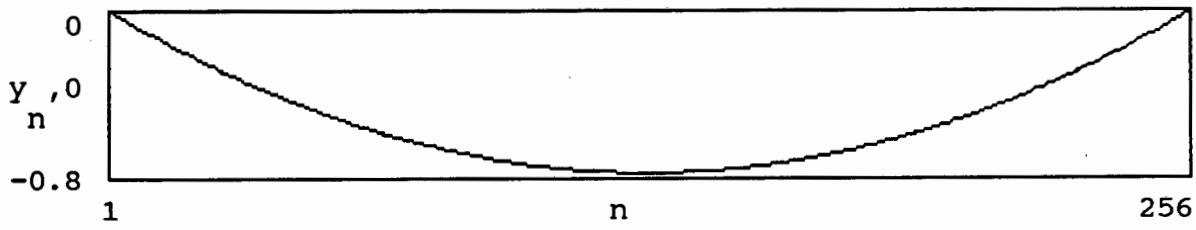

--- The maximum amount of range curvature that occurs over the azimuth length, is calculate. ---

$$\left| y_T \right| = 0.77191648$$

==========

APPENDIX D

APPENDIX D1

MENU TAPE FOR THE SIR-B EXPERIMENT.

SIR-B
DIGITALLY CORRELATED IMAGERY
MENU TAPE

ANNOTATION PARAMETERS

SITE NAME: AGULHAS/MOLOPO
DATA TAKE-SCENE NO.: X1-035.60-079
CENTER LAT/LONG: -32 Deg 16.5 Min / 25 Deg 38.9 Min
CENTER RESOLUTION (GROUND RANGE x AZIMUTH): 24.0 M x 29.2 M
TRACK (DEG TO TRUE NORTH): 139.9

CENTER TIME (GMT): 281/15:20:11.755
CORRELATION DATE: 06/23/90
CENTER INCIDENCE ANGLE: 35.8
PIXEL SIZE: 12.5
BITS PER SAMPLE: 6

SHUTTLE PARAMETERS

FOR IMAGE CENTER

X POSITION: 282.449
Y POSITION: -5637.355
Z POSITION: -3419.207
SLANT RANGE TO NEAR EDGE: 272.67
ALTITUDE: 226.96
YAW: .0

X VELOCITY: 4763.469
Y VELOCITY: 3359.391
Z VELOCITY: -5143.152
EARTH RADIUS AT TARGET: 6372.07
ROLL: 85.0
PITCH: .0

RADAR PARAMETERS

RECEIVER GAIN: 89.68
BORE ANGLE : 59.6

PRF: 1463.8
DATA WINDOW POSITION: 43

CALIBRATOR LEVEL SETTING: 2
DOWNLINK RATE: 30.4

IMAGE PARAMETERS

STARTING SAMPLE NO.: 1
NO. SAMPLES/SLANT RANGE IMAGE LINE: 4352

NO. SAMPLES PER IMAGE LINE: 6972
NO. SLANT RANGE IMAGE RECORDS: 1202

NO. IMAGE RECORDS: 1614
LINES PER REF. UPDATE: 8

COEFFICIENTS USED TO CALCULATE DOPPLER FREQUENCY

ACROSS TRACK: FD:A= .00 Hz FD:B= 89.21 Hz FD:C= 1859.70 Hz

COEFFICIENTS USED TO CALCULATE DOPPLER FREQUENCY RATE

ACROSS TRACK: FR:D= .00 Hz/S FR:E= -65.85 Hz/S FR:F= 1725.06 Hz/S
ALONG TRACK : FR:A1= .00 Hz/S FR:A2= .13 Hz/S FR:A3= -551.15 Hz/S

EARTH RADIUS AT NADIR: 6372.32 KM
GROUND RANGE PIXEL SIZE: AZIMUTH = 19.9 M

AZIMUTH SKEW: -42
RANGE = 16.9 M

SQUINT ANGLE: .58 Deg
SWATH VELOCITY: 7.2668 KM/S

CORNER COORDINATES

NEAR EARLY LATITUDE:	-31 Deg 54.4 Min	NEAR EARLY LONGITUDE: 25 Deg 27.5 Min
NEAR LATE LATITUDE :	-32 Deg 31.9 Min	NEAR LATE LONGITUDE : 26 Deg .4 Min
FAR EARLY LATITUDE :	-32 Deg 1.2 Min	FAR EARLY LONGITUDE : 25 Deg 17.5 Min
FAR LATE LATITUDE :	-32 Deg 38.7 Min	FAR LATE LONGITUDE : 25 Deg 50.3 Min

CALIBRATION LEVEL ESTIMATE: 39.84
BLOCKS PER FDDOT AZIMUTH INCREMENT: 12
SIGNAL TO NOISE RATIO: 5.18 DB

BIT ERROR RATE: -99.99
FR AZIMUTH INCREMENT FLAG: 0
NOISE: 44.21

SCALE FACTOR: 145.28
START TIME (GMT):281/15:20:03
REQUEST NUMBER: 3008

PROCESSOR SOFTWARE VERSION NO.: 2.3

REMARKS:

APPENDIX D2

TOPOGRAPHICAL MAP OF CRADOCK AREA.

AERIAL PHOTOGRAPH OF BUFFELSKOP IN THE GANNAHOEK MOUNTAIN RANGE SOUTH OF CRADOCK.

1/30 000
3
27/7/86
895

1:250 000 SOUTH AFRICA
SUID-AFRIKA